Università degli Studi di Cagliari

PHD DEGREE

INGEGNERIA CIVILE E ARCHITETTURA

Cycle XXX

Thesis presented for the degree of Doctor of Philosophy to:
University of Cagliari and Institut National de la Recherche Scientifique (Québec)

A comparative assessment of hydrologic models of varying complexity applied to a semi-arid region (Sardinia, Italy) for climate change studies

Scientific Disciplinary Sector
ICAR/02 Costruzioni idrauliche e marittime e idrologia

PhD Student: Enrica Perra

Coordinator of the PhD Programme Prof. Roberto Deidda

Supervisors Prof. Roberto Deidda and Prof. Claudio Paniconi

Final exam Academic Year 2016 – 2017
Thesis defence: February-March 2018 Session

UNIONE EUROPEA
Fondo sociale europeo

REGIONE AUTONOMA DELLA SARDEGNA

FSE 2007-2013
POR SARDEGNA
obiettivo competitività regionale e occupazione

Enrica Perra gratefully acknowledges Sardinia Regional Government for the financial support of her PhD scholarship (P.O.R. Sardegna F.S.E. Operational Programme of the Autonomous Region of Sardinia, European Social Fund 2007-2013 - Axis IV Human Resources, Objective l.3, Line of Activity l.3.1.).

Abstract

Assessing the hydrologic impacts of climate change is of great importance in the Mediterranean basins, which are heavily sensitive to climate variability, with significant impacts on water resources and hydrologic extremes. Modeling such complex systems to manage water resources and predict hydrologic extremes is a difficult task. The overall aim of the work described in this thesis is to bring a contribution in developing a modeling approach that allows evaluation of local hydrologic impacts of climate changes in two Mediterranean catchments located in Sardinia. This contribution revolves around two main themes: understanding how physical representation of hydrologic models can affect hydrologic impact assessment under climate change on a semi-arid basin of the Mediterranean region, the Rio Mannu catchment, and demonstrating how advanced hydrologic modeling can help in defining adaptation measures in a complex water system, the Flumendosa basin, under climate change.

The work to achieve the general objective is elaborated into three stages. The effects of climate change are evaluated on the Rio Mannu catchment through comparison of the results from five hydrologic models, CATchment HYdrology (CATHY), Soil and Water Assessment Tool (SWAT), TIN-based Real time Integrated Basin Simulator (tRIBS), TOPographic Kinematic APproximation and Integration-eXtended (TOPKAPI-X), and Water flow and balance Simulation Model (WASIM), and using as atmospheric input outputs of four climate global (GCM) and regional (RCM) model combinations. In order to evaluate uncertainties, a recently proposed metric is used: climate and hydrologic models results are compared in terms of agreement with each other in reference and future periods using Pearson correlation values and Duveiller bias. Notwithstanding some differences, overall the five hydrologic models show good agreement, and they respond similarly to the reduced precipitation and increased temperatures

predicted by the climate models, lending strong support to a future scenario of increased water shortages for this region of the Mediterranean, with negative consequences especially for the agricultural sector. Detailed comparison of the responses obtained with three physically based hydrologic models, but to varying degrees as regards physical processes and terrain features representation – CATHY, tRIBS, and TOPKAPI-X – on the same catchment is carried out, with the aim to test the transferability of parameters between the three hydrologic models, focusing in particular on the calibration and validation difficulties. While the three hydrologic models responded similarly during the calibration year, significant differences were found for the drier validation period for the CATHY model, which produced very low streamflow. To obtain satisfactory results for the CATHY model, an hypothesis of soil crusting was assumed and the first soil layer was modeled with a lower saturated hydraulic conductivity. Finally, the TOPKAPI-X model is applied on a large Sardinian basin prone to extreme flood events, the Flumendosa basin, to assess the hydrologic impact of climate change at much larger scale. The model responds with decreasing value of discharge, soil water content, and actual evapotranspiration to the reduced precipitation and increased temperature predicted by the climate models, lending strong support to a future scenario of increased water shortages also in this basin of the Mediterranean region.

Riassunto

La valutazione dell'impatto idrologico del cambiamento climatico riveste particolare importanza per i bacini del Mediterraneo, sensibili ad eventi idrologici estremi. Modellizzare dei sistemi così complessi per la gestione della risorse idriche è una sfida difficile. L'obiettivo globale di questo lavoro è contribuire allo sviluppo di un approccio modellistico che consenta la valutazione dell'impatto idrologico del cambiamento climatico su due bacini del Mediterraneo localizzati in Sardegna. Questo contributo si focalizza su due temi principali: capire come la rappresentazione fisica dei modelli idrologici incida sulla valutazione dell'impatto idrologico dovuto al cambiamento climatico su un bacino con un clima semi-arido, il Rio Mannu di San Sperate, e dimostrare come la modellizzazione avanzata possa aiutare nel definire misure di adattamento in un sistema idrico complesso incline ad eventi estremi, il Flumendosa, in condizioni di cambiamento climatico.

Per raggiungere tale obiettivo il lavoro si articola in tre fasi. Gli effetti del cambiamento climatico sul bacino del Rio Mannu sono stati valutati attraverso il confronto dei risultati di cinque modelli idrologici, CATchment HYdrology (CATHY), Soil and Water Assessment Tool (SWAT), TIN-based Real time Integrated Basin Simulator (tRIBS), TOPographic Kinematic APproximation and Integration-eXtended (TOPKAPI-X), and Water flow and balance Simulation Model (WASIM), utilizzando come forzante atmosferica gli output di quattro combinazioni di modelli climatici globali (GCM) e regionali (RCM). Per valutare le incertezze è stata utilizzata una metrica recentemente proposta: i risultati dei modelli sono stati comparati durante un periodo di riferimento e futuro, utilizzando l'indice di correlazione di Pearson e il bias di Duveiller. Pur con qualche differenza, complessivamente i modelli idrologici mostrano una buona concordanza tra loro, e rispondono in maniera simile alla riduzione della precipitazione e

all'incremento della temperatura previsti dai modelli climatici. Ci si aspetta pertanto che il bacino nel futuro sarà soggetto ad una riduzione della disponibilità di risorsa idrica, con conseguenze negative in particolare per il settore agricolo. È stato effettuato un confronto dettagliato delle risposte ottenute sullo stesso bacino con tre modelli idrologici fisicamente basati di diverso grado per quanto riguarda la rappresentazione dei processi fisici e delle caratteristiche del terreno, CATHY, TOPKAPI-X, tRIBS, con lo scopo di testare la trasferibilità dei parametri tra i tre modelli idrologici, concentrandosi sulle difficoltà riscontrate nei periodi di calibrazione e validazione. Mentre i tre modelli hanno risposto in maniera simile durante il periodo di calibrazione, sono state riscontrate significative differenze durante il periodo di validazione, caratterizzato da un clima molto secco, con il modello CATHY, che ha prodotto una portata molto bassa. Pertanto, per ottenere risultati soddisfacenti con il modello CATHY, è stata assunta l'ipotesi di soil crusting, sulla base della quale il primo strato di suolo è stato modellato con una ridotta conducibilità idraulica satura. Infine il modello TOPKAPI-X è stato implementato su uno dei principali bacini sardi di importanza strategica per il sistema idrico della regione, il Flumendosa, per valutare gli effetti del cambiamento climatico a scala maggiore. Il modello risponde con una diminuzione dei valori di portata, contenuto idrico ed evapotraspirazione reale alla riduzione della precipitazione ed incremento della temperature previsto dai modelli climatici, dando supporto ad uno scenario futuro di carenza della risorsa idrica anche in questo bacino dell'area Mediterranea.

Résumé

L'évaluation de l'impact hydrologique du changement climatique présente une importance particulière pour les bassins de la Méditerranée, qui sont très sensibles aux événements hydrologiques extrêmes. La modélisation des systèmes aussi complexes pour la gestion des ressources hydriques est un défi difficile. L'objectif global de ce travail est de contribuer au développement d'une approche de modélisation qui permette l'évaluation de l'impact hydrologique du changement climatique sur deux bassins de la Méditerranée, localisés en Sardaigne. Cette contribution se concentre sur deux sujets principaux: comprendre comment la représentation physique des modèles hydrologiques grave sur l'évaluation de l'impact hydrologique dû au changement climatique sur un bassin avec un climat semi-aride, le Rio Mannu di San Sperate, et montrer comme le modélisation avancé puisse aider à définir de mesures de modération et adaptation dans un système complexe enclin aux événements hydrique extrêmes, le Flumendosa, en conditions de changement climatique.

Pour atteindre cet objectif le travail s'articule en trois phases. Les effets du changement climatique sur le bassin du Rio Mannu sont évalués à travers la comparaison des résultats de cinq modèles hydrologiques, CATchment HYdrology (CATHY), Soil and Water Assessment Tool (SWAT), TIN-based Real time Integrated Basin Simulator (tRIBS), TOPographic Kinematic APproximation and Integration-eXtended (TOPKAPI-X), and Water flow and balance Simulation Model (WASIM), en utilisant comme forçage atmosphérique les données de quatre combinaisons de modèles climatiques globaux (GCM) et régionaux (RCM). Pour évaluer les incertitudes une métrique récemment proposée est utilisée: les résultats des modèles sont comparés pendant une période de référence et future, en utilisant l'index de corrélation de Pearson et le bias de Duveiller. Même si certaines différences existent, en tout les modèles

hydrologiques montrent une bonne concordance, et ils répondent de manière semblable à la réduction de la précipitation et à l'accroissement de la température prévu par les modèles climatiques. Il s'attend donc que le bassin dans l'avenir sera sujet à une réduction de la disponibilité de ressource hydrique, avec des conséquences négatives en particulier pour le secteur agricole. Une comparaison détaillée des réponses obtenue sur le même bassin avec trois modèles hydrologique à base physique avec différent degré pour ce qui concerne la représentation des procès physiques et des caractéristiques du terrain, CATHY, TOPKAPI-X, tRIBS, est effectué dans le but de tester la transférabilité des paramètres entre les trois modèles hydrologiques, avec une attention particulière sur les difficultés relevées dans les périodes de calibrage et validation. Tandis que les trois modèles ont répondu de manière semblable pendant la période de calibrage, significatives différences ont été relevées pendant la période de validation, caractérisé par un climat très sec, avec le modèle CATHY, qu'il a produit un très bas décharge. En conséquence, pour obtenir résultats satisfaisants avec le modèle CATHY, l'hypothèse de croûtage de sol a été assumée, sur la base dont la couche premier de sol a été modelée avec une conductibilité hydraulique saturée réduite. Finalement le modèle TOPKAPI-X est implémenté sur un des principaux bassins de la Sardaigne, d'importance stratégique pour le système hydrique de la région, le Flumendosa, afin d'évaluer les effets du changement climatique à plus grande échelle. Le modèle répond avec une diminution des valeurs de décharge, contenu hydrique et évapotranspiration réelle à la réduction de la précipitation et accroissement des températures prévus par les modèles climatiques en donnant aussi support à une scène future de carence de la ressource hydrique dans ce bassin de la zone Méditerranéenne.

Acknowledgements

I am sincerely grateful to my advisors, Prof. Roberto Deidda, for giving me the opportunity of this doctoral research and his support toward a critical approach in hydrologic science, and Prof. Claudio Paniconi, for his precious reviews and fundamental contribution to the development of this thesis, and his hospitality at Institut National de la Recherche Scientifique.

My gratitude goes to all my colleagues and friends, who kindly supported my doctoral research, in particular to Monica for her continuous encouragement and help, Domenico and Francesco for their support, Jacopo, Laura, and Michela, who shared this PhD experience with me, and Carlotta, Gaetano, Michela, Silvia, my family in Canada.

Last, but not least my special thanks to my husband, my family and friends for always having believed in me. Thank you for everything and forever.

Contents

Synthèse

S.1 Introduction

Les études climatiques conviennent que la zone méditerranéenne sera particulièrement affectée par des changements dus au réchauffement climatique [*IPCC,* 2014]. Il a été distingué comme un "des points chauds" dans les prédictions du changement climatique futures [*Giorgi*, 2006], susceptible aux événements extrêmes plus fréquents et plus intenses. Pendant les décennies dernières, une augmentation des températures moyennes et extrêmes a été observée dans les régions méditerranéennes [*Xoplaki et al*., 2003; *Del Río et al*., 2011; *El Kenawy et al*., 2011; *Acero et al*., 2014], accompagnée par réductions saisonnières des précipitations [*Giorgi and Lionello*, 2008; *Sousa et al*., 2011; *Vicente-Serrano and Cuadrat-Prats*, 2007].

À cause des changements climatiques et anthropiques (comme l'expansion des cultures vers zones semi-arides, la dépopulation des montagnes, l'intensification d'utilisation des terres, le déboisement et les feux forestiers) les flux hydrologiques et les caractéristiques physiques peuvent évoluer dans le sens de la désertification [*Cudennec et al*., 2007; *Puigdefabregas and Mendizabal*, 1998; *Tooth*, 2007]. En raison de sa position géographique avec beaucoup des montagnes environnantes, le bassin Méditerranéen est aussi régulièrement exposé à des précipitations intenses ainsi que inondations [*Adamovic*, 2016], qui représentent le danger le plus destructif dans la région méditerranéenne [*Gaume et al*., 2009].

Les récentes inondations intenses ont causé des pertes socio-économiques importantes [*Chessa et al*., 2004; *Silvestro et al*., 2012], tandis que les périodes de sécheresse persistantes ont limité la disponibilité d'eau, causant des restrictions qui ont affecté le secteur agricole, le pilier de l'économie locale [*Piras*, 2014]. Dans des régions où le stress d'eau est déjà haut, l'impact combiné de l’augmentation des besoins en raison des activités humaines et de la diminution de la

disponibilité d'eau en raison du changement climatique pourrait engendrer un sévère manque d'eau et des conflits majeurs de son utilisation [*Grouillet et al*., 2015; *Milano et al*., 2013a].

Dans ce contexte il est donc important d'évaluer les effets du changement climatique au niveau local du bassin hydrologique pour fournir des possibles scénarios aux décideurs et aux parties prenantes intéressées [*Cudennec et al.*, 2007]. Les évaluations d'impact du changement climatique forment la base pour le développement de stratégies d'adaptation appropriées [*Gädeke et al*., 2014]. Les impacts du changement climatique à l'échelle du bassin peuvent être évalués par l'accouplement des modèles climatiques globaux (GCM) et régionaux (RCM) avec des modèles hydrologiques distribués utilisant des techniques de réduction d'échelle pour rapprocher la disparité entre l'échelle des modèles climatiques et hydrologiques [*Piras*, 2014]. Ceci est d'habitude conduit par une procédure en trois étapes [*Xu et al.,* 2005] consistant en: (i) sélectionner des GCM et RCM pour fournir des scénarios climatiques futurs sous l'effet de gaz à effet de serre croissants; (ii) développer et appliquer des techniques de réduction d'échelle pour adapter l'échelle des GCM et RCM à celle des modèles hydrologiques; et (iii) utiliser des outputs à échelle réduite comme forçage pour les modèles hydrologiques afin de simuler les effets du changement climatique sur les régimes hydrologiques [*Abbaspour et al*., 2009; *Liuzzo et al*., 2010; *Sulis et al*., 2011, 2012; *Montenegro and Ragab*, 2012; *Piras et al*., 2014 ; *Majone et al*., 2016; *Meyer et al*., 2016]. Toutes ces phases sont affectées par des incertitudes [*Xu and Singh*, 2004] qui ont été explorées dans beaucoup des papiers précédents: choix du scénario d'émission et forçage climatique [*Giorgi and Mearns*, 2002; *Tebaldi et al.*, 2005], technique de réduction d'échelle [*Wood et al*., 2004; *Fowler et al*., 2007; *Im et al*., 2010], moyens hydrologiques utilisés pour évaluer les impacts locaux et données observées pour les calibrer [*Clark et al.*, 2008; *Jiang et al*., 2007; *Dams et al*., 2015]. Une approche pour l'évaluation et la réduction d'incertitudes est

d'utiliser de multiple modèles climatiques et hydrologiques [*Bosshard et al*., 2013; *Cornelissen et al*., 2013; *Gädeke et al*., 2014; *Najafi et al*., 2011].

S.1.1 État de l'art sur l'intercomparaison de modèles et transférabilité de paramètre

Le but principal de la modélisation hydrologique est simuler les processus hydrologiques aux échelles différentes, pour guider la formulation de stratégies de gestion de ressource en eau et aussi comme outils d'enquête scientifique [Dingman, 2008]. Un modèle hydrologique est essentiellement un modèle de simulation, une représentation d'une part du monde naturel ou construit d'homme, qui peut reproduire certains, mais pas tous les processus en jeu [Dooge, 1986]. En général, trois classes principales de modèles de simulation existent: modèles physiques, modèles analogues et modèles mathématiques. Les premiers sont des représentations à l'échelle d'une partie du monde naturel. Les deuxièmes utilisent observations d'un processus pour simuler un processus naturel physiquement analogue. Les modèles mathématiques sont un ensemble séquentiel explicite d'équations qui convertissent des données numériques en résultats numériques. Ces derniers modèles sont devenus la classe plus largement utilisée de modèle hydrologique, grâce à la disponibilité de calculateurs numériques dans lesquels exécuter les codes [*Dingman*, 2008].

Une première classification des modèles mathématiques utilisés dans l'hydrologie a été présentée par Clarke [1973]. Dans cette classification, on considère des modèles stochastiques, avec des variables qui montrent une variation aléatoire, ou déterminée, avec des variables considérées libres de la variation aléatoire. Les modèles tant stochastiques que déterministes sont classifiés comme conceptuels quand ils utilisent des schématisations de phénomènes physiques, à base physique quand ils résolvent les équations physiques des processus différents et empiriques quand ils ne représentent pas les phénomènes physiques parce qu'ils sont basés seulement sur

l'observation des données et des résultats, sans explicitement représenter le processus de conversion. Dans ces groupes, les modèles pourraient être linéaires ou non-linéaires et regroupés ou distribués. Les modèles regroupés sont définis comme ceux qui ne représentent pas la distribution spatiale des données ou des paramètres. Les modèles distribués, au contraire, représentent la variabilité spatiale des données.

Les modèles hydrologiques à base physique sont des outils utiles pour simuler la réponse hydrologique, afin de guider la formulation de stratégies de gestion de ressource en eau et aussi comme outils d'enquête scientifique [*Abbott et al.,* 1986; *Kampf and Burgess,* 2007; *Paniconi and Putti*, 2015; *Fatichi et al*., 2016]. Le fait d'utiliser des paramètres avec une signification physique, en plus, peut permettre la transférabilité du calibrage de leur valeur parmi des modèles différents. Les modèles hydrologiques à base physique peuvent représenter un processus spécifique, comme le flux d'eau souterraine dans milieu poreux saturé et variablement saturé [*Huyakorn et al*., 1986; *Jones and Woodward*, 2001; *Kirkland et al*., 1992] ou l'écoulement de surface [*Gottardi and Venutelli*, 1993; *Jaber and Mohtar*, 2003; *Taylor et al*., 1974], ou processus multiples et leurs interactions [*Gunduz and Aral*, 2005; *Panday and Huyakorn*, 2004; *VanderKwaak and Loague*, 2001], comme les modèles superficiels-souterrains couplés. Grâce aux avances récentes de télédétection, des systèmes d'information géographiques (GIS) et des techniques géophysiques depuis quelques années, les modèles hydrologiques à base physique qui représentent les interactions atmosphère–terrain ont été développés comme des outils utiles pour simuler et prévoir des flux d'eau, tant dans des domaines appliqué/opérationnel qu'en recherche/théorique. Ces modèles ont été appliqués par exemple pour étudier deux phénomènes qui sont très importants: changement climatique et événements d'inondation [*Artan et al.,* 2001; *Kite*, 1995; *Liu and Todini*, 2002; *Wigmosta et al*., 1994].

Étant donné que les modèles hydrologiques sont des représentations du monde réel, on ne peut pas prévoir lequel offre plus de précision pour spécifiques bassins et conditions hydrologiques [*Seiller et al*., 2012]. Dans telles circonstances, l'intercomparaison de modèles fournit des moyens utiles pour conduire des évaluations de prestation, y compris l'évaluation de l'effet de la structure du modèle sur leur résultats [*Chiew et al*., 1993; *Refsgaard and Knudsen*, 1996; *Perrin et al*., 2001; *Reed et al*., 2004; *Breuer et al*., 2009; *Gorgen et al*., 2010; *Bae et al.*, 2011; *Clark et al*., 2011; *Koch et al*. 2016]. La plupart des études d'intercomparaison de modèles hydrologiques se sont concentrés sur la décharge simulée, une mesure intégrée de réponse hydrologique au débouché de bassin [*Cornelissen et al*., 2013; *Dams et al*., 2015; *Goslin et al*., 2011; *Kollet et al*., 2017; *Ludwig et al*. 2009], et ont montré qu'il existe une variété de modèles hydrologiques, avec une vaste gamme d'algorithmes pour décrire des processus hydrologiques, qui permettent de simuler la décharge fluviale avec une précision similaire [*Refsgaard and Knudsen*, 1996; *Pitman and Henderson-Sellers*, 1998; *Smith et al*., 2004, 2012; *Duan et al.*, 2006; *Safari et al*., 2012; *Vansteenkiste et al*., 2014a,b]. Cependant, dans ces comparaisons chaque modèle hydrologique a été indépendamment calibré.

Un défi pour les modélisateurs hydrologiques concerne la façon dont la connaissance gagnée d'un modèle peut être transférée à un autre modèle. La littérature sur la transférabilité de paramètre est surtout reliée à la transférabilité des paramètres spatio-temporels. Par exemple, Patil et al. [2015] ont comparé trois plans différents de transfert de paramètre, temporel, spatial et spatiotemporel, utilisant un modèle hydrologique concentré, EXP-HYDRO, sur 294 bassins à travers les États-Unis. Les résultats ont montré que la stabilité des paramètres des modèles hydrologiques a tendance à être plus haut dans le domaine temporel que dans le domaine spatial. Ren et al. [2016] ont évalué le potentiel de transférabilité des paramètres des modèles

hydrologiques dans Community Land Model (CLM) par des analyses de sensibilité et classification à travers des bassins aux États-Unis. Ils ont constaté que l'utilisation des mêmes valeurs de paramètre pour des sites appartenant à la même classe ne pourrait pas apporter la meilleure prestation du modèle si le sol et les conditions climatiques varient considérablement dans la classe. La littérature de la transférabilité de paramètre à travers des modèles hydrologiques est limitée. Seulement en Yen et al. [2015] trois sources de données d'utilisation de terrain ont été mises en œuvre sur un bassin situé en Maryland, États-Unis, pour examiner l'impact potentiel de transfert des paramètres de calibrage optimaux entre trois versions du modèle SWAT. Il a montré que les paramètres sont transmissibles temporellement (paramètres transférés dans période de simulation différente) ou dans l'espace (paramètres transféré dans des sites voisins non mesurés) mais non structurellement (par exemple les paramètres ne sont pas transmissibles dans des versions différentes du modèle SWAT).

De la même façon dans les modèles hydrologiques, l'ensemble multi-modèle est généralement utilisé dans la météorologie et la climatologie pour quantifier l'incertitude de prévisions météorologiques et de simulations de changement climatique [*Murphy et al*., 2004] et a été utilisé aussi pour conduire des simulations hydrologiques multi-modèle. Bae et al. [2011] ont comparé dans un bassin coréen trois modèles hydrologiques semi-distribué forcés avec les données de treize GCM et trois scénarios d'émission de gaz serre. Les résultats montrent que les modèles hydrologiques peuvent produire des différences majeures sur le changement d'écoulement dans les mêmes simulations climatiques, en particulier pendant la saison sèche. Bastola et al. [2011] ont examiné le rôle d'incertitudes des modèles hydrologiques (paramètre et incertitude structurelle) en utilisant six scénarios de changement climatique et quatre modèles hydrologiques conceptuels dans les méthodes d'évaluation d'incertitude de probabilité

généralisée (GLUE) et le modèle Bayésien atteignant moyenne (BMA). Les résultats pour les quatre bassins irlandais considérés ont montré une tendance de flux croissant en hiver et diminuant en été. Thompson et al. [2013] ont démontré pour la rivière du Mékong dans l'Asie du Sud-Est que l'incertitude concernant les GCM dans les projections de changement climatique est généralement plus grande que cela liée à l'utilisation de trois modèles hydrologiques, qui simulent la même direction de changement de la décharge moyenne. Cependant, l'incertitude liée au modèle hydrologique n'est pas négligeable et dans certains cas est d'une ampleur semblable à l'incertitude concernant les GCM. Velázquez et al. [2013] ont appliqué plusieurs scénarios de changement climatique et quatre modèles hydrologiques avec des complexités structurelles variables (modèles concentrés, semi-distribués et distribués) sur un bassin au Canada et un en Allemagne. Les résultats ont démontré une forte influence du modèle hydrologique choisi sur le flux simulé sous les scénarios de changement climatique, particulièrement pour les flux bas prévus. Les changements de hauts flux étaient au lieu de cela moins sensibles au choix de modèle hydrologique. Vansteenkiste et al. [2014a] ont utilisé un ensemble de modèles hydrologiques, entre concentré conceptuel et distribués à base physique, pour simuler l'impact du changement climatique à Grote Nete (Belgique). L'incertitude dans les résultats d'impact hydrologique a été évaluée avec le changement relatif de volumes de décharge et avec les extrêmes (pics et écoulement faible) entre les conditions climatiques historiques et futures. De grandes différences de prédictions modèles ont été trouvées, particulièrement dans des conditions de flux basses. Maurer et al. [2010] ont comparé un modèle distribué et un modèle concentré, forcés par vingt-deux productions des modèles climatiques pour trois bassins en Californie. Les changements de la décharge mensuelle n'ont pas significativement différé entre les deux modèles, sauf pendant l'été et pour des flux extrêmes. Néanmoins, dans ces études la zone

climatique des bassins analysés varie entre arctique et sous-arctique, humide tempéré, à tropical et subtropical. L'intercomparaison des modèles reste un champ inexploré dans des bassins caractérisés par un climat méditerranéen.

S.1.2 Objectifs et structure de la thèse

Dans ce contexte ma recherche a pour but d'apporter une contribution dans le développement d'une approche qui permet l'évaluation des impacts hydrologiques locaux dus au changement climatique sur deux bassins méditerranéens. Il y a trois buts spécifiques que je veux atteindre. Ceux-ci sont:

1. Tester la transférabilité de paramètre entre trois modèles hydrologiques à base physique, mais avec degrés variables en ce qui concerne les processus physiques et la représentation des caractéristiques du terrain – CATchment HYdrology (CATHY), TIN-based Real time Integrated Basin Simulator (tRIBS), and TOPographic Kinematic APproximation and Integration-eXtended (TOPKAPI-X) – sur un bassin de petite taille situé en Sardaigne (Italie) et caractérisé par un climat semi-aride, le Rio Mannu de San Sperate, se concentrant en particulier sur le calibrage et les difficultés de validation. Trois ans consécutifs ont été choisis pour le calibrage (1930) et la validation (1931-1932), la première étant une année assez humide tandis que la dernière période est caractérisée par un climat très sec. Les trois modèles hydrologiques ont répondu de la même façon pendant l'année de calibrage, tandis que des différences significatives ont été trouvées pendant la période de validation. Particulièrement pour obtenir des résultats satisfaisants pendant la période sèche 1931-1932, pour le modèle CATHY une hypothèse de croûtage

de sol a été assumée, sur la base de laquelle la première couche de sol a été modelée avec une conductivité hydraulique saturée plus bas.

2. Caractérisation de l'accord entre les prévisions tant climatiques qu'hydrologiques sur le bassin Rio Mannu, représentant du climat méditerranéen et questions socio-économiques liées aux extrêmes hydrologiques. Pour ce but un ensemble de modèles climatique et hydrologiques, y compris quatre combinaisons de GCM et RCM et un ensemble de cinq modèles hydrologiques avec complexité structurelle variable, entre conceptuel et à base physique, sera utilisé. Les modèles examinés sont: CATHY, Soil and Water Assessment Tool (SWAT), TOPKAPI-X, tRIBS et WAter balance SImulation Model (WASIM). Ceci est la première étude où une vaste gamme de modèles hydrologiques distribués forcés avec les outputs de modèles climatiques différents est appliquée sur un bassin méditerranéen pour évaluer l'impact dus au changement climatique. En plus, contrairement à beaucoup d'études précédentes, elle est centrée est sur un ensemble de variables caractérisant l'équilibre hydrique à l'échelle du bassin, y compris la précipitation, la température de l'air, la décharge, le contenu d'eau du sol dans le premier mètre et l'évapotranspiration réelle. Les résultats sont discutés dans le contexte des représentations de processus pour chaque modèle et avec une analyse rigoureuse de concordance. En particulier, pour le dernier, une nouvelle métrique, proposé par Duveiller et al. [2016], sera utilisée pour comparer les résultats des modèles pendant les période de référence et future utilisant des coefficients de biais et corrélation.
3. L'évaluation préliminaire d'impact hydrologique du changement climatique à une beaucoup plus grande échelle, par la mise en œuvre du modèle hydrologique TOPKAPI-

X sur un des bassins hydrographiques le plus économiquement importants en Sardaigne, le bassin de Flumendosa.

Le reste de la thèse est structuré comme suit:

Le Chapitre 2 contient la description des bassins Rio Mannu et Flumendosa;

Le Chapitre 3 présente les modèles hydrologiques et climatiques utilisés;

Le Chapitre 4 discute les résultats principaux quant aux les trois objectif de cette étude;

Le Chapitre 5 récapitule le contenu de cette dissertation.

S.2 Domaines d'études

Cette section contient la description des deux domaines d'étude considérés, situé en Sardaigne (Italie). La Section S.2.1 décrit le bassin Rio Mannu de San Sperate, tandis que la section S.2.2 illustre le bassin Flumendosa.

S.2.1 Le bassin Rio Mannu de San Sperate

La première zone d'étude, le Rio Mannu de San Sperate, est située dans le sud de la Sardaigne et il draine une région de 473 km^2 avec élévation variant entre 66 m et 963 m (Figure 1). La topographie est essentiellement plate, à part une zone montagneuse située à Sud-Est et la pente moyenne est environ 17%. Le bassin est caractérisé par un climat méditerranéen typique, avec des périodes humides à partir d'octobre jusqu'au moi d'avril et des périodes sèches pendant le reste de l'année. La précipitation annuelle moyenne est environ 600 mm, principalement concentré dans la période pluvieuse (94%). La température mensuelle moyenne varie entre 9°C en hiver et 25°C en été. Le régime de débit est caractérisé par des flux bas (moins de 1 m^3/s) pour la majeure partie de l'année, avec peu d'événements d'inondation en automne et en hiver, causé par des systèmes frontaux [*Mascaro et al*., 2013a]. La disponibilité de données de ce bassin est limitée: la précipitation, la température et les données de décharge sont collectés à une durée quotidienne et pendant des périodes non-coïncidentes. Pour fournir des données en entrée à l'échelle nécessaire pour le calibrage et la validation des modèles hydrologiques, deux stratégies de réduction d'échelle ont été développées, qui ont rapporté la précipitation et l'évapotranspiration potentielle à une durée horaire [*Mascaro et al*., 2013b].

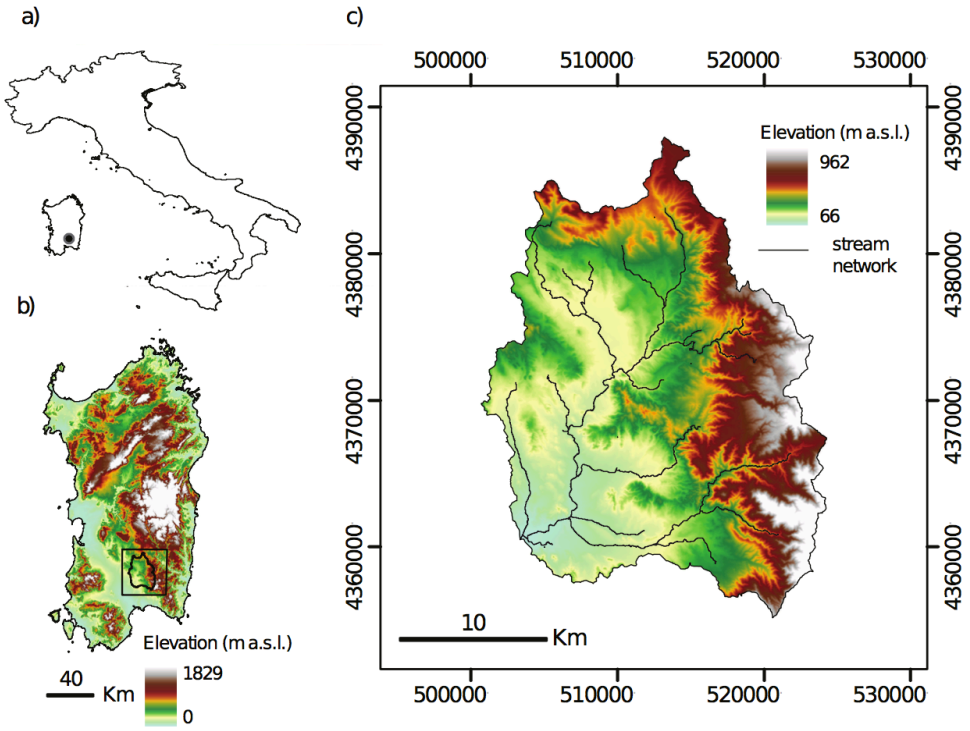

Figure 1. Localisation du bassin Rio Mannu dans a) l'Italie et b) l'île de la Sardaigne. Modèle d'élévation digital (DEM) du bassin Rio Mannu incluant coordonnées UTM.

Les données géospatiales pour le bassin du Rio Mannu ont été fourni du Gouvernement de la Région de la Sardaigne et incluent les suivantes: (i) un modèle d'élévation digital (DEM) à résolution de 10 m (Figure1c); (ii) la carte du couverture du terrain (LC) dans le format digital, dérivé du projet COORDINATION de l'INformation sur l'Environnement (CORINE) de l'Agence européenne pour l'environnement (EEA) pour l'année 2008; (iii) une copie d'une carte pédologique de la Sardaigne à échelle 1:250 000 [*Aru et al.*, 1992]; et (iv) des orthophotos de l'île entière pendant les années 1954 et 2006. Le LC et les cartes de texture de sol ont été prétraités pour être utilisés comme données pour les modèles. Les classes originales CORINE LC ont été regroupées dans 8 groupes, obtenant la carte montrée dans la Figure2b [*Mascaro et al.*, 2013b]. Selon ce reclassement, les classes dominantes sont l'agriculture (~ 48 %) et la végétation clairsemée (~ 26 %), y compris la forêt méditerranéenne. D'autres catégories incluent

les olives, les forêts, les pâturages, les vignobles et les zones urbaines, avec des pourcentages mineurs. La carte pédologique a été numérisée et géoréférencée venant en 17 classes pour le bassin du Rio Mannu. Pour chaque classe de la carte, Aru et al., [1992] fournissent une gamme de texture du sol et une description qualitative des profondeurs du sol. Pour réduire l'incertitude de la classification de texture du sol, une série de campagnes du terrain a été conduite en 2011 par le projet décrit dans Ludwig et al. [2010], pendant lequel un total de 50 échantillons du sol de profondeur de 80 cm ont été rassemblés partout dans le bassin et analysés pour caractériser la texture. Ces données ont été utilisées comme un guide pour agréger les 17 classes et réduire la gamme de types de texture du sol possibles pour chaque classe. On montre la carte résultante dans la Figure 2a.

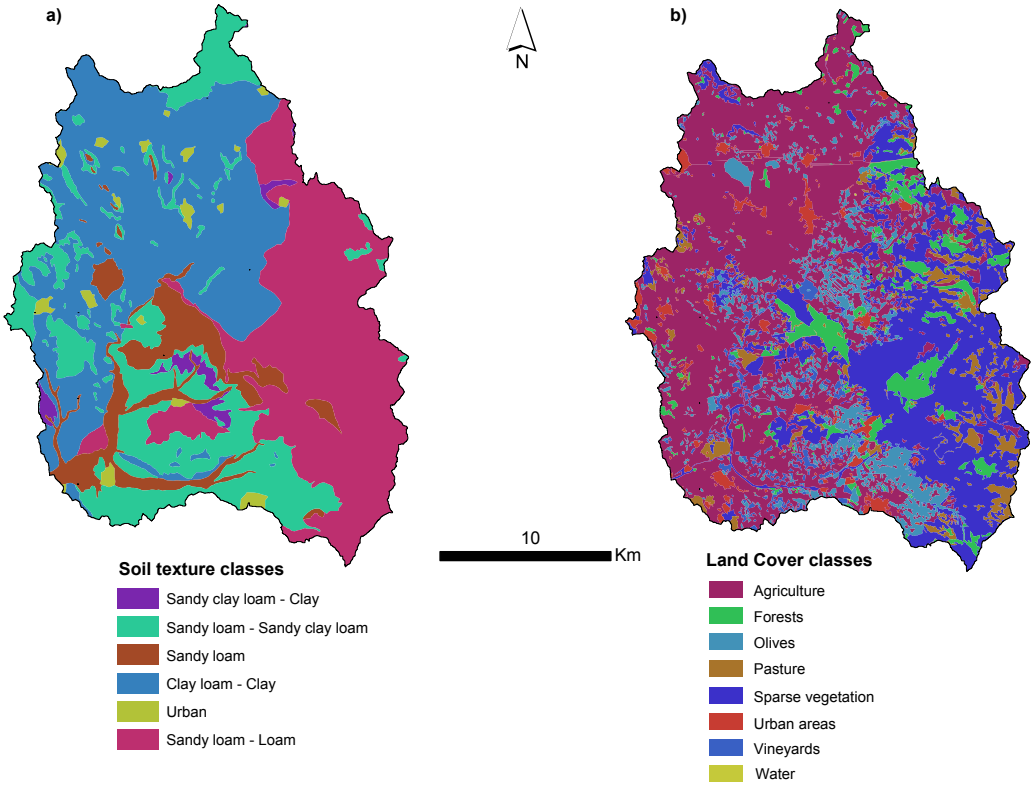

Figure 2. a) Texture du sol et b) carte de Couverture du Terrain utilisées pour le bassin Rio Mannu.

S.2.2 Le bassin Flumendosa

Le deuxième domaine d'étude, le bassin Flumendosa, est un des bassins sardes principaux, avec une pertinence stratégique pour le réseau hydrographique de la région (Figure 3). Il est localisé dans le sud-est de la Sardaigne et il draine un domaine de 1826 km^2. Il s'étend du sommet le plus haut de l'île (montagne Gennargentu, 1834 m) à l'embouchure sur la mer Tyrrhénienne. La pente moyenne est environ 36%. La précipitation annuelle moyenne est environ 900 mm et montre une forte corrélation avec l'orographie [*Seoni*, 2015]. La température mensuelle moyenne varie entre 6°C en hiver et 24°C en été. Prés du fleuve Flumendosa et ses tributaires ont été construits trois réservoirs que, avec une capacité totale de 600 millions de mètres cubes, constituent la ressource en eau principale pour les utilisations domestiques, irriguées et industrielles en Sardaigne du sud. Cette région est cependant aussi encline à de longues périodes de sécheresse, ainsi que des problèmes sociaux et économiques créés par des conflits parmi des utilisations différentes d'eau. De plus, quelques villages dans le bassin (par exemple Ballao, San Vito, Muravera et Villaputzu) ont subi des épisodes d'inondation extrêmes, qui ont exigé l'intervention de l'agence de protection civile et cela a causé, dans quelques cas, la perte de vies humaines.

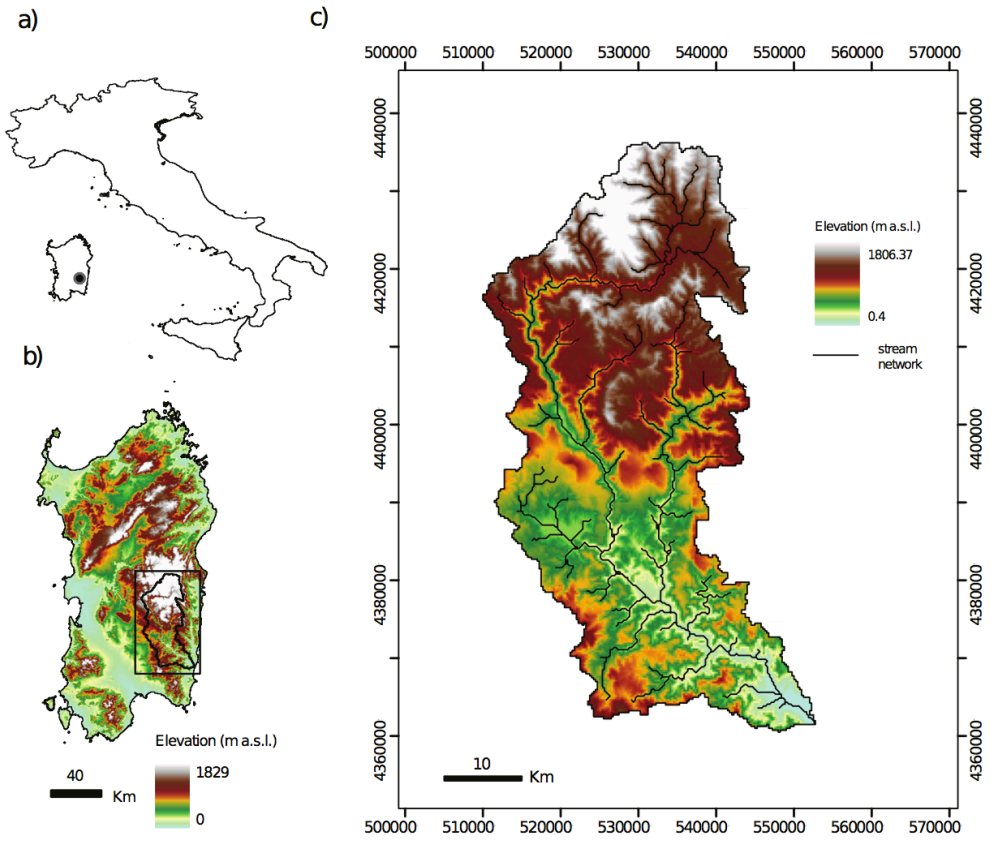

Figure 3. Localisation du bassin Flumendosa dans a) l'Italie et b) l'île de la Sardaigne. Modèle d'élévation digital (DEM) du bassin Rio Mannu incluant coordonnées UTM.

Les données géospatiales pour le bassin du Flumendosa ont été fourni du Gouvernement de la Région de la Sardaigne et incluent les suivantes: (i) un modèle d'élévation digital (DEM) à résolution de 10 m (Figure4c); (ii) la carte du couverture du terrain (LC) dans le format digital, dérivé du projet COORDINATION de l'INformation sur l'Environnement (CORINE) de l'Agence européenne pour l'environnement (EEA) pour l'année 2008; (iii) une copie d'une carte pédologique de la Sardaigne à échelle 1:250 000 [*Aru et al.*, 1992].

Le LC et les cartes de texture du sol ont été prétraités pour être utilisés comme données pour les modèles. Les classes originales CORINE LC ont été regroupées dans 8 groupes, obtenant la carte montrée dans la Figure 4a. Selon ce reclassement, les classes dominantes sont la forêt méditerranéenne (~ 38 %) et les forêts latifoliées (~ 22 %). D'autres catégories incluent

l'agriculture, les forêts, les pâturages et les zones urbaines, avec des pourcentages mineurs. La carte pédologique a été numérisée et géoréférencée venant en 26 classes pour le bassin Flumendosa. Pour chaque classe de la carte, Aru et al., [1992] fournissent une gamme de texture du sol et une description qualitative des profondeurs du sol. Ces données ont été alors agrégées dans 7 classes basées sur l'acronyme du sol et le pourcentage de zone du bassin occupée dans la carte originale. On montre la carte résultante dans la Figure 4b.

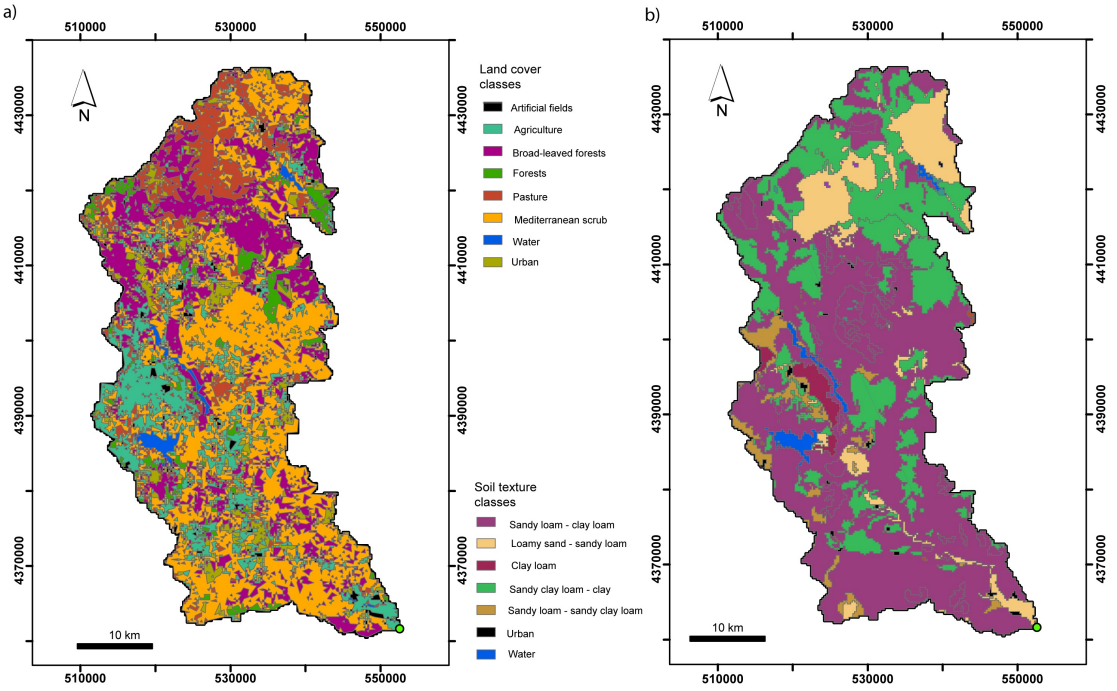

Figure 4. a) Carte de couverture du terrain et b) texture du sol pour le bassin Flumendosa.

S.3 Méthodologie

Certaines des études commencées pendant le projet CLIMB (CLimate Induced Changes on the hydrology of Mediterranean Basins) [*Ludwig et al*., 2010] dans le bassin Rio Mannu sont maintenant complétées et leurs résultats sont ici analysés pour exécuter une évaluation multi-modèle d'impacts hydrologique du changement climatique. Spécifiquement une comparaison détaillée des réponses obtenues avec les trois modèles hydrologiques à base physique, Catchment Hydrology (CATHY), TIN-based Real Time Integrated Basin Simulator (tRIBS), Topographic Kinematic Approximation and Integration eXtended (TOPKAPI-X), est appliquée, concentrant en particulier sur les difficultés lors du calibrage et validation. Puisque le modèle tRIBS a été précédemment mis en œuvre sur le bassin Rio Mannu pendant le projet CLIMB, pour les deux autres modèles les mêmes ensembles de données ont été adoptés, y compris les données géospatiales de propriétés de surface de terrain et la contrainte hydraulique-météorologique, pour tester la transférabilité de paramètres entre les trois modèles hydrologiques à base physique. Les modèles considérés représentent les processus physiques et les caractéristiques de terrain d'une façon différente et ceci mène aux résultats différents, particulièrement pendant la période de validation, caractérisée par beaucoup de temps de sécheuse comparé avec la période de calibrage.

Les résultats de cinq différents modèles hydrologiques forcés avec quatre modèles climatiques du projet ENSEMBLE sont comparé sur le bassin Rio Mannu. Les modèles examinés – CATHY, Soil and Water Assessment Tool (SWAT), TOPKAPI-X, tRIBS, and Water Flow and Balance Simulation (WASIM) – diffèrent grandement dans leur représentation des caractéristiques du terrain, des processus physiques et de la complexité numérique, mais tous les modèles considérés peuvent représenter de façon distribuée l'apport météorologique, les

variables hydrologiques et les propriétés du bassin. Les modèles ont été indépendamment calibrés et validés pour le bassin Rio Mannu et ensuite appliqués en cascade avec les modèles climatiques pour évaluer les effets du changement climatique pour une période de référence (1971-2000) et une future (2041-2070).

Finalement le modèle TOPKAPI-X est mis en œuvre sur un système complexe, le bassin Flumendosa, pour évaluer les impacts du changement climatique à une échelle beaucoup plus grande. Le modèle hydrologique a été calibré et validé et appliqué ensuite en cascade avec des modèles climatiques pour évaluer les effets du changement climatique pendant cinq périodes de 30 ans (1951-1980, 1981-2010, 2011-2040, 2041-2070, 2071-2100).

Chaque modèle hydrologique utilisé dans cette étude est décrit dans la section 3.1 et la Table 1 présente les caractéristiques de chaque modèle en montrant leurs différences principales, tandis que la sélection des modèles climatiques est rappelée dans la section 3.2.

S.3.1 Modèles hydrologiques

CATHY est un modèle distribué à base physique qui permet la description détaillée des écoulements souterrains et de surface et leur interaction [*Camporese et al.,* 2010]. CATHY est composé de deux modules principaux qui représentent la surface et les processus souterrains. Le module superficiel est basé sur la résolution, utilisant la méthode de différence finie, d'une approximation diffusive unidimensionnelle de l'équation de Saint Venant [*Orlandini and Rosso*, 1996, 1998]. Le module souterrain résout, utilisant la méthode d'élément finie, l'équation de Richards qui décrit le flux dans les médias poreux variablement saturés [*Paniconi and Wood*, 1993; *Paniconi and Putti*, 1994]. L'équation 3D de Richards est discrétisée par un schéma d'élément fini Galerkin dans l'espace utilisant des éléments tétraédriques et selon un schéma

d'Euler amont dans le temps avec le pas de temps adaptatif [*Scudeler et al*., 2017]. Le module souterrain traite la contrainte atmosphérique en mettant en œuvre un cas spécial de condition de à la limite, pour diviser les flux (atmosphériques) potentiels en flux réels à travers la surface du terrain (l'infiltration, l'exfiltration comme évaporation et l'exfiltration comme flux de retour) et en changements du stockage superficiel (ponding heads). De cette manière, le module souterrain contrôle les échanges avec le module superficiel. Les deux modules utilisent un réseau régulier pour la représentation topographique. CATHY est appliqué principalement dans des objectifs de recherche tant en sites de référence que dans des bassins [*Camporese et al*., 2010; *Gauthier et al*., 2009] pour illustrer la capacité du modèle de reproduire une variété de processus hydrologiques et évaluer l'impact du changement climatique [*Sulis et al*., 2011].

SWAT est un modèle conceptuel, semi-distribué, continu dans le temps, capable de simuler des longues périodes pour calculer les effets des changements de gestion [*Arnold et al., 1998*]. Il permet l'évaluation du climat et des impacts d'utilisation du terrain sur les ressources hydrique, des sédiments et des produits chimiques agricoles à travers une représentation physique des processus hydrologiques, da température du sol, de la croissance des plantes, des substances nutritives, des pesticides et de l'utilisation du terrain. Dans SWAT, un bassin est divisé dans multiples sous bassins, qui sont encore subdivisés dans des unités de réponse hydrologiques (HRUs) qui consistent des unités homogènes d'utilisation du terrain, de gestion, et de caractéristiques topographique et du sol. Les HRUs sont représentés comme un pourcentage de sous bassin et ils peuvent être non contigus ou identifié dans l'espace. Le pas de temps journalier est adopté dans la simulation des processus hydrologiques. L'écoulement superficiel est évalué en utilisant la procédure du Curve Number Soil Conservation Service (SCS) et le mouvement d'humidité du sol verticalement dans le profil du terrain est simulé en utilisant une

approche 1D "tipping bucket" approche, où la précipitation effective remplit la couche du sol jusqu'à la capacité du terrain en commençant avec la couche supérieure. Ses applications s'étendent de buts d'ingénierie/pratiques aux études de recherche [*Arnold et al*., 1999a; *Mausbach and Dedrick*, 2004; *Volk et al*., 2007].

TOPKAPI-X est un modèle distribué à base physique qui combine la topographie du bassin avec l'approche cinématique [*Todini and Ciarapica*, 2001; *Liu and Todini*, 2002]. Le modèle consiste en cinq modules principaux qui simulent les processus hydrologiques principaux incluant le flux souterrain, le ruissellement, le flux dans les canaux, l'évapotranspiration et la neige, en utilisant des pas de temps définissables (de peu de minutes aux pas de temps horaires ou journalières). Quatre équations non-linéaires différentielles de réservoir, obtenues en combinant les équations de conservation de masse et de l'impulsion et résolues avec la méthode de différence finie 2D, sont utilisées pour décrire le flux souterrain dans la première et deuxième couche, le ruissellement et le flux du canal. TOPKAPI-X utilise un réseau régulier pour la représentation topographique et exige de bas temps informatiques, compatibles avec les temps nécessaires pour que l'événement d'inondation prédise en temps réel. Il peut être couplé avec des modèles hydrauliques et météorologiques. TOPKAPI-X a déjà été mis en œuvre avec succès comme modèle hydrologique opérationnel et de recherche dans plusieurs bassins dans le monde [*Liu and Todini*, 2002; *Bartholomes and Todini*, 2005; *Liu et al.*, 2005; *Martina et al*., 2006].

TRIBS est un modèle à base physique entièrement distribué qui reproduit plusieurs processus hydrologiques [*Ivanov et al*., 2004a, 2004b]: l'interception de la canopée et la transpiration, l'évaporation des sols nus et végétés, l'infiltration et la redistribution d'humidité du sol, le transport souterrain, l'écoulement dans les canaux et le ruissellement. Le schéma d'infiltration est basé sur la résolution du modèle bidimensionnel modifié de Green-Ampt dans

des sols hétérogènes et anisotropes [*Cabral et al*., 1992]. Une onde cinématique est utilisée pour simuler le transport d'eau dans le réseau du canal. Les flux latéraux dans la zone non saturée et l'eau souterraine sont déterminés par la topographie et permettent quatre mécanismes de génération de débit. Un pas de temps fixe de 3.75 minutes est adopté pour la simulation des processus hydrologiques. Les caractéristiques du terrain sont représentées via Triangulated Irregular Networks (TINs) qui réduisent le nombre de nœuds informatiques en ce qui concerne les modèles avec la grille [*Vivoni et al*., 2004, 2005]. Les polygones Voronoi dérivés par TINs sont les éléments de base pour le calcul de l'énergie et d'équilibre d'eau à travers l'approche de volume de contrôle différence finie. Les applications de tRIBS concernent de projets d'inter-comparaison [*Fatichi et al*., 2016; *Reed et al*., 2004; *Vivoni et al*., 2007], l'hydrométéorologie [*Mascaro et al*., 2010; *Moreno et al*., 2014], l'évaluation de l'impact du changement climatique [*Liuzzo et al*., 2010], l'éco-hydrologie [*Mahmood and Vivoni*, 2014; *Vivoni et al*., 2014].

WASIM est un modèle hydrologique distribué à base physique [*Schulla*, 2015], à l'origine développé pour évaluer l'influence du changement climatique sur l'équilibre d'eau et le régime de débit dans des bassins pré alpins et alpins [*Schulla*, 1997]. Le temps de discrétisation peut être choisi variablement, de quelques minutes jusqu'à un jour. WASIM est caractérisé par une structure basée sur une grille et représente les flux verticaux dans la zone non saturée en utilisant l'équation 1D de Richards, qui est résolue numériquement avec le schéma de différence fini. Le cheminement de la décharge est exécuté par une approche cinématique en utilisant des vitesses de flux différentes pour des niveaux différents d'eau dans le canal. WASIM est composé en sous-modules, qui sont traités pour chaque pas de temps et pour la grille du bassin entière. La complexité des sous-modules utilisés peut être ajustée selon les caractéristiques des bassins et la disponibilité de données. Les différents modules calculent des variables hydrologiques diverses

comme l'interception, la décharge, la fusion de la neige, l'évapotranspiration etc. WASIM est adopté pour le but de recherche [*Cornelissen et al*., 2013; *Jasper et al*., 2002; *Meyer et al*., 2016].

La Table 1 récapitule les caractéristiques de chaque modèle hydrologique montrant leurs différences principales. Pour plus de détails le lecteur est renvoyé aux références fournies ci-dessus pour chaque modèle.

Model	Discretization scheme	Infiltration/Subsurface flow	Surface flow	Topographic representation
CATHY	Finite element	Richards' equation	Diffusive wave	Regular grid
SWAT	Subwatershed	Tipping bucket	Soil Conservation Service (SCS)	Homogeneous hydrologic units
TOPKAPI-X	Finite difference	Kinematic wave	Kinematic wave	Regular grid
tRIBS	Finite difference control volume	Modified Green-Ampt	Kinematic wave	Triangulated irregular network
WASIM	Finite difference	Richards' equation	Kinematic wave	Regular grid

Table 1. Comparaison de la structure et des caractéristiques des cinq modèles hydrologiques.

S.3.2 Modèles climatiques

Deidda et al. [2013] ont analysés les productions de quatorze combinaisons GCM-RCM du projet ENSEMBLES dans les sept régions d'étude du projet CLIMB pour identifier ceux exposant la meilleure prestation en termes de représentation de la variabilité intra-annuelle de la précipitation et température dans le climat présent. Les modèles choisis pour le bassin Rio Mannu sont inscrits dans la Table 2, y compris les acronymes utilisés dans ce travail (ECH-RCA, ECH-REM, ECH-RMO et HCH-RCA). Le choix a été contraint par la condition de garder au moins un RCM forcé par deux GCM (ECH-RCA et HCH-RCA) et plus RCMS emboîtés dans le

même GCM (ECH-RCA, ECH-REM, ECH-RMO), pour explorer un degré minimal d'incertitude climatique tant dans les représentations de GCM que RCM. Pour ces modèles, les productions ont été extraites sur le bassin Rio Mannu pour une période de référence (1971-2000) et future (2041-2070) sous le scénario d'émission A1B [*Nakićeović et al*., 2000], qui a été considéré comme un de plus raisonnable et a fourni l'ensemble de données le plus complet dans les modèles ENSEMBLES. Pour limiter les différences principales (particulièrement dans de petits bassins) dans la reproduction de caractéristiques climatologiques et la saisonnalité observée [*Lucarini et al*., 2007; 2008; *Hasson et al*., 2013; 2014], une correction de biais à grande échelle a été appliqué à la précipitation et aux champs de température utilisant la méthode de la translation journalier [*Wood et al*., 2004; *Maurer and Hildago*, 2008; *Sulis et al*., 2012] en utilisant l'ensemble de données E-OBS [*Haylock et al*., 2008] comme référence. En plus, des techniques de réduction d'échelle ont été appliqué pour désagréger la précipitation et les grilles de température de la résolution grossière des modèles climatiques (25 km, 24 h) aux résolutions raffiné (5 km, 1 heure) approprié pour la modélisation hydrologique. Pour la précipitation, le modèle multifractale de Deidda et al. [1999] et Deidda [2000] a été utilisé, tandis que la température a été interpolée dans l'espace en tenant compte des corrections lapse rate comme dans Liston and Elder [2006]. Enfin, les biais résiduels dans la précipitation, principalement en raison du grossièreté de réseau de pluie des données E-OBS, ont été corrigés selon une procédure de correction de biais d'échelle locale. Plus de détails sur la correction de biais et les techniques de réduction d'échelle sont fournit dans Piras et al. [2014].

	Climatological center and model	Acronym
Global Climate Models, GCMs	Hadley Centre for Climate Prediction, Met Office, UK HadCM3 Model	HCH
	Max Planck Institute for Meteorology, Germany ECHAM5 / MPI Model	ECH
Regional Climate Models, RCMs	Swedish Meteorological and Hydrological Institute (SMHI), Sweden RCA Model	RCA
	Max Planck Institute for Meteorology, Hamburg, Germany REMO Model	REM
	Koninklijk Nederlands Meteorologisch Instituut (KNMI), Netherlands RACMO2 Model	RMO

Table 2. Liste des Modèles Climatiques Globale (GCM) et Modèles Climatiques Régionaux (RCM) du project CLIMB avec la correspondance du centre climatologique et modèle et acronymes adoptés dans ce travail. Les quatre combinaisons GCM-RCM utilisées sont ECH-RCA, ECH-REM, ECH-RMO et HCH-RCA.

Puisque les projections climatiques du projet CLIMB ne couvrent pas le bassin Flumendosa, pour le dernier et les mêmes modèles climatiques inscrits dans la Table 2 une approche paramétrique pour la correction simultanée de biais et réduction d'échelle statistique a été appliqué aux champs de précipitation [*Mamalakis et al*., 2017]. Pour les données de température au lieu de cela, les grilles horaires de température obtenues pour le bassin Rio Mannu ont été utilisées pour dériver les valeurs de grille horaires de température sur le bassin Flumendosa adoptant la même méthode décrite dans Caracciolo et al. [2017].

S.4 Résultats

S.4.1 Une application de transférabilité de paramètre entre trois modèles hydrologiques distribués physiquement basés

Dans ce paragraphe est montré une comparaison détaillée des réponses obtenues avec les trois modèles hydrologiques à base physique, CATHY, tRIBS, TOPKAPI-X, mis en œuvre sur un bassin méditerranéen caractérisé par un climat semi-aride, le Rio Mannu. Puisque le modèle tRIBS a été précédemment mis en œuvre sur le bassin Rio Mannu pendant le projet CLIMB, pour les deux autres modèles les mêmes ensembles de données ont été adoptés, y compris les données géospatiales de propriétés de surface de terrain et la contrainte hydrométéorologique, pour tester la transférabilité de paramètres entre les trois modèles hydrologiques à base physique. Les paramètres du sol et de couverture de terrain calibrés pour l'application du modèle tRIBS ont été utilisés pour guider le calibrage des deux autres modèles hydrologiques. L'hypothèse de transférabilité des valeurs de paramètres a été explorée. Tandis que ceci a mené aux performances satisfaisantes pour TOPKAPI-X et CATHY pendant la période de calibrage, CATHY a produit une très basse décharge dans la période de validation beaucoup plus sèche. Pour contourner ceci, pour le modèle CATHY, une hypothèse de croûtage de sol a été assumée et la première couche de sol a été modelée avec une conductivité hydraulique saturée plus bas.

Dans un bassin avec un climat semi-aride, les contrastes de conditions climatiques entre les années pourraient être importants. Plusieurs auteurs ont proposé, adapté, ou ont appliqué des tests pour évaluer la capacité des modèles d'avoir de bons résultats dans des conditions climatiques contrastées [*Refsgaard and Knudsen*, 1996; *Xu*, 1999; *Donnelly-Makowecki and Moore*, 1999; *Seibert*, 2003*; Xu et al*., 2005; *Refsgaard et al., 2006*; *Gorgen et al*., 2010; *Vaze et*

al., 2010; *Merz et al*., 2011]. Tous se sont inspirés du principe "Differential Split-Sample Test" (DSST), formulé par Klemes [1986], qui recommande de calibrer le modèle sur des données pré-changement et le valider sur des données post-changement, donc des observations existant avec des caractéristiques climatiques dissemblables peuvent être utilisées pour calibrer et valider les modèles [*Seiller et al*., 2012]. Particulièrement Klemes suggère d'utiliser une période humide pour le calibrage et une période de séche pour la validation, particulièrement quand le modèle hydrologique est utilisé pour évaluer les effets du changement climatique. Pour calibrer et valider les modèles tRIBS, trois ans consécutifs ont été choisis (1930-1932) où la courbe de tarage ne présente pas de variations significatives. Parmi ces trois ans, l'année 1930 a présenté le nombre majeur d'événements d'inondation et a été alors choisie pour le calibrage, tandis que 1931 et 1932 ont été utilisés pour valider la performance du modèle.

Différents séries de simulations utilisant comme apport atmosphérique un ensemble de 50 série de précipitation à échelle réduite qui ont été assumé comme forçant pour le modèle tRIBS, chacun représente un scénario statistiquement possible, ont été effectués avec les trois modèles hydrologiques pendant la période de calibrage (année 1930) et validation (années 1931 et 1932).

La Figure 5 montre la comparaison de décharge simulée et observée pendant l'année 1930 de calibrage avec les trois modèles tRIBS, TOPKAPI-X et CATHY, utilisant l'ensemble de 50 séries de précipitation à échelle réduite. Dans les deux encarts il est possible de mieux visualiser la comparaison de deux périodes avec des événements d'inondation significatifs. Pour chaque encart, est tracée aussi la différence entre la précipitation à échelle réduite et journalière moyenne d'ensemble (MAP_D) et observée (MAP_O). Malgré l'incertitude dans les apports hydrométéorologiques, les modèles ont reproduits, avec une raisonnable exactitude, la forme et le moment des événements d'inondation majeurs, avec quelques différences. En particulier les

trois modèles ne peuvent pas reproduire les sommets étiquetés comme M (manqué), en raison d'une période précédente de précipitation sous-estimée (négatif MAP_D- MAP_O), mais avec degrés différents de sous-estimation. En fait CATHY et TOKPAPI-X simulent assez bien les courbes de récession, tandis que tRIBS montre une tendance à les simuler plus raides. De même, le moment des sommets d'inondation peut être aussi affecté par les différences de MAP observée et simulée, comme illustré par l'étiquette D (retardé). Nous pouvons aussi noter que le modèle CATHY ne peut pas reproduire le pic finale de décharge pendant 1930: en fait, puisque le sol se dessèche après les mois chauds, le modèle permet à l'eau de s'infiltrer dans le sol, donc il peut ne pas reproduire l'écoulement d'Horton observé.

Table 3 rapporte l'index de Nash-Sutcliffe (NS) [*Nash and Sutcliffe*, 1970] pendant l'année de calibrage évaluée utilisant le volume observé et simulé d'eau pour les trois modèles hydrologiques. Ce paramètre peut varier de -∞ à 1, avec la meilleure prestation près de 1. Spécifiquement, les valeurs minimum, moyennes et maximales des 50 ensembles sont rapportées pour des temps d'accumulation différents (journalier, hebdomadaire et mensuellement). Clairement, les valeurs les plus basses de NS ont été obtenues à la résolution quotidienne, car à cette échelle la correspondance directe entre l'observation et les simulations est plus affectée par le pas de temps différent d'échantillonnage et les différences dans la contrainte désagrégée [*Piras*, 2014]. Quand de plus grandes durées sont considérées, NS augmente et arrive à une valeur moyenne de 0.55 à la résolution mensuelle pour le modèle tRIBS, 0.61 pour TOPKAPI-X et 0.62 pour CATHY.

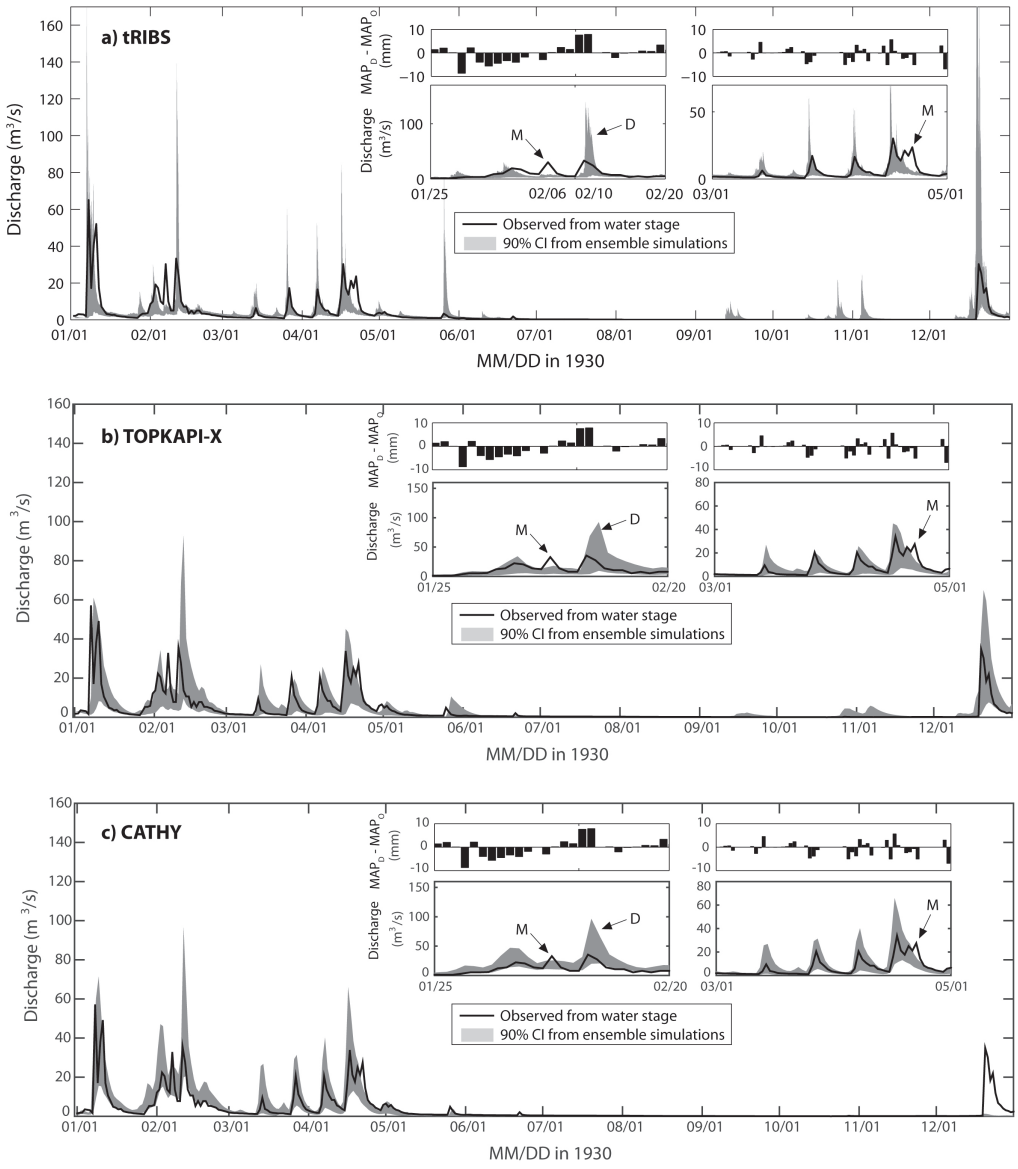

Figure 5. Résultats pendant l'année 1930 de calibrage pour les modèles tRIBS (a), TOPKAPI-X (b), et CATHY (c) en comparant la décharge observée contre les intervalles de confiance de 90 % (CI) obtenu des 50 simulations d'ensemble des modèles tRIBS, TOPKAPI-X et CATHY. Dans les encarts est montré un agrandissement sur deux périodes avec des événements d'inondation significatifs pour mieux visualiser la comparaison et la différence entre MAP_D journalier et MAP_O (voir le texte pour la définition).

	tRIBS	TOPKAPI-X	CATHY
Time scale	**Calibration NS Min, Mean, Max**	**Calibration NS Min, Mean, Max**	**Calibration NS Min, Mean, Max**
Daily	-3.53, 0.07, 0.61	-2.77, 0.27, 0.63	-0.20, 0.40, 0.66
Weekly	-5.50, 0.46, 0.83	-1.85, 0.48, 0.81	-0.07, 0.56, 0.80
Monthly	-0.06, 0.55, 0.89	-1.59, 0.61, 0.95	0.08, 0.62, 0.85

Table 3. Index de Nash-Sutcliffe (NS) pendant l'année de calibrage 1930, évalué en utilisant le volume observé et simulé d'eau à l'échelle journalier, hebdomadaire et mensuelle, pour les trois modèles hydrologiques.

Les résultats pendant la période de validation, caractérisée par un climat très sec (années 1931 et 1932), sont montrés dans la Figure 6. On peut noter des bonnes prestations dans la reproduction de la série de décharge au cours de l'année 1931 et la plupart de 1932 pour tRIBS et TOPKAPI-X. Dans la période depuis Octobre jusqu'à Décembre 1932, les deux modèles simulent un certain nombre de sommets qui n'ont pas été observés, tandis que sous-estime parfois la décharge, à cause des mêmes raisons discutées pendant la période de calibrage. CATHY n'est pas capable de produire n'importe quelle décharge, seulement un peu au début de 1931. Ceci est dû à la même raison discutée pour le pic finale manqué à la fin de 1930. Pour cette raison pour le modèle CATHY une hypothèse de croûtage de sol a été assumée pendant la période de validation, sur la base de laquelle la première couche mince est modelisée avec une conductivité hydraulique à saturation plus basse. Assouline [2013] a fourni une revue des approches proposées pour modeler l'infiltration dans des sols croûtés. Hillel et Gardner [1969, 1970] était le premier à formuler l'hypothèse qu'un sol croûté pourrait être modelisé comme un profil de sol uniforme étonné avec une couche mince saturée de perméabilité basse. Ceci a été appliqué dans des études différentes [*Ahuja*, 1974, 1983; *Moore*, 1981a; *Parlange et al*., 1984b].

Des variations et des extensions de cette approche de base ont inclus la simulation d'infiltration avec la croûte dépendant de temps [*Farrell and Larson*, 1972; *Whisler et al*., 1979; *Moore*, 1981b; *Ahuja*, 1983; *Brakensiek and Rawls*, 1983; *Chu et al*., 1986; *Vandervaere et al*., 1998]. Quand pendant l'été le sol est sec (à température élevée), l'eau est enlevé du sol et les particules sont laissées compacts les unes contre les autres. Où le sol est scellé (sol couvert d'une croûte) la pluie ne peut pas pénétrer et ruisselle, ainsi nous represéntons ce mécanisme en utilisant pour la première couche mince une conductivité hydraulique basse. En fait la période de validation est caractérisée par un climat très sec, mais il y a un écoulement observé de Horton, donc nous avons fait l'hypothèse qu'un mécanisme dépendant de temps de croûtage de sol a été développé. La Figure 7 montre la comparaison de décharge simulée et observée pendant la période de validation pour le modèle CATHY avec la supposition de croûtage de sol, tandis que la Table 4 rapports les indices de Nash-Sutcliffe (NS) pour les trois modèles hydrologiques. Avec cette supposition les indices de Nash-Sutcliffe (NS) obtenues avec le modèle CATHY sont comparable avec ceux des autres modèles: même s'il y a quelques différences, ils ont le même ordre de grandeur.

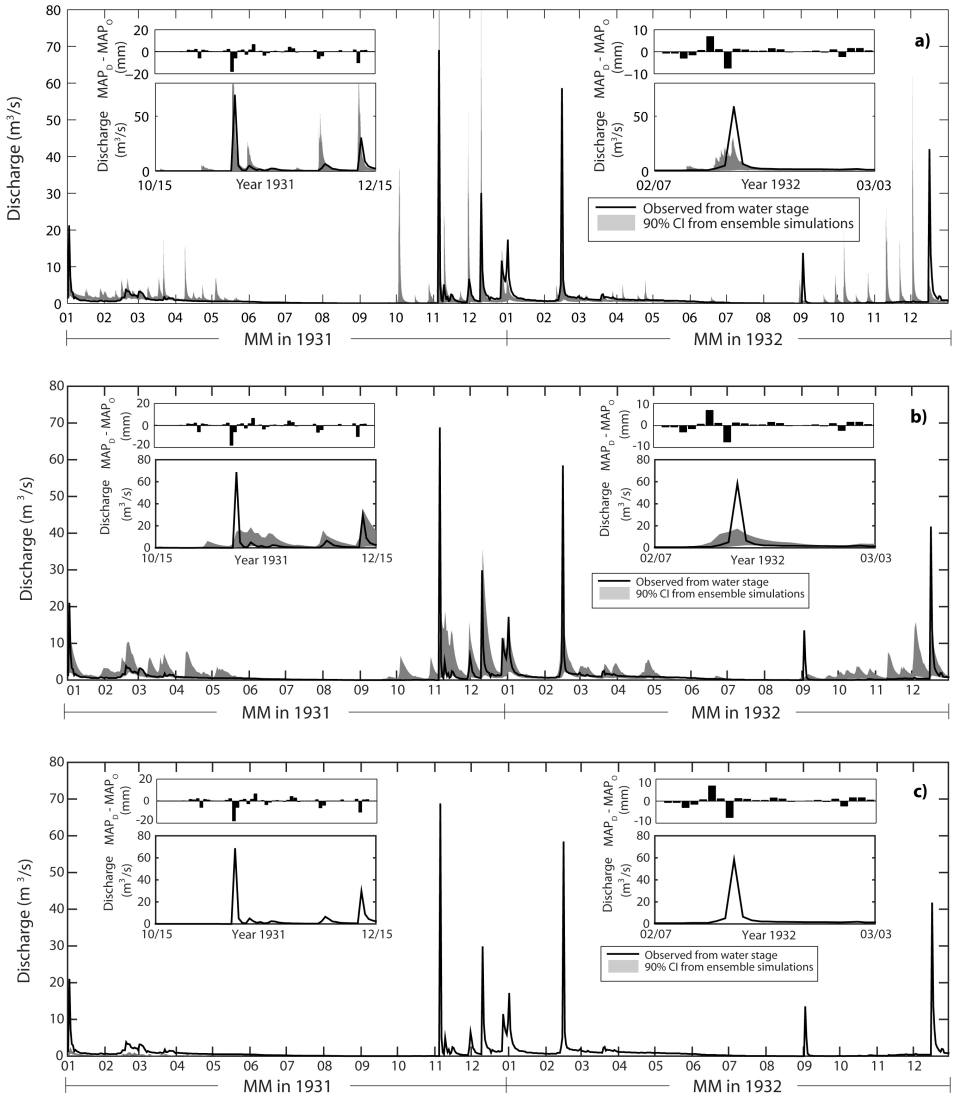

Figure 6. Résultats pendant les années de validation 1931-1932 pour les modèles tRIBS (a), TOPKAPI-X (b), et CATHY (c), comparant la décharge observée contre les intervalles de confiance de 90 % (CI) tiré des 50 simulations d'ensemble des modèles tRIBS, TOPKAPI-X et CATHY. Dans les encarts, on montre un agrandissement sur deux périodes avec des événements d'inondation significatifs pour mieux visualiser la comparaison et la différence entre MAP_D quotidien et MAP_O.

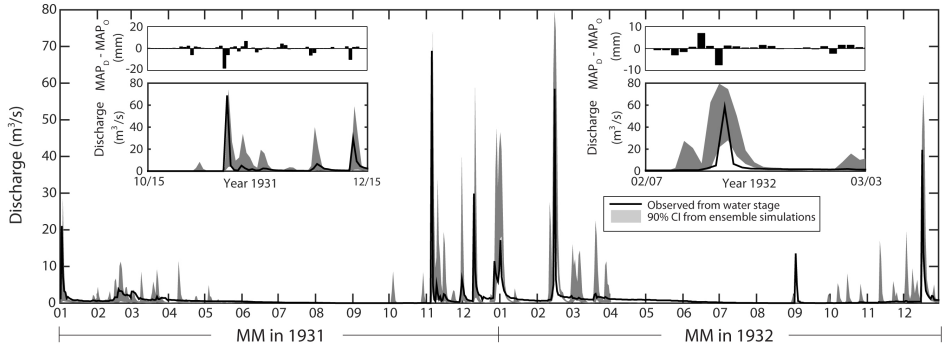

Figure 7. Résultat pour le modèle CATHY pendant les années de validation 1931-1932, avec l'hypothèse de sol couvert d'une croûte.

	tRIBS	**TOPKAPI-X**	**CATHY**
Time scale	**Calibration NS Min, Mean, Max**	**Calibration NS Min, Mean, Max**	**Calibration NS Min,Mean,Max**
Daily	-0.99, 0.02, 0.42	-1.92, -0.03, 0.23	-1.37, -0.37, -0.01
Weekly	-0.72, 0.13, 0.47	-1.89, 0.09, 0.56	-0.64, 0.06, 0.54
Monthly	0.03, 0.25, 0.74	-1.45, 0.40, 0.84	-0.38, 0.26, 0.62

Table 4. Index de Nash-Sutcliffe (NS) pendant les années de validation 1931-1932, évalué en utilisant le volume observé et simulé d'eau à l'échelle journalier, hebdomadaire et mensuelle, pour les trois modèles hydrologiques. Pour le modèle CATHY a été assumé l'hypothèse de croûtage de sol.

S.4.2 Évaluation multi-modèle des impacts hydrologiques induits par changement climatiques pour le bassin Rio Mannu

Pendant le projet CLIMB, une évaluation d'impact a été développé pendant laquelle les quatre combinaisons GCM-RCM plus performantes du projet ENSEMBLE [*van der Linden et al.*, 2009] ont été choisi pour chacun des sept sites d'étude. Les outputs journaliers des GCM-RCM à la résolution de 25 km pour une période de référence (1971-2000) et future (2041-2070) ont été corrigés sur les biais et statistiquement réduit d'échelle. Pour le bassin Rio Mannu, les données réduit d'échelle ont été alors utilisées pour forcer cinq modèles hydrologiques - CATHY, SWAT, TOPKAPI-X, tRIBS, WASIM - pour les périodes de référence et futures. Les modèles hydrologiques ont été indépendamment calibrés et validés contre des données observées: chaque groupe de modélisation a utilisé le type de données les plus appropriées pour son modèle, comme l'humidité de sol à l'échelle de terrain, l'évapotranspiration et la décharge [Cau et al., 2005; Mascaro et al., 2013b; Meyer et al., 2016; Perra et al., in preparation].

Pour comparer les outputs (i) des quatre modèles climatiques et (ii) des cinq modèles hydrologiques forcés par les quatre modèles climatiques pendant la période de référence et future, les moyens mensuels climatologiques ont été d'abord dérivés. Ensuite, la différence entre chaque paire des modèles hydrologiques ou climatiques est quantifiée en utilisant le coefficient de corrélation Pearson r et le coefficient de biais α, proposé par Duveiller et al. [2016], défini comme:

$$r = \frac{\sum_{i=1}^{n}(X_i - \bar{X})(Y_i - \bar{Y})}{n\sigma_X\sigma_Y} \quad (1)$$

$$\alpha = \begin{cases} \dfrac{2}{\frac{\sigma_X}{\sigma_Y} + \frac{\sigma_Y}{\sigma_X} + \frac{(\bar{X}-\bar{Y})^2}{\sigma_X\sigma_Y}} & , \ r > 0 \\ 0 & , \ r \leq 0 \end{cases} \quad (2)$$

où X_i, Y_i sont les valeurs mensuelles moyennes sur 30 ans d'une certain variable de réponse

simulée par une paire de modèles, $\bar{X}$ et $\bar{Y}$ leurs moyens, σ_X et $\sigma_Y$sont leurs écarts-types et n =12 est le nombre de mois par an.

Le coefficient de Pearson, qui peut s'étendre entre -1 et 1, est une mesure largement utilisée du degré de dépendance linéaire entre deux ensembles de données, mais il ne donne aucune indication en ce qui concerne l'accord en grandeur entre les données; le coefficient de biais, variant entre 0 (biais plein, aucun accord) et 1 (aucun biais, accord parfait), évalue possible additif ou multiplicatifs biais entre les outputs des modèles, seulement si le coefficient de Pearson est positif, donc on considère que données négativement corrélé n'ont aucun accord.

Ces deux indices ont été récemment utilisés dans une étude d'inter-comparaison de modèles hydrologiques [*Kollet et al*., 2017] pour évaluer l'accord entre sept modèles superficiels-souterrains pour une série de scénarios de test de référence. Dans cette étude les deux index *r* et α ont été calculés pour toutes les paires de variables représentatives climatiques et hydrologiques. Les résultats sont présentés dans des images matricielles où chaque élément représente la comparaison de paires de modèles, qui permette de comparer chaque combinaison avec tous les autres.

La contrainte météorologique principale, précipitation et température, projetée par les modèles climatiques est d'abord présentée et analysée en termes de variations entre la période future et de référence avec le but de prévoir le changement climatique dans le bassin Rio Mannu. La concordance de résultats des modèles climatiques est alors évalué en termes d'accord pendant la période future et de référence en utilisant les valeurs de corrélation de Pearson et le biais de Duveiller, comme dans Kollet et al. [2017]. Par la suite, l'impact du changement climatique projeté est examiné avec l'application de cinq modèles hydrologiques différents. La disponibilité

d'eau et des flux en termes de décharge, de contenu d'eau du sol et d'évapotranspiration réelle sont analysés en termes de tendances et de concordance inter-modèle.

Toutes les combinaisons GCM-RCM reconnaissent que dans la période future il y aura une diminution de la précipitation annuelle moyenne, en moyenne de 12%, tandis que à l'échelle mensuelle le signe de la variation dépend du mois et modèle (Figure 8a and 8c). La tendance de la température montre moins d'incertitude en ce qui concerne la précipitation (Figure 8b and 8d). Toutes les combinaisons GCM-RCM prévoient des valeurs moyennes croissantes qui varient de 11% (1.9°C) à 19% (3°C) selon le modèle. La comparaison mensuelle reproduit une tendance semblable pour les quatre combinaisons, avec des variations positives en chaque saison dans la période future, d'environ 7% (ECH-REM en juin) à 30% (HCH-RCA en mars). En analysant précipitation et température mensuelle moyenne dans la période de référence et future, nous pouvons observer que les valeurs du coefficient de corrélation de Pearson et le biais de Duveiller sont élevées, tous les deux sont près de 1 (Figure 9). Ainsi, l'incertitude en raison des modèles climatiques peut être considérée bas et due principalement à la contrainte GCM que exerce l'influence majeure sur le changement climatique projeté.

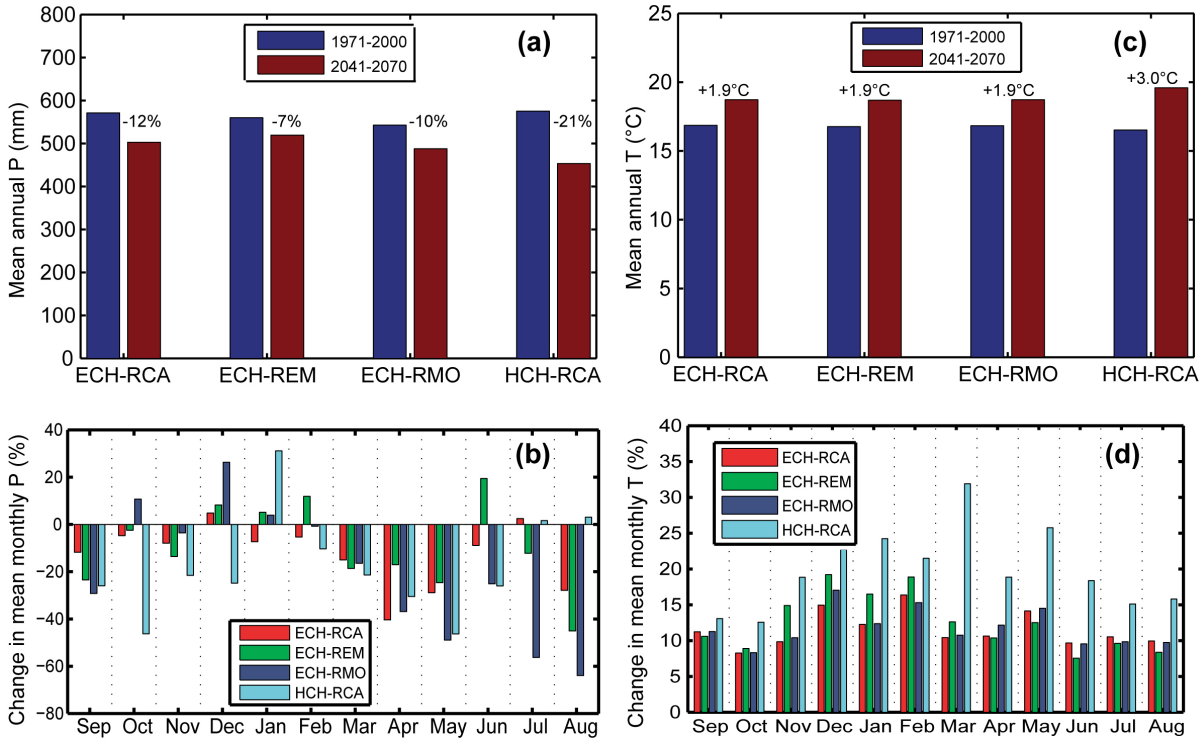

Figure 8. Précipitation P (a) et température T (c) annuelle moyenne prévu par les quatre modèles climatiques pendant les périodes de référence (1971-2000), barres bleues, et futur (2041-2070), barres rouges. Changement relatif de précipitation P (b) et température T (d) mensuelle moyenne entre les périodes de référence et future calculés avec les quatre modèles climatiques.

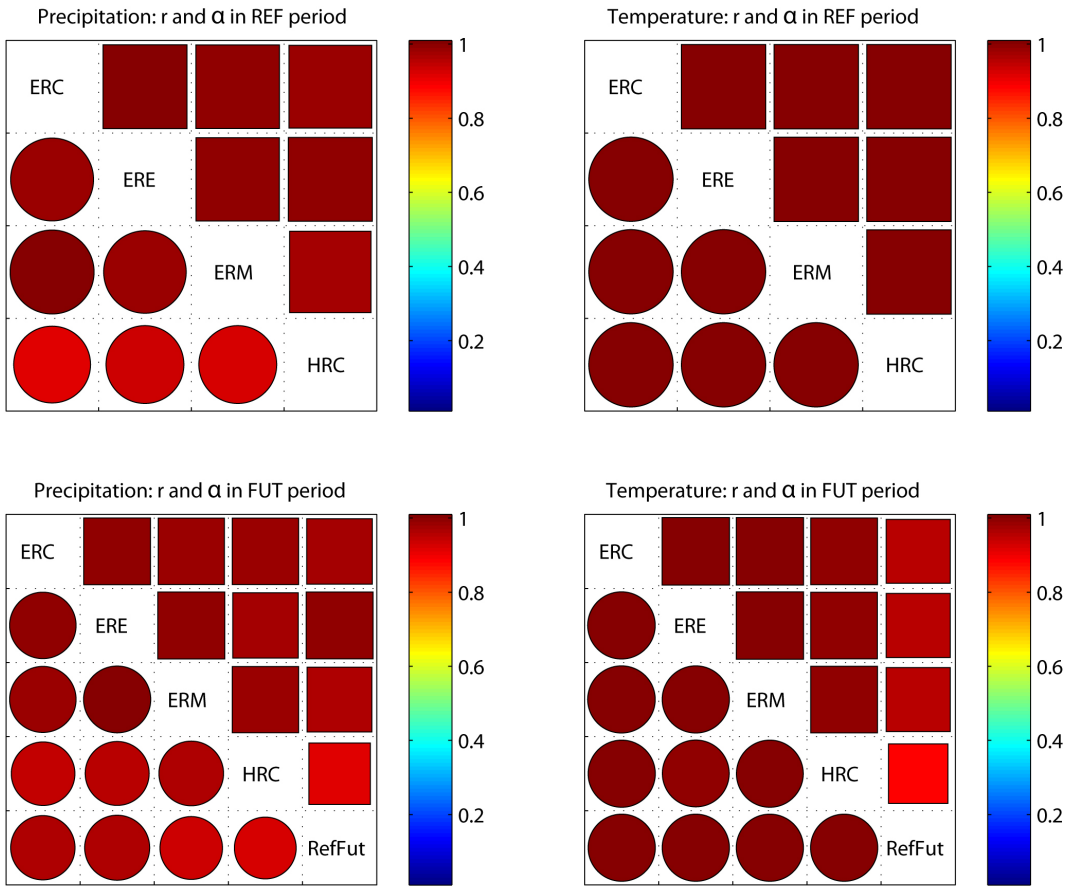

Figure 9. Résultats de l'analyse d'accord pour la précipitation et la température mensuelle moyenne parmi les quatre modèles climatiques (ERC = ECH-RCA, ERE = ECH-REM, ERM = ECH-RMO, HRC = HCH-RCA) dans la période de référence (REF, 1971-2000) et futur (FUT, 2041-2100). Les valeurs de corrélation ($-1 \le r \le 1$) sont représentées avec des cercles en-dessous de la diagonale, tandis que le biais ($0 \le \alpha \le 1$) est tracé comme des carrés au-dessus de la diagonale. La taille et la couleur de symboles sont proportionnelles aux valeurs des coefficients. Les entrées matricielles blanches correspondent à $r = 0$ ou $\alpha = 0$.

Les variations du forçage climatique influencent les différents composants de la réponse hydrologique du bassin. Les simulations avec les cinq modèles hydrologiques montrent pour la période future de valeurs décroissantes de débit annuel moyen (Figure 10a). Nous pouvons observer lors de l'analyse des données à l'échelle mensuelle de plus grandes variations non

perceptibles à l'échelle annuelle. Il est prévu une réduction de la décharge dans la période future dans tous les mois à part janvier et février (Figure 10d). En terme d'accord pendant la période de référence on peut observer une bonne concordance entre chaque paire de modèles hydrologiques (Figure 11), avec des différences majeures pour le futur: le modèle qui diffère considérablement des autres est CATHY, qui produit la décharge la plus basse dans le futur et ce résultat est reflété aussi dans les valeurs du paramètre de biais. Les simulations hydrologiques montrent aussi une réduction du contenu d'eau du sol à la profondeur de 1m (Figure 12a), confirmé à l'échelle mensuelle pendant l'année avec l'ampleur de variation qui dépend du modèle hydrologique considéré (Figure 12b). De nouveau le modèle CATHY présente la corrélation la plus basse avec les autres modèles (Figure 13), suivis par tRIBS: les deux modèles, en fait, montrent des variations limitées du contenu d'eau du sol pendant l'hiver et le printemps aux valeurs de mois d'été en ce qui concerne les autres, et ce fait est reflété aussi dans la valeur de biais. L'évapotranspiration réelle diminuera selon quatre modèles hydrologiques (Figure 14a), tandis qu'il montera dans la prédiction du modèle CATHY, qui simule le plus haut contenu d'eau dans le première mètre du sol, et aussi selon WASIM dans le mois de janvier et février qui prévoit plutôt les plus fortes réductions en été (Figure 14d), En ce qui concerne l'analyse d'accord de l'évapotranspiration réelle, les indices de Pearson et biais sont semblables pour CATHY, tRIBS et TOPKAPI-X (qui sont forcés avec les mêmes valeurs d'évapotranspiration potentielle) (Figure 15). De plus ces modèles atteignent les valeurs les plus hautes d'évapotranspiration réelle pendant les mois d'été. Dans la période futur cet accord est maintenu avec une corrélation forte entre tRIBS et TOPKAPI-X. Au sujet du SWAT-WASIM ils anticipent le sommet d'évapotranspiration réelle au printemps où des températures modérées coïncident avec l'activité

de végétation. On peut voir ceci dans la période de référence et moins dans le futur, quand le valeur du coefficient de biais est légèrement plus basse.

Pour conclure, malgré leurs différences, les cinq modèles hydrologiques ont répondu de la même façon à la précipitation réduite et températures augmentées prévues des modèles climatiques et prêtent fort support d'un scénario futur de manques accrus d'eau, avec des conséquences négatives particulièrement pour le secteur agricole.

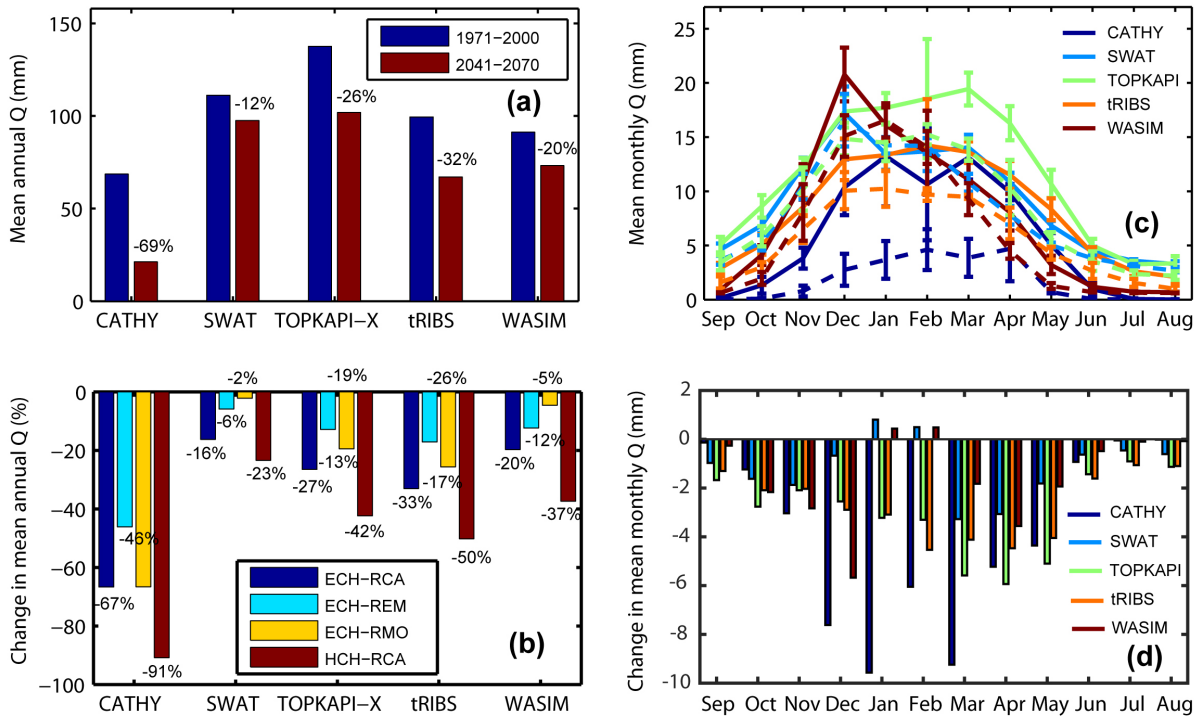

Figure 10. Décharge (Q) pour chaque modèle hydrologique forcé avec le quatre modèle climatique choisi, pendant la période de référence (REF, 1971-2000) et futur (FUT, 2041-2100). (a) Q annuel moyenne pendant les périodes REF et FUT, obtenues comme moyenne parmi les quatre modèles climatiques. (b) Changement relatif de Q annuel moyenne entre les périodes de REF et FUT forcé avec les quatre modèles climatiques. (c) Distribution saisonnière de Q mensuel moyen pendant les périodes REF (ligne continue) et FUT (lignes pointées) et écarts-types correspondant (barres verticales), obtenu comme moyenne parmi les quatre modèles climatiques. (d) Distribution

saisonnière de changement relatif de Q mensuel moyenne entre les périodes de REF et FUT, obtenu comme moyenne parmi les quatre modèles climatiques.

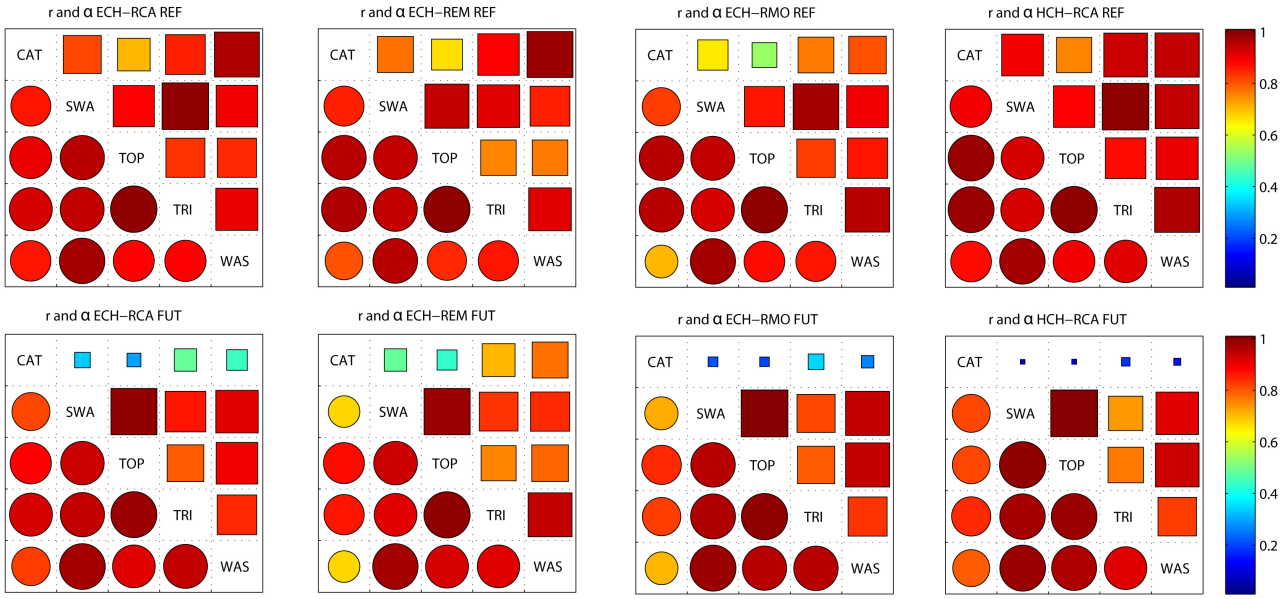

Figure 11. Comme la Figure 9, mais pour l'analyse des accords de la décharge mensuelle moyenne entre les cinq modèles hydrologiques (CAT = CATHY, SWA = SWAT, TOP = TOPKAPI-X, TRI = tRIBS, WAS = WASIM) pendant la période de référence (REF, sommet) et futur (FUT, en bas)).

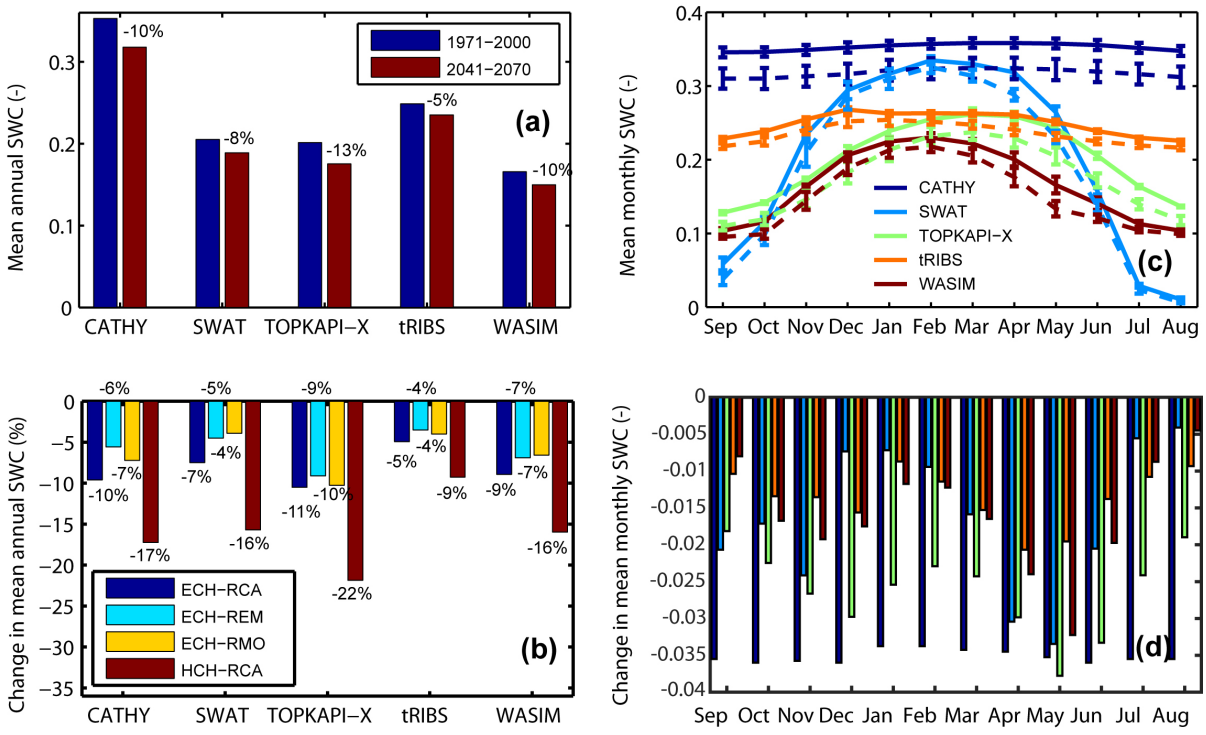

Figure 12. Comme la Figure 10, mais pour le contenu d'eau du sol (SWC) simulé par chaque modèle hydrologique forcé avec les quatre modèles climatique choisi, pendant la période de référence (REF, 1971-2000) et futur (FUT, 2041-2100).

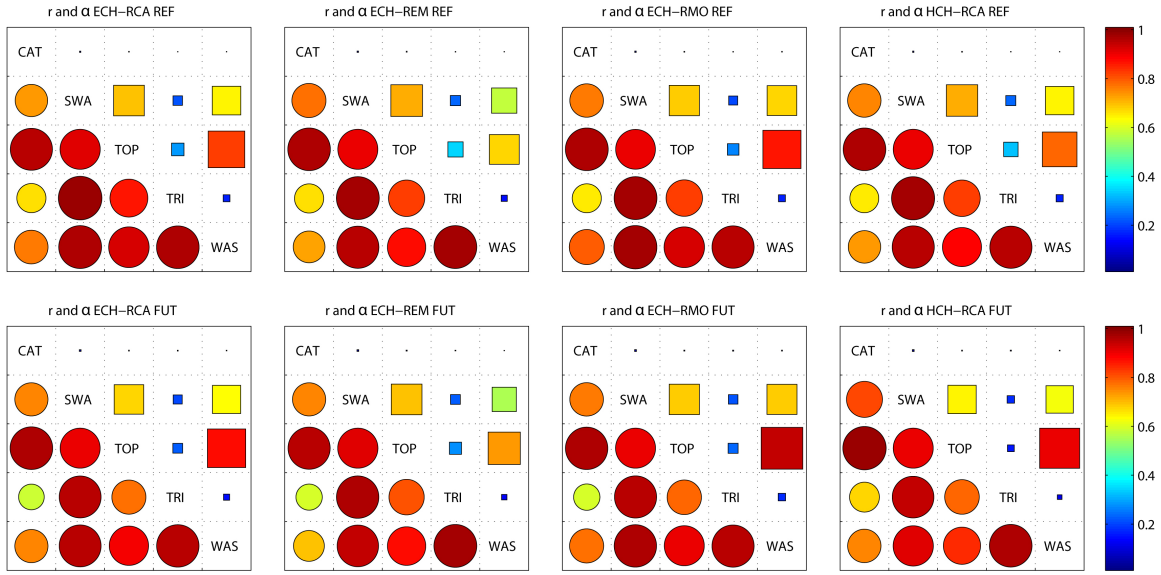

Figure 13. Comme la Figure 6, mais pour l'analyse des accords du contenu d'eau du sol mensuelle moyenne entre les cinq modèles hydrologiques (CAT = CATHY, SWA = SWAT, TOP = TOPKAPI-X, TRI = tRIBS, WAS = WASIM) pendant la période de référence (REF, sommet) et futur (FUT, en bas)).

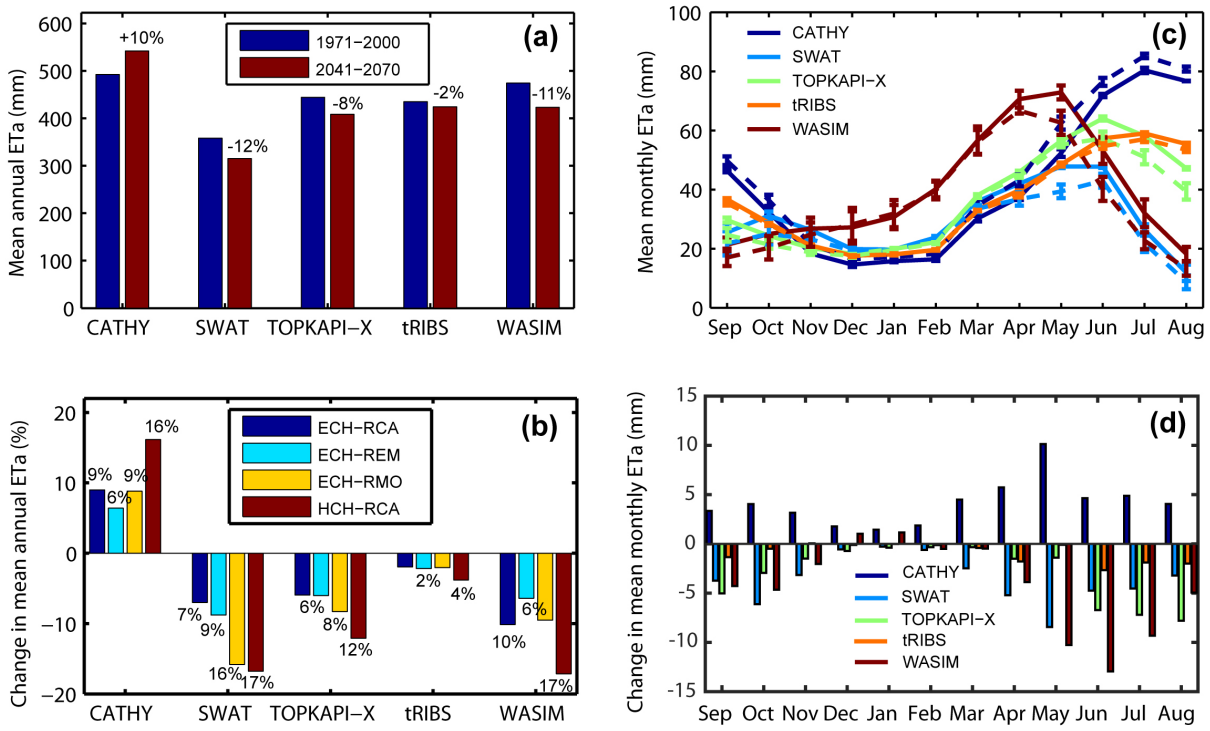

Figure 14. Comme la Figure 10, mais pour l'évapotranspiration réelle (ET_a) simulé par chaque modèle hydrologique forcé avec les quatre modèles climatique choisi, pendant la période de référence (REF, 1971-2000) et futur (FUT, 2041-2100).

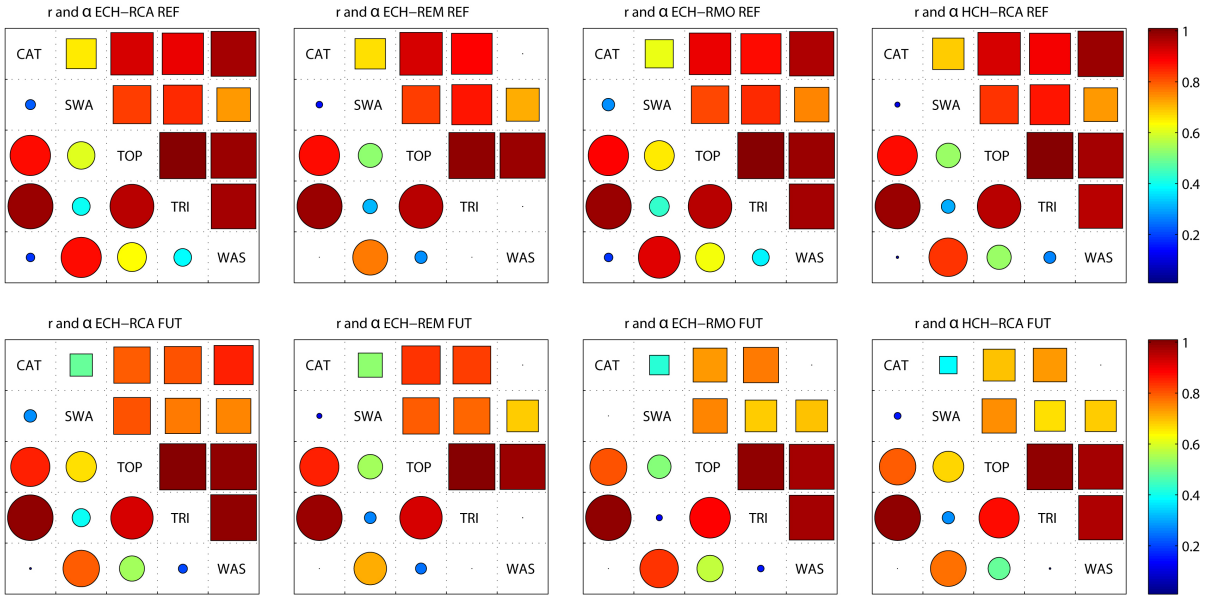

Figure 15. Comme la Figure 6, mais pour l'analyse des accords de l'évapotranspiration réelle mensuelle moyenne entre les cinq modèles hydrologiques (CAT = CATHY, SWA = SWAT, TOP = TOPKAPI-X, TRI = tRIBS, WAS = WASIM) pendant la période de référence ((REF, sommet) et futur (FUT, en bas)).

S.4.3 Évaluation d'impact du changement climatique préliminaire sur le bassin Flumendosa

Pour exécuter le modèle TOPKAPI-X sur le bassin Flumendosa nous nous concentrons sur la période avant la construction de réservoirs, depuis l'année 1926 jusqu'à 1936. Dans cette période la précipitation quotidienne de 14 indicateurs de pluie, la température minimale et maximale quotidienne de 5 stations thermométriques et des données de décharge quotidiennes d'une station hydrométrique ont été publiés dans les rapports techniques annuels de l'Enquête Hydrologique italienne (appelé "Annali idrologici). Puisque le modèle TOPKAPI-X fonctionne au pas de temps horaire, la précipitation quotidienne a été divisée également pendant les 24 heures, tandis que pour obtenir des données horaires de température la température minimale et maximale quotidienne a été linéairement interpolée. De plus, parce que le modèle a besoin du même nombre de stations météorologiques pour la précipitation et la température, nous avons appliqué une procédure semblable décrite ci-dessus dans la section 3.2 pour calculer les données de température pour les 14 stations d'indicateur de pluie, basées sur les données de température des 5 stations thermométriques, en suivant l'approche décrite dans Caracciolo et al. [2017]. Une résolution de 250 m a été choisie pour tracer le bassin Flumendosa, comme compromis entre le temps informatique et l'exactitude. Le calibrage du modèle a été exécuté en utilisant les données hydrométéorologiques décrites ci-dessus pendant les années 1927-1931, tandis que les données d'évapotranspiration potentielles sont estimées en TOPKAPI-X en utilisant la formule du Thornthwaite et Mather [*Thornthwaite and Mather*, 1955]. Une période de montée en régime de 1 année a été utilisée avant le début de la période de calibrage. Les données disponibles pendant la période 1932-1936 ont été utilisées pour valider la performance du modèle. Une conjecture initiale pour les paramètres du modèle a été dérivée de la carte de types de sol disponible (Figure

4b), en assumant des valeurs de paramètre prises de la littérature [*Rawls et al.*, 1982]. En suivant Ciarapica et al. [2002] et les résultats d'une analyse de sensibilité, les paramètres les plus influents se sont révélés être la conductivité hydraulique à saturation à la surface (K_S) et le coefficient de Manning (n). Les valeurs de K_S ont été modifiées dans les gammes typiques pour les classes de texture de sol correspondantes (Figure 4b). Pour le coefficient de Manning du réseau de drainage nous avons assumé des valeurs de littérature allant de 0.03 à 0.04 $m/s^{1/3}$ [*Chow*, 1959], tandis que pour d'autres paramètres nous avons adopté des valeurs de littérature pour des propriétés de sol semblables [Rawls et al., 1983]. Les valeurs rapportées dans la Table 5 ont été assumées pour les classes de texture de sol principales. Pour le modèle TOPKAPI-X seulement deux couches sont possibles pour représenter le sol, superficiel et profond: la première couche mince est assumée de 0.4 m de profondeur, le couche de sol profonde de 0.7 m de profondeur. Pour la couche profonde les valeurs de K_S ont été prises un ordre de grandeur plus bas.

La performance du modèle est quantifiée utilisant l'index de Nash-Sutcliffe, évalué sur la base du volume d'eau journalier observé et simulée. La Figure 16 montre la comparaison entre la décharge observée et simulée pendant les années de calibrage, produisant une mesure de performance de NS = 0.79. Malgré quelques désaccords dans les sommets probablement en raison de la désagrégation de précipitation journalier en parte égales pendant la journée, le modèle peut capturer tout à fait bien la dynamique du captage tant dans l'augmentation que dans les courbes de récession de l'hydrogramme. La Figure 17 montre les résultats pendant les années de validation, qui confirment une bonne performance du modèle avec NS = 0.75.

Soil Properties	Variable (unit)	Sandy loam – Clay loam	Sandy clay loam – Clay	Loamy sand – Sandy loam
Saturated hydraulic conductivity	K_s (m/s)	$1.86 \cdot 10^{-4}$	$3.79 \cdot 10^{-5}$	$9.53 \cdot 10^{-4}$
Saturated soil moisture	θ_s (-)	0.458	0.436	0.445
Residual soil moisture	θ_r (-)	0.058	0.079	0.038
Head suction	ψ_a (m)	0.159	0.267	0.087
Exponent of the horizontal flow	α	2.5	2.5	2.5

Table 5. Les valeurs de paramètres du modèle TOPKAPI-X pour les classes de sol majeures du bassin Flumendosa.

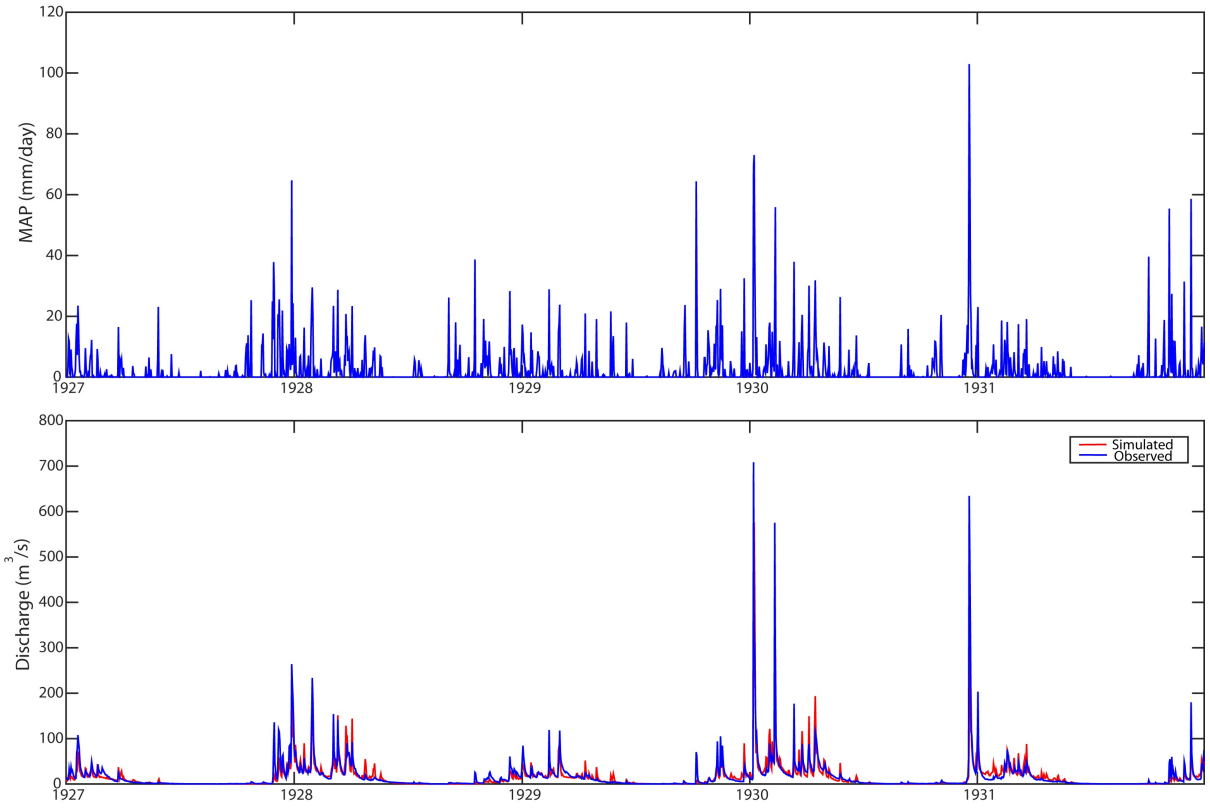

Figure 16. Simulation de calibrage pour le modèle hydrologique TOPKAPI-X appliqué au bassin Flumendosa. La décharge observée est comparée contre la simulé. Dans le panneau supérieur la série de précipitation régionale moyenne calculée avec les 14 indicateurs de pluie pendant la période 1927-1931 est rapportée.

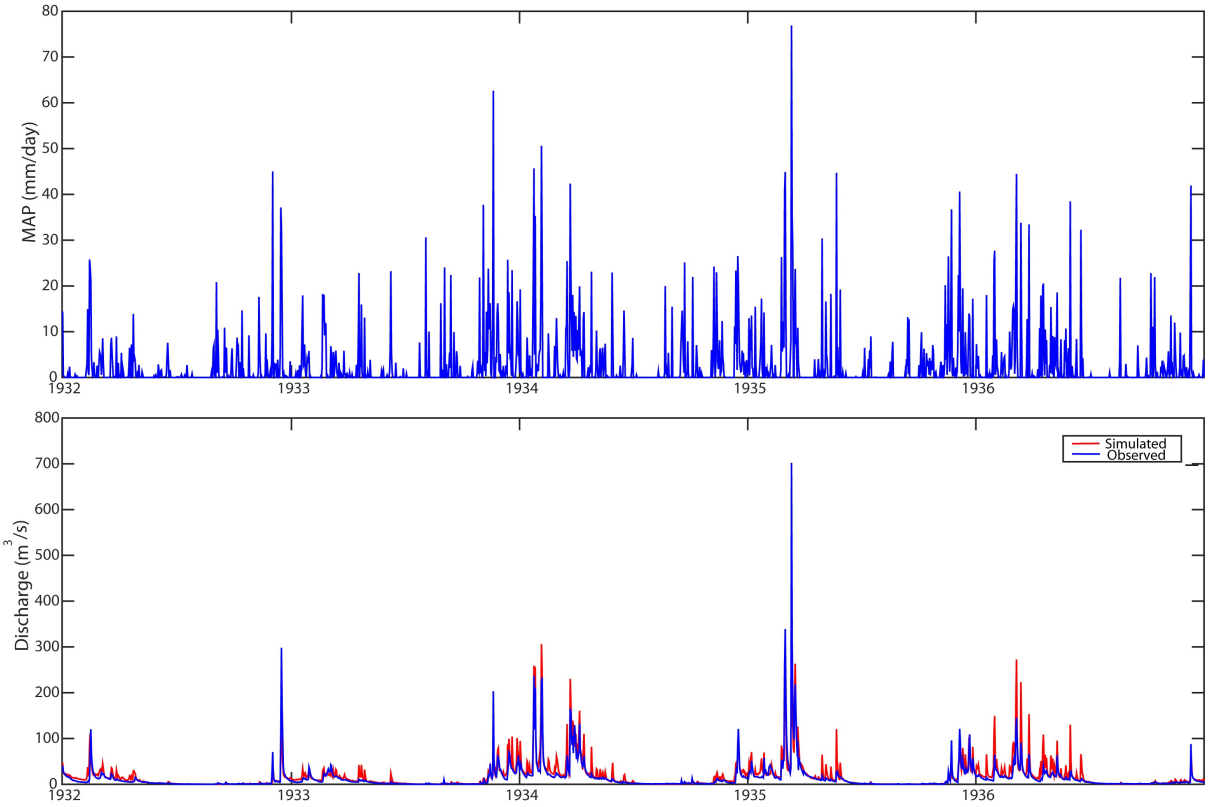

Figure 17. Simulation de validation pour le modèle hydrologique TOPKAPI-X appliqué au bassin Flumendosa. La décharge observée est comparée contre la simulé. Dans le panneau supérieur la série de précipitation régionale moyenne calculée avec les 14 indicateurs de pluie pendant la période 1932-1936 est rapportée.

Les moyens climatologiques de précipitation (P) et température (T) sur le bassin et parmi les quatre modèles climatiques ont été calculés aux échelles annuelles et mensuelles. La Figure 18 compare les résultats pendant les cinq périodes de 30 ans considérés (1951-1980, 1981-2010, 2011-2040, 2041-2070, 2071-2100). Les modèles prévoient une diminution de P annuel moyen depuis la période 2011-2040 jusqu'à la période 2071-2100, avec le changements pour cent d'environ 27% et une augmentation de 2% dans la deuxième période 1981-2010 (Figure 18a). En ce qui concerne la distribution saisonnière de la précipitation nous pouvons remarquer un sommet pendant Octobre (Figure 18b). Le modèle prévoit aussi une augmentation de T parmi toutes les cinq périodes d'environ 3.4 º C (Figure 18c) et pendant tous les mois (Figure 18d).

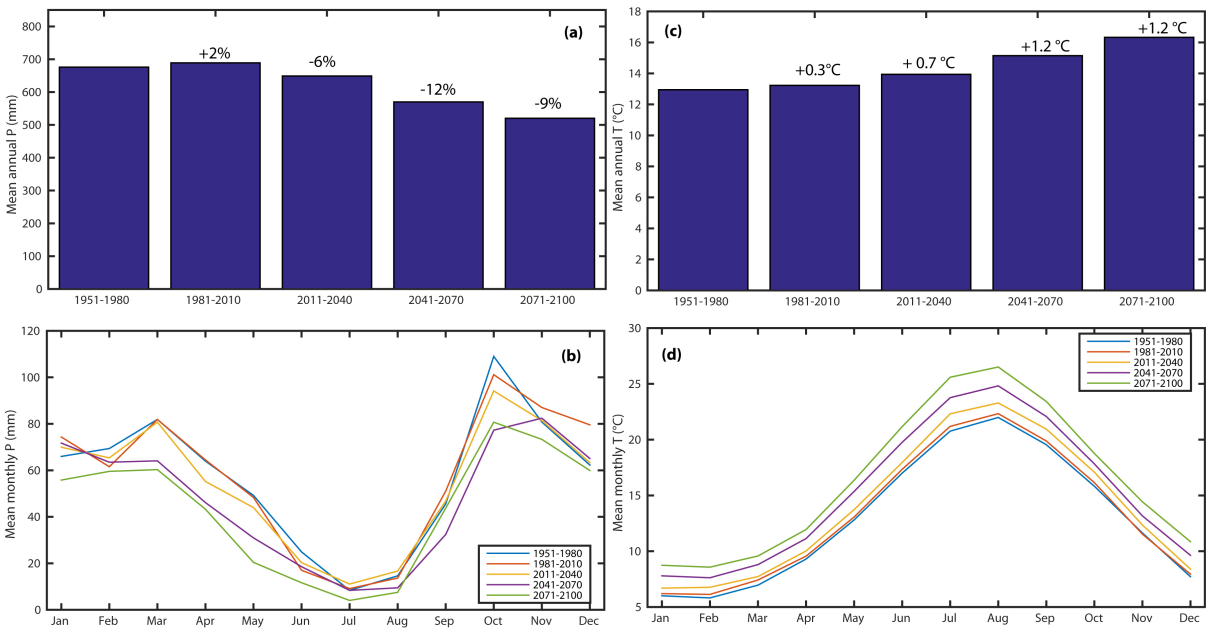

Figure 18. Précipitation P (a) et température T (c) annuelle moyenne obtenu comme moyenne parmi les quatre modèles climatiques pendant les cinq périodes de 30 ans (1951-1980, 1981-2010, 2011-2040, 2041-2070, 2071-2100). La distribution saisonnière de précipitation P (b) et température T (d) mensuelle moyenne pendant les cinq périodes de 30 ans considérées.

Un résumé des climatologies annuelles et mensuelles moyenne sur le bassin de l'évapotranspiration potentielle (ETP), décharge (Q), contenu d'eau de sol (SWC) et évapotranspiration réelle (ET_a) simulé par le modèle TOPKAPI-X, obtenu comme moyenne parmi les quatre modèles climatiques, est rapporté dans des Figures 19-22. Chaque Figure montre: la variable annuelle simulée dans chaque période, y compris le changement pour cent entre chaque (panneau a); la distribution saisonnière des valeurs mensuelles moyennes de chaque variable pendant les cinq périodes (panneau b).

L'ETP est calculé dans TOPKAPI-X en utilisant la formula de Thornthwaite et Mather, que produit un moyen annuel d'environ 650 mm pendant la période 1951-1980, qui est compatible avec des évaluations précédentes pour cette région [*Pulina et al.*, 1986]. Une augmentation de

ETP est prévu pendant toutes les périodes considérées à l'échelle annuelle (Figure 19a) et mensuelle (Figure 19b), surtout en raison de l'incrément projeté de T.

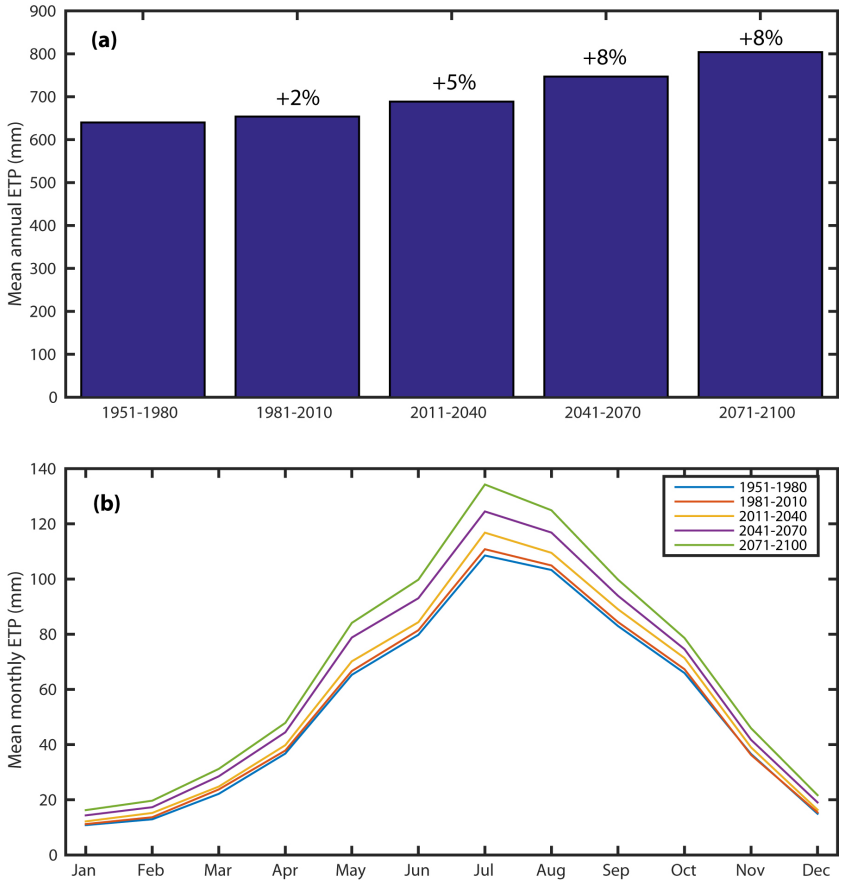

Figure 19. Évapotranspiration potentielle (ETP) pour le modèle TOPKAPI-X obtenu comme moyenne parmi le quatre modèles climatiques pendant les cinq périodes de 30 ans (1951-1980, 1981-2010, 2011-2040, 2041-2070, 2071-2100). (a) ETP annuelle moyenne pendant les cinq périodes de 30 ans. (b) Distribution saisonnière d'ETP mensuelle moyenne pendant les cinq périodes de 30 ans.

Les résultats en termes de Q sont analysés dans la Figure 20: est prévue une diminution de la décharge est prévue de la période 2011-2040 jusqu'à la période 2071-2100, avec de changements pour cent d'environ -60%, en suivant la tendance de la précipitation, et une augmentation de 3% dans la deuxième période 1981-2010 (Figure 20a). La Figure 20b se réfère à

la moyenne mensuelle Q, montrant la saisonnalité moyenne pendant les cinq périodes considérées.

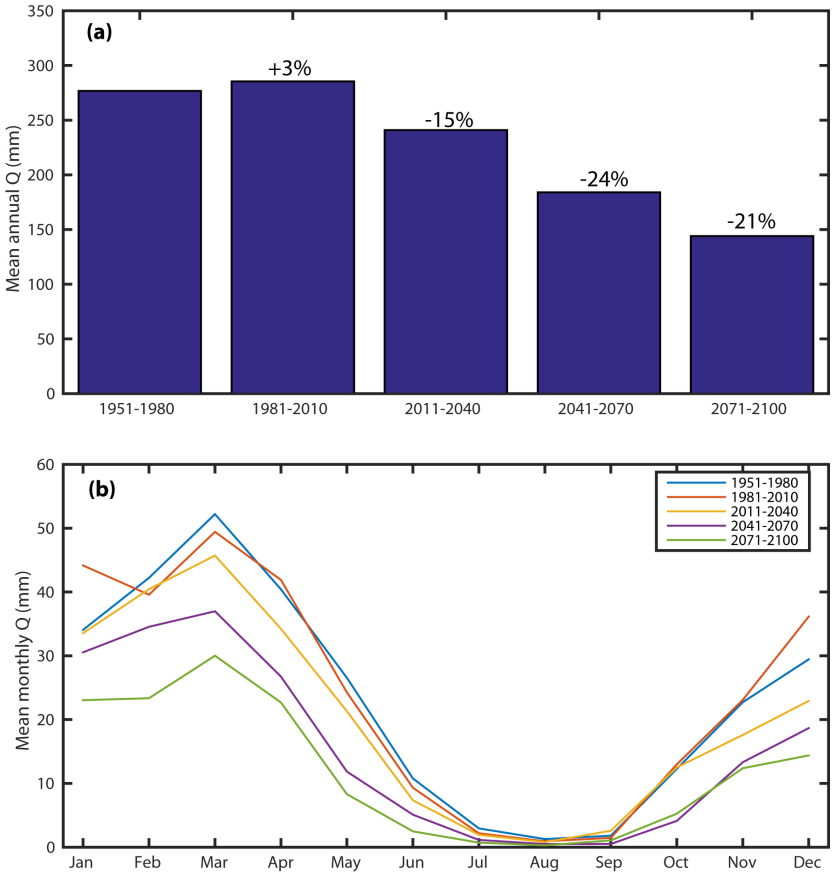

Figure 20. Comme en Figure 19, mais pour la décharge (Q).

La Figure 21 montre les valeurs moyennes de SWC: nous pouvons encore remarquer une diminution de valeurs du contenu d'eau de sol de la période 2011-2040 jusqu'à la période 2071-2100, avec des changements d'environ -20%, en suivant la tendance de la précipitation, et une légère augmentation des valeurs (+0.3 %) dans la deuxième période 1981-2010 (Figure 21a). La distribution saisonnière mensuelle moyenne de SWC est rapportée dans la Figure 21b: nous pouvons observer des valeurs croissantes de SWC dans la deuxième période considérée dans les mois d'hiver, comme pour les valeurs de précipitation et décharge.

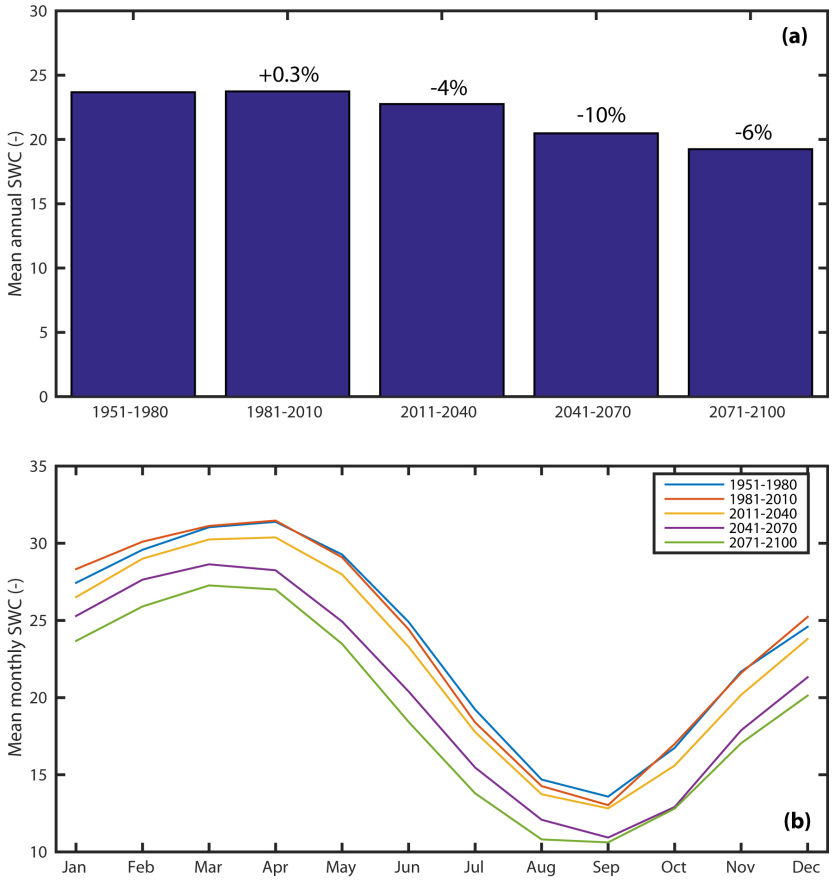

Figure 21. Comme en Figure 19, mais pour le contenu d'eau de sol (SWC).

La simulation des résultats en termes de ET_a est rapportée dans la Figure 22. Une diminution des valeurs annuelles moyennes est prévue de la période 2011-2040 jusqu'à la période 2071-2100, avec des changements d'environ -5%, en suivant la tendance de contenu d'eau de sol, et une légère augmentation (+0.02 %) dans la deuxième période 1981-2010 (Figure 22a). La Figure 22b se réfère à la moyenne mensuelle de ET_a, montrant la saisonnalité moyenne pendant les cinq périodes considérées. Nous pouvons remarquer les valeurs les plus hautes pendant les mois d'été, quand l'évapotranspiration potentielle et la température sont plus hautes et une augmentation aussi pendant Octobre, probablement en raison de l'eau disponible dans la surface à cause de l'augmentation de la précipitation.

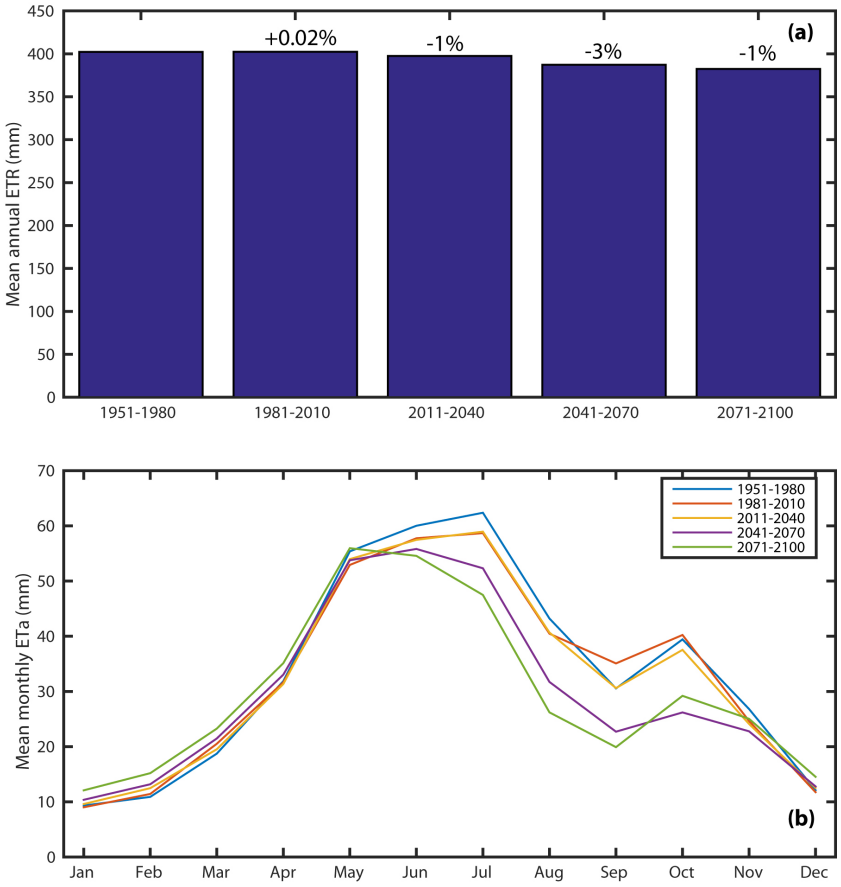

Figure 22. Comme en Figure 19, mais pour l'évapotranspiration réelle (ET_a).

S.5 Conclusions

Les contributions principales de ces travaux de recherche sont récapitulées dans ce chapitre final. L'objectif principal de cette thèse est de développer une approche de modélisation pour évaluer l'impact hydrologique du changement climatique sur deux bassins méditerranéens, situés en Sardaigne, Italie. Le travail pour réaliser cet objectif général est élaboré dans trois étapes. Une comparaison détaillée des réponses obtenues avec trois modèles hydrologiques à base physique, mais avec différent degré en ce qui concerne la représentation des processus physiques et de caractéristiques de terrain - CATchment HYdrology (CATHY), TIN-based Real time Integrated Basin Simulator (tRIBS), et TOPographic Kinematic APproximation and Integration-eXtended (TOPKAPI-X) - sur un bassin méditerranéen semi-aride situé en Sardaigne, le Rio Mannu, est effectuée, avec le but de tester la transférabilité des paramètres entre les trois modèles hydrologiques, concentrant en particulier sur les difficultés de validation et calibrage. Tandis que les trois modèles hydrologiques ont répondu de la même façon pendant l'année de calibrage, des différences significatives ont été trouvées pendant la période de validation très seche pour le modèle CATHY, qui a produit une très basse décharge. Pour obtenir des résultats satisfaisants pour le modèle CATHY, une hypothèse de croûtage de sol a été assumée et la première couche de sol a été modelée avec une conductivité hydraulique saturée plus bas.

Les effets du changement climatique sont alors évalués sur le bassin Rio Mannu à travers la comparaison des résultats de cinq modèles hydrologiques, CATHY, Soil and Water Assessment Tool (SWAT), TOPKAPI-X, tRIBS et Water flow and balance Simulation Model (WASIM) et utilisant comme forçage atmosphérique les données de quatre combinaisons de modèles climatiques globaux et régionaux. Pour évaluer les incertitudes une métrique récemment

proposé par Duveiller et al. (2016), est utilisée: les résultats des modèles ont été comparés pendant une période de référence (1971-2000) et future (2041-2070), en utilisant l'index de corrélation de Pearson et le bias de Duveiller comme dans Kollet et al. (2017). Malgré quelques différences, en général les cinq modèles hydrologiques montrent un bon accord et ils ont répondu de la même façon à la précipitation réduite et températures augmentées prévues des modèles climatiques, en prêtant un fort support d'un scénario futur de manques accrus d'eau pour cette région de la Méditerranée, avec des conséquences négatives particulièrement pour le secteur agricole.

Finalement, on montre une mise en œuvre préliminaire du modèle TOPKAPI-X sur un grand bassin sarde enclin aux événements extrêmes, le Flumendosa, avec le but de tester l'impact hydrologique du changement climatique à plus grande échelle pendant cinq périodes de 30 ans (1951-1980, 1981-2010, 2011-2040, 2041-2070, 2071-2100), en utilisant comme forçage atmosphérique les résultats de quatre combinaisons GCM-RCM. Le modèle TOPKAPI-X répond avec valeur diminuante de décharge, de contenu d'eau de sol et d'évapotranspiration réelle à la précipitation réduite et à la température accrue prévue par les modèles climatiques depuis la période 2011-2040 à la période 2071-2100, en prêtant un fort support à un scénario futur de manque accrus d'eau aussi dans ce bassin de la région méditerranéenne.

1. Introduction

1.1 Climate change impact modeling

Several climate model predictions agree that the Mediterranean area will be affected by changes due to global warming [*IPCC,* 2014]. Giorgi [2006] singled out this region as one of the hotspots in future climate change predictions, susceptible to more frequent and intense extreme events. In addition, in Mediterranean regions during the last decades increasing temperatures have been observed [*Xoplaki et al*., 2003; *Del Río et al*., 2011; *El Kenawy et al*., 2011; *Acero et al*., 2014], associated with seasonal reductions in precipitation [*Giorgi and Lionello*, 2008; *Sousa et al*., 2011; *Vicente-Serrano and Cuadrat-Prats*, 2007].

As a result of climatic and anthropogenic changes (such as expansion of cultivation to former pasture and semi-arid areas, depopulation of remote mountains, land-use intensification, deforestation and forest fires) hydrologic fluxes and physical characteristics may evolve in the sense of desertification [*Cudennec et al*., 2007; *Puigdefabregas and Mendizabal*, 1998; *Tooth*, 2007]. The Mediterranean basin is also usually exposed to typical convective mesoscale systems, due to its geographic position with many surrounding mountains, and this lead to heavy precipitation and flash floods [*Adamovic*, 2016], which represent the most destructive hazard in the Mediterranean region, involving loss of life and high economic and social impact [*Gaume et al*., 2009].

In the recent past intense flood events as well as drought periods have caused important socioeconomic losses [*Chessa et al*., 2004; *Silvestro et al*., 2012], affecting the agricultural sector, the pillar of the local economy [*Piras*, 2014]. In regions where water stress is already high, the combined effect of decreasing water availability due to climate change and increasing needs due to human activities may lead to critical water shortages and water use conflicts

[*Grouillet et al*, 2015; *Milano et al*., 2013a]. In this backdrop it is therefore crucial evaluate the effects of climate change at the basin scale in order to develop suitable adaptation strategies [*Gädeke et al.*, 2014].

Climate change impacts at the catchment scale can be evaluated by coupling global and regional climate models with distributed hydrologic models using downscaling techniques to bridge the scale mismatch between climate and hydrologic models [*Piras,* 2014]. This is usually conducted through the following procedure [e.g. *Xu et al.,* 2005]: (i) selection of a set of global climate models (GCM) and regional climate models (RCM) to provide future climate predictions; (ii) application of downscaling techniques to increase the coarse scale of climate model outputs to the finer resolutions required by hydrologic models; and (iii) use of downscaled outputs as forcing for calibrated hydrologic models to evaluate the basin hydrologic response [*Abbaspour et al*., 2009; *Liuzzo et al*., 2010; *Sulis et al*., 2011, 2012; *Montenegro and Ragab*, 2012; *Piras et al*., 2014; *Majone et al*., 2016; *Meyer et al*., 2016]. Each of these steps are affected by uncertainties [*Xu and Singh*, 2004] that have been explored in many previous papers: choice of emission scenario and climate forcing [*Giorgi and Mearns*, 2002; *Tebaldi et al.*, 2005], downscaling technique [*Wood et al*., 2004; *Fowler et al*., 2007; *Im et al*., 2010], hydrologic tools used to assess the local impacts and observed data used to calibrate it [*Clark et al.*, 2008; *Jiang et al*., 2007; *Dams et al*., 2015]. One approach to dealing with uncertainties is to use multiple climate and hydrologic models [*Bosshard et al*., 2013; *Cornelissen et al*., 2013; *Gädeke et al*., 2014; *Najafi et al*., 2011].

1.2 State of the art about model intercomparison and parameter transferability

The main purpose of hydrologic modeling is to simulate hydrologic processes at different scales, in order to guide the formulation of water resource management strategies and also as tools of scientific inquiry [*Dingman*, 2008]. A hydrologic model is essentially a simulation model, a representation of a portion of the natural or human-constructed world, which can reproduce some but not all of the characteristics thereof [*Dooge*, 1986]. The essential feature of a simulation model is that it produces an output or a series of outputs in response to an input or series of inputs. In general, three main classes of simulation models exist: physical models, analog models, and mathematical models. The first are scale representations of a portion of the natural world. The second use observations of one process to simulate a physically analogous natural process. Mathematical models are an explicit sequential set of equations and numerical and logical steps that convert numerical inputs to numerical outputs. These last models have become the hydrologic model class most widely used, thanks to the availability of powerful digital computers on which to implement codes, modeling techniques, and software [*Dingman*, 2008].

An early classification of mathematical models used in hydrology was introduced by Clarke [1973]. In this classification, models are considered either stochastic, with model variables displaying random variation, or deterministic, with model variables regarded as free from random variation. Both stochastic and deterministic models are classified as conceptual when they use schematizations of physical phenomena, as physically based when they solve the physics equations of the different processes, and empirical when they don't represent the physical phenomena because they are based only on the observation of inputs and outputs, without explicitly representing the conversion process. Within these groups, models could be

either linear or nonlinear and either lumped or distributed. Lumped models are defined as those that do not account for the spatial distribution of input variables or parameters. Distributed models, in contrast, account for spatial variability of input variables.

In order to guide the formulation of water resource management strategies and also as tools of scientific inquiry, physically based hydrologic models are useful tools for simulating hydrologic response [*Abbott et al.,* 1986; *Kampf and Burgess,* 2007; *Paniconi and Putti*, 2015; *Fatichi et al*., 2016]. There are three main objectives behind their development: to account for the spatial variability of physiographic watershed characteristics; to have process-based models based on physical laws and parameters assessed a priori; and to simulate the spatio-temporal variability of different hydrologic variables, such as soil moisture, groundwater flow and runoff generation. Moreover, using parameters with a physical meaning can allow the transferability of the calibration of their value among different models. Physically based hydrologic models can represent a specific process, such as groundwater flow in saturated and variably saturated porous media [*Huyakorn et al.*, 1986; *Jones and Woodward*, 2001; *Kirkland et al*., 1992] or surface flow [*Gottardi and Venutelli*, 1993; *Jaber and Mohtar*, 2003; *Taylor et al*., 1974], or multiple processes and their interactions [*Gunduz and Aral*, 2005; *Panday and Huyakorn*, 2004; *VanderKwaak and Loague*, 2001], such as coupled surface-subsurface models. Many researchers have recently recognized the relevance of surface and subsurface water interactions to correctly describe hydrologic processes at the catchment scale [*Fleckenstein et al.*, 2010; *Kollet and Maxwell*, 2006; *Maxwell et al*., 2007]. Consequently many efforts have been undertaken to develop coupled models that, together with laboratory and field experimental studies, underline the fact that it is necessary to consider the catchment as an integral surface-subsurface domain to better determine the variables of interest (groundwater level, volumetric water content,

discharge, etc.). Thanks to recent advances in remote sensing, geographic information systems (GIS), and geophysical techniques over the last few years, physically based hydrologic models that represent land-atmosphere interactions have been developed as useful tools to simulate and predict water fluxes, both in applied/operational and research/theoretical fields. These models are applied for example to study two phenomena that are of great importance: climate change and flood events [*Artan et al.,* 2001; *Kite*, 1995; *Liu and Todini*, 2002; *Wigmosta et al*., 1994].

Because hydrologic models are representations of real systems, it cannot be anticipated which one offers more accuracy and predictive capability for specific catchments and hydrologic conditions [*Seiller et al*., 2012]. Under such circumstances, model intercomparison provides a useful means for conducting performance assessments, including evaluation of the effect of model structure on model output [*Chiew et al*., 1993; *Refsgaard and Knudsen*, 1996; *Perrin et al*., 2001; *Reed et al*., 2004; *Breuer et al*., 2009; *Gorgen et al*., 2010; *Bae et al.*, 2011; *Clark et al*., 2011; *Koch et al*., 2016]. Most intercomparison studies of hydrologic models have focused on simulated discharge, an integrated measure of hydrologic response at basin outlet [*Cornelissen et al*., 2013; *Dams et al*., 2015; *Goslin et al*., 2011; *Kollet et al*., 2017; *Ludwig et al*. 2009], and have shown that there exist a variety of hydrologic models, with a wide range of algorithms to describe hydrologic processes, that allow to simulate river discharge with a similar accuracy [*Refsgaard and Knudsen*, 1996; *Pitman and Henderson-Sellers*, 1998; *Smith et al*., 2004, 2012; *Duan et al.*, 2006; *Safari et al*., 2012; *Vansteenkiste et al*., 2014a,b]. However in these comparisons each hydrologic model has been independently calibrated.

A challenge facing hydrologic modelers is how the knowledge gained from one model can be transferred to another model. The literature on parameter transferability is above all related to spatiotemporal parameter transferability. For example, Hogue et al. [2005], investigate

the performance of the National Centers for Environmental Prediction (NCEP) Noah land surface model to evaluate the transferability of calibrated parameters between two semiarid sites in southern Arizona. Their results showed that in the absence of calibration data, a proxy basin set of parameters can be applied with a moderate decline in performance. Patil et al. [2015] compared three different schemes of parameter transferability, temporal, spatial, and spatiotemporal, applying the EXPonential bucket HYDROlogic model (EXP-HYDRO) in 294 catchments across the continental United States. Results showed that the stability of hydrologic model parameters tends to be higher in the temporal domain than in the spatial domain. Ren et al. [2016] evaluated the potential of transferring hydrologic model parameters in Community Land Model (CLM) through sensitivity analyses and watershed classification across 431 basins in the United States. They found that using the same parameter values for sites belonging to the same class as regards climate, soil, land cover/use, or geographic locations, could not yield the best model performance if the soil and climate conditions vary substantially within the class.

Literature about parameter transferability across hydrologic models is limited. Only in Yen et al. [2015] three sources of land use data were implemented on a watershed situated in Maryland, United States, to investigate the potential impact of cross transferring optimal calibration parameters between three version of the SWAT model. It has been shown that model parameters are transferable temporally (parameter transferring in different simulation time period) or spatially (parameter transferring in nearby ungauged sites) but not structurally (e.g. parameters are not transferable in different versions of SWAT).

Similarly to hydrologic models, the multi-model ensemble is commonly used in meteorology and climatology to quantify the predictive uncertainty of weather forecasts and climate change simulations [*Murphy et al*., 2004], and has been utilized also to drive multi-

model hydrologic simulations. Bae et al. [2011] compared in a Korean basin three semi-distributed hydrologic forced with outputs from thirteen GCMs and three greenhouse gas emission scenarios. They results show that the hydrologic models can produce major differences in runoff change under the same climate simulations, in particular during the dry season. Bastola et al. [2011] examined the role of hydrologic model uncertainties (parameter and structural uncertainty) using six climate change scenarios and four conceptual hydrologic models within the generalised likelihood uncertainty estimation (GLUE) framework. The results for the four Irish catchments considered showed a tendency of increasing flow in winter and decreasing flow in summer. Thompson et al. [2013] demonstrated for the Mekong river in southeast Asia that GCM-related uncertainty in climate change projections is generally larger than that related to the use of three hydrologic models, which simulate the same direction of change in mean discharge. However, hydrologic model related-uncertainty is not negligible and in some cases is of a similar magnitude to GCM-related uncertainty. Vansteenkiste et al. [2014a] utilized an ensemble of hydrologic models, from lumped conceptual to distributed physically based, to evaluate the impact of climate change on the Grote Nete (Belgium). The uncertainty in the hydrologic impact results was assessed by the relative change in runoff volumes and peak and low flow extremes from historical and future climate conditions. Large differences in model predictions were found, especially under low flow conditions. Using the ANOVA approach, Bosshard et al. [2013] assessed uncertainties induced by climate models, two different bias correction methods and hydrological models using the output of eight RCM that are fed into two hydrologic models of the Upper Rhine. The results indicate that none of the investigated uncertainty sources is negligible, and some of the uncertainties are not attributable to individual modeling chain components, but rather depend upon their interactions, while in total, climate model uncertainty

has the largest contribution to the entire uncertainty. Maurer et al. [2010] applied a lumped and a distributed model forced by twenty-two climate model outputs on three California watersheds. The projected percent changes in monthly discharge differed between the two models above all during the summer season and for extreme flows. Nevertheless in these studies the climatic zone of the basins analyzed varies from Arctic and sub-Arctic, humid temperate, to tropical and sub-tropical. Model intercomparison remains an unexplored field in basins characterized by a Mediterranean climate.

1.3 Research objectives and thesis outline

In this context my research aims to bring a contribution in developing a modeling approach that allows evaluation of local hydrologic impacts of climate changes in two Mediterranean basins. There are three specific goals that I want to reach. These are:

1. Test the parameter transferability between three hydrologic models that are physically based to varying degrees as regards processes and terrain features representation – CATchment HYdrology (CATHY), TIN-based Real time Integrated Basin Simulator (tRIBS), and TOPographic Kinematic APproximation and Integration-eXtended (TOPKAPI-X) – on a small Mediterranean basin located in a semiarid region in Sardinia (Italy), the Rio Mannu catchment, focusing in particular on the calibration and validation difficulties. Three consecutive years were chosen for the calibration (1930) and validation (1931-1932), the former being a quite wet year while the latter period is characterized by much drier weather. The three hydrologic models responded similarly during the calibration year, whereas significant differences were found for the validation period. In particular, to obtain satisfactory results during the 1931-1932 dry period, for the CATHY

model an hypothesis of soil crusting was assumed, on the basis of which the first soil layer was modeled with a lower saturated hydraulic conductivity.

2. Characterization of the agreement between both climate and hydrologic predictions in the Rio Mannu cathment, representative of Mediterranean climate and socioeconomic issues related to hydrologic extremes. For this aim an ensemble of climate and hydrologic models, including four combination of GCMs and RCMs and a set of five hydrologic models of varying structural complexity, from conceptual to physically-based, will be used. The examined models are: CATHY, Soil and Water Assessment Tool (SWAT), TOPKAPI-X, tRIBS, and WAter balance SImulation Model (WASIM). This is the first study wherein a wide range of distributed hydrologic models forced with outputs of different climate models is applied to a Mediterranean catchment to assess the impact of climate change. Moreover, unlike many previous studies, the focus is on a set of variables characterizing and affecting the water balance at the catchment scale, including precipitation, air temperature, discharge, soil water content in the first meter, and actual evapotranspiration. The results are discussed in the context of the process representations for each model and within a rigorous analysis of agreement framework. For the latter a new metric, proposed by Duveiller et al. [2016], will be used to compare model results for reference and future periods using correlation and bias coefficients.
3. Preliminary evaluation of climate change impacts at a much larger scale, through the implementation of the hydrologic model TOPKAPI-X on one of the most economically important river basins in Sardinia, the Flumendosa basin.

The rest of the thesis is structured as follows:

Chapter 2 contains the description of the Rio Mannu and Flumendosa basins and related dataset;

Chapter 3 presents both the hydrologic and climate models used in this study;

Chapter 4 discusses the main results regarding the three objective of this study;

Chapter 5 summarizes the contents of this dissertation.

2. Study area and available dataset

This section contains the description of the two study areas considered, both located in Sardinia (Italy), and the available dataset. Section 2.1 describes the Rio Mannu catchment, while section 2.2 illustrates the Flumendosa basin.

2.1 Rio Mannu catchment

The first study site is the Rio Mannu di San Sperate at Monastir basin, located in southern Sardinia, Italy (Figure 2.1). It drains an area of 473 km^2 with elevation varying from 66 m to 963 m. The topography is mostly gently rolling, except for a mountainous zone in the southeastern part ("Sette Fratelli chain"), and the mean slope is about 17%. The main physiographic properties, including elevation, slope and river network features, are reported in Table 2.1. The principal land use in the region is agriculture, which is especially dominating in the valley area (Campidano plain). The most important crops grown are wheat, maize, beans and artichokes [*Meyer et al*., 2016].

The basin is characterized by a typical Mediterranean climate with wet periods from October to April and dry periods during the rest of the year. Figure 2.2 shows the mean monthly values of precipitation, discharge, and temperature in the catchment. Precipitation in the form of snow occurs rarely due to the topographic characteristics and the geographic position, and can be neglected in hydrologic simulations [*Mascaro et al*., 2013b]. The mean annual precipitation is about 600 mm and the mean temperature ranges from 9 °C in January to 25 °C in July-August. The discharge regime is characterized by low flows (less than 1 m^3/s) for the main part of the year and few flood events in autumn and winter [*Mascaro et al*., 2013a].

The Rio Mannu basin was one of the seven study sites of a European research project (CLIMB, CLimate Induced changes on the hydrology of Mediterranean Basins) change [*Ludwig et al*., 2010] aimed at assessing the impact of climate change on the hydrologic cycle and on stakeholders in different Mediterranean catchments. Amongst the reasons for selecting the Rio Mannu site for CLIMB is the presence of an agricultural research station within its boundaries, where extensive field characterization studies could be undertaken, and the vulnerability of this region to climatic extremes (e.g., several prolonged drought periods over the past decades). Over the course of the CLIMB project, several field and modeling activities of direct or indirect relevance to this study were undertaken, including geophysical and remote sensing surveys, geostatistical analyses of field data, and several model implementations [e.g., *Cassiani et al*., 2012; *Marras et al*., 2014; *Filion et al*., 2016; *Meyer et al.*, 2016].

Daily discharge data at the Rio Mannu catchment outlet section were collected and published for 11 years, from 1925 to 1935. During the same period 12 rain gages provided daily rainfall data and one thermometric station registered daily minimum (T_{min}) and maximum (T_{max}) temperature. To provide forcings at resolutions needed for the application of tRIBS, Mascaro et al. [2013b] developed two downscaling strategies to generate hourly precipitation grids at spatial resolution of ~13 km and basin-averaged hourly potential evapotranspiration (ETP). These tools were calibrated and tested with high-resolution data available at more recent times. Specifically, the multifractal downscaling model known as Space Time RAINfall (STRAIN) [*Deidda et al*., 1999; *Deidda*, 2000] was applied to disaggregate precipitation from the coarse resolution of 104 km, 24 h to the fine resolution of 13 km, 1 h. This model was calibrated with high-resolution (1 min) rain gauges available over the period 1986-1996 in the coarse domain of 104 km x 104 km that contains the Rio Mannu catchment. Basin-averaged hourly estimates of ETP were instead

obtained through a downscaling method based on dimensionless functions that reproduce, for each month, the average daily cycle of ETP using T_{min} and T_{max} as inputs. This routine was calibrated and tested by applying the Penmamn Monteith equation with hourly meteorological data collected in Cagliari from 1995 to 2010. More details on the downscaling tools can be found in Mascaro et al. [2013].

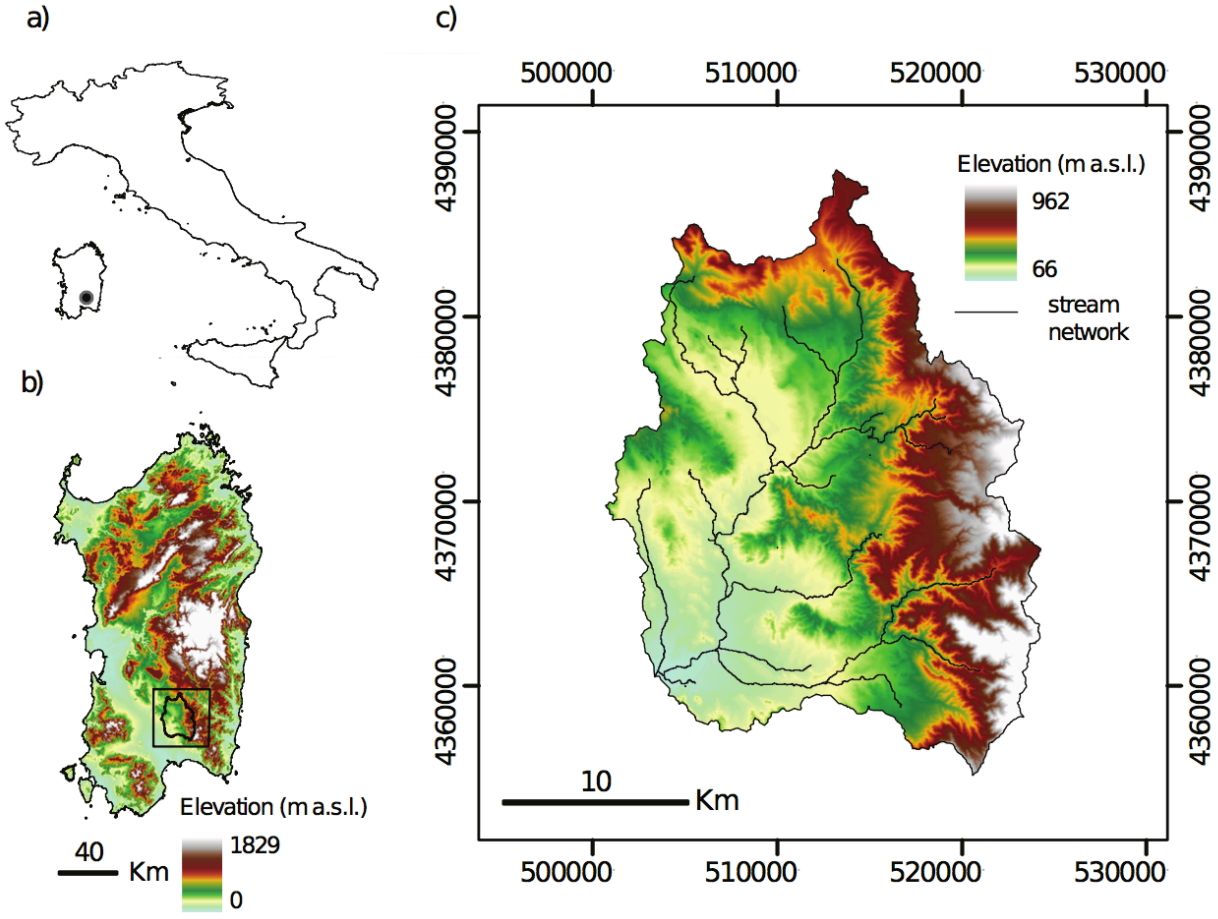

Figure 2.1. Location of the Rio Mannu basin within (a) Italy, and (b) Sardinia. (c) Boundaries in WGS84 UTM coordinates, elevation and stream network of the basin.

A_b [Km^2]	z_{min} [m a.s.l.]	z_{max} [m a.s.l.]	z_{mean} [m a.s.l.]	β_{bmean} [%]	L_m [Km]	T_c [h]
473	66	962	296	17	39	12

Table 2.1. Physiographic characteristics of the Rio Mannu catchment including area A_b, minimum (z_{min}), maximum (z_{max}) and mean (z_{mean}) elevation, mean slope (β_{mean}), length of the main reach (L_m), and concentration time (T_c), computed using the Giandotti [1934] formula.

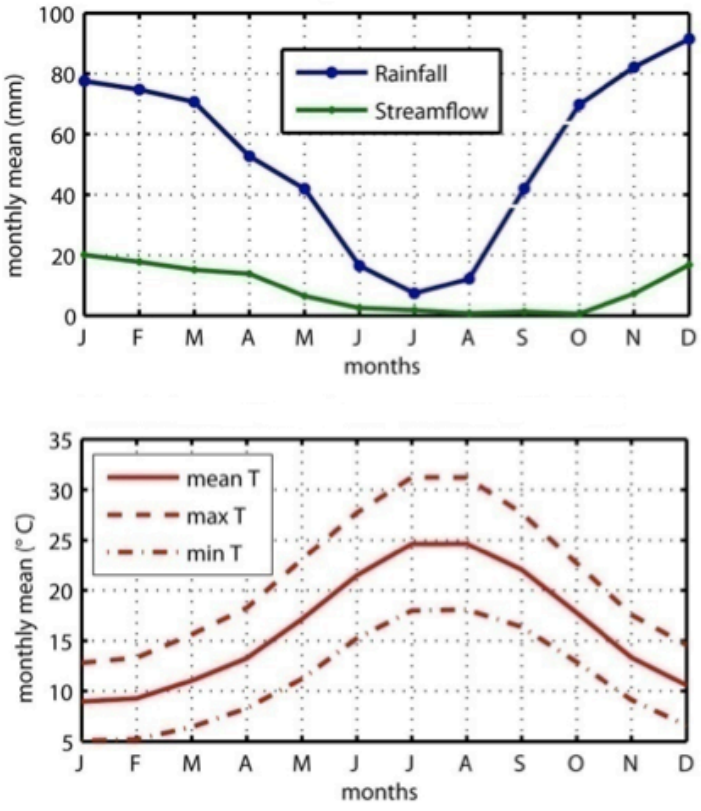

Figure 2.2. Mean monthly precipitation discharge and temperature in Rio Mannu catchment computed in different periods in which daily data were available.

Geospatial datasets characterizing the spatially-variable basin land surface properties include the following. A digital elevation model (DEM) at 10-m resolution obtained from the Sardinian Region Government (Figure 2.1c). The land cover map was provided by the COoRdination de l'INformation sur l'Environnement (CORINE) project, and reclassified into 8 groups. As shown in Table 2.2, the dominant classes are agriculture (~ 48 %) and sparse vegetation (~ 26 %) (Figure 2.3b). The pedologic map of Aru et al. [1992] was used to characterize the soil properties. For this aim, the map was aggregated on the basis of field campaigns conducted as part of the CLIMB project and described in Ludwig et al. [2010]. The resulting map is shown in Figure 2.3a, while the percentage of the basin area for each class is reported in Table 2.2 [*Piras*, 2014]. The soil depth map was obtained combining the DEM and the soil texture information (Figure 2.4), following a procedure described on the website of the Distributed Hydrology Soil Vegetation Model (http://www.hydro.washington.edu/Lettenmaier/Models/DHSVM/tools.shtml).

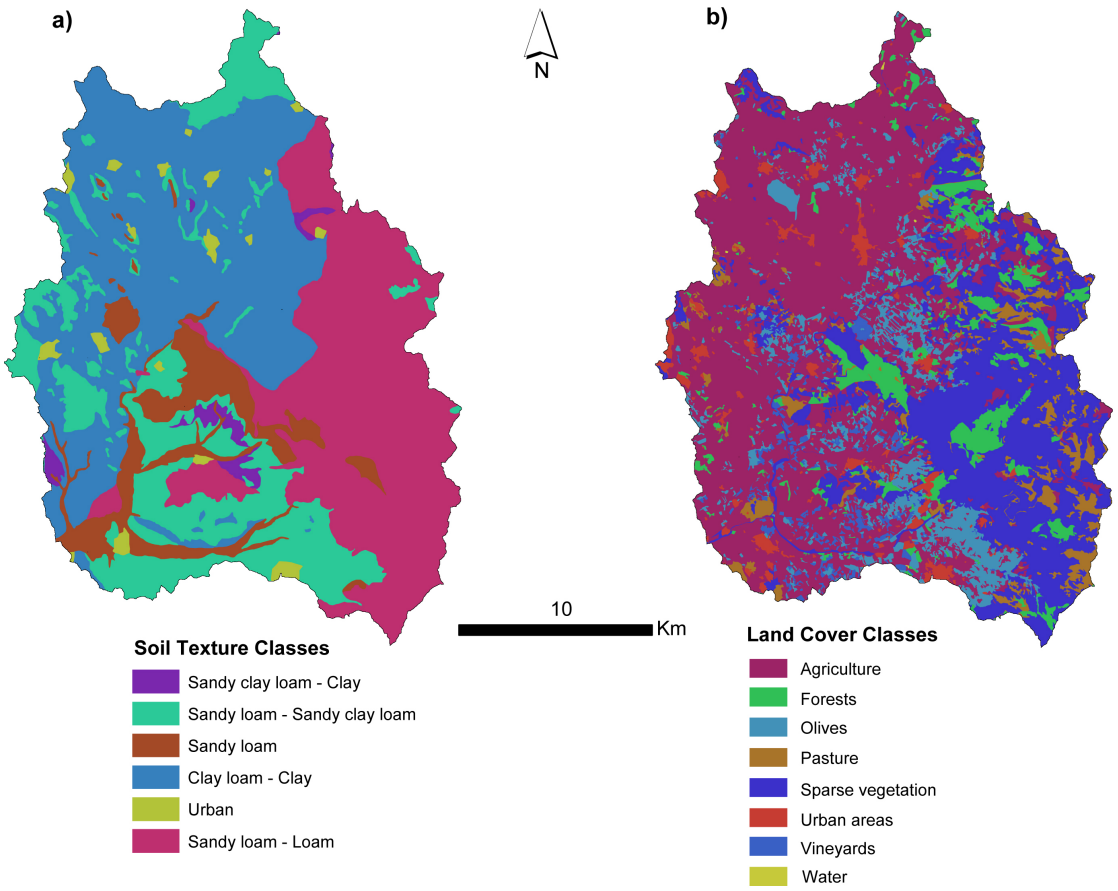

Figure 2.3. a) Soil texture and b) land cover maps used for the Rio Mannu basin.

Land Cover Class	% Basin Area	Range of Soil Texture Classes	% Basin Area
Agriculture	47.64	Sandy clay loam - clay	1.57
Forests	7.09	Sandy loam - sandy clay loam	19.59
Olives	8.07	Sandy loam	8.84
Pastures	5.43	Clay loam - clay	36.66
Sparse vegetation	26.08	Urban	1.52
Urban areas	3.25	Sandy loam - loam	31.82
Vineyards	2.44		
Water	0.02		

Table 2.2. Land Cover, range of soil texture classes and percentage of basin area for the Rio Mannu catchment.

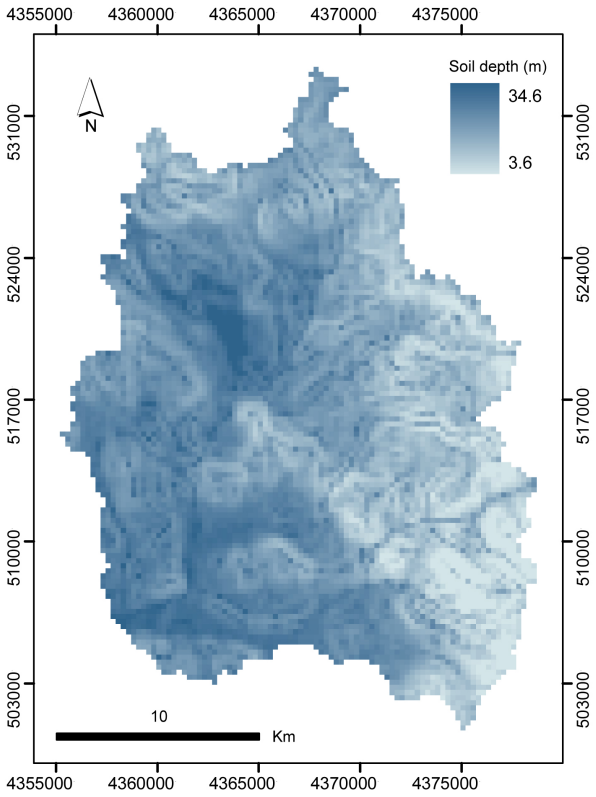

Figure 2.4. Base map for the Rio Mannu catchment, obtained from the DHSVM model.

2.2 Flumendosa basin

The second study area, the Flumendosa basin, is one of the main Sardinian basins, with a strategic relevance for the region's water system (Figure 2.5). It is located in southeast Sardinia and it drains an area of 1826 km^2. It extends from the highest peak of the island (Mount Gennargentu, 1834 m) to the outlet on the Tyrrhenian Sea. The mean slope is about 36%. The main physiographic properties, including elevation, slope and river network characteristics, are reported in Table 2.3. The mean annual precipitation is about 900 mm and shows a strong correlation with orography [*Seoni*, 2015], while the mean monthly temperature ranges from 6°C in winter to 24°C in summer.

The basin is the main source of water supply for the whole southern part of Sardinia, the most populated area. Along the Flumendosa river and its tributary, in fact, three reservoirs were constructed that, with a total capacity of 600 million cubic meters, constitute the main water resource for domestic, irrigated, and industrial uses in southern Sardinia. This region however is also prone to prolonged periods of drought, together with social and economic problems created by conflicts amongst different water uses. In addition, some villages within the basin (for instance Ballao, St. Vito, Muravera, and Villaputzu) have suffered extreme flood episodes that required the intervention of the civil protection agency and that caused, in some cases, loss of human lives.

Hydrometeorological data from the Italian Hydrologic Survey (the 'Annali Idrologici') were collected within and around the Flumendosa basin at a daily time scale from 1926 to 1936, and included daily precipitation measurements from 14 rain gages, daily minimum and maximum temperature from 5 thermometric stations, and daily discharge data from one hydrometric station. Figure 2.6 shows the mean monthly values of precipitation, temperature, and streamflow, while Figure 2.7 shows the location of the hydrometeorological stations.

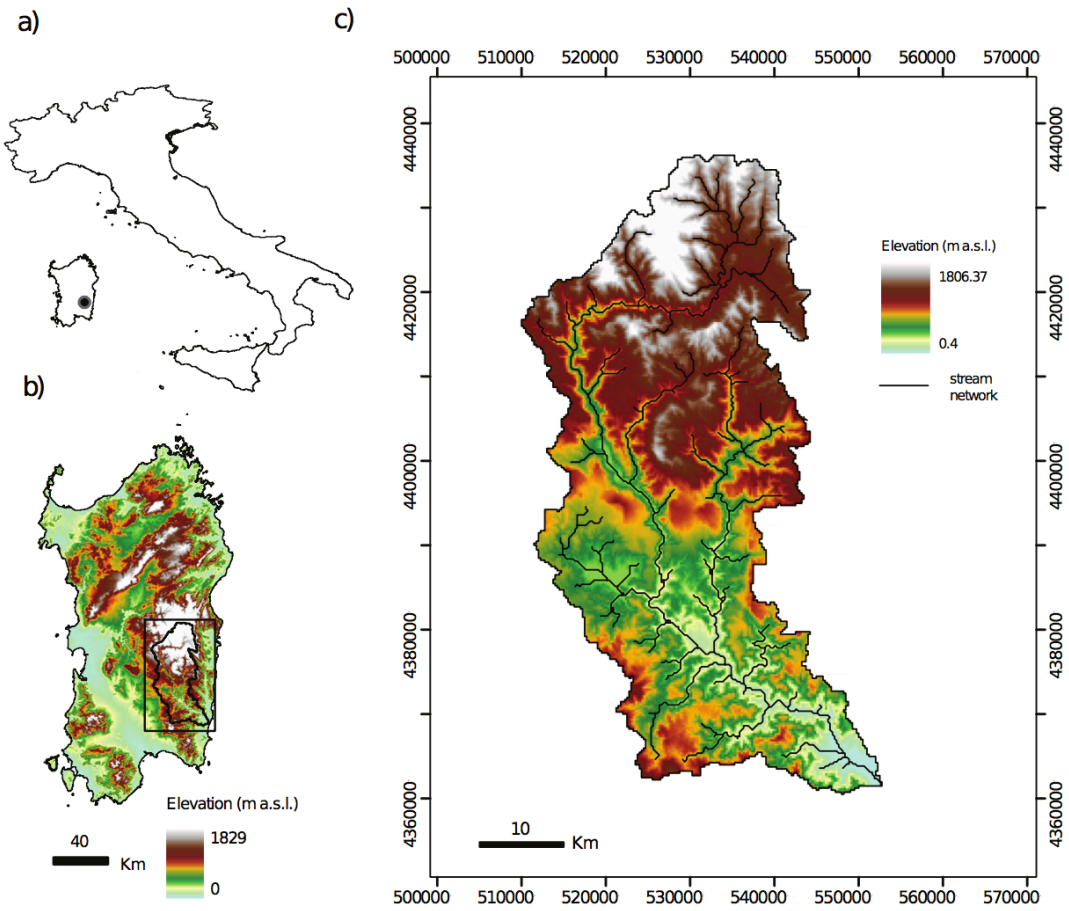

Figure 2.5. Location of the Flumendosa basin within a) Italy and b) the island of Sardinia. Digital elevation model of the Flumendosa basin including UTM coordinates.

A_b [Km^2]	z_{min} [m a.s.l.]	z_{max} [m a.s.l.]	z_{mean} [m a.s.l.]	β_{bmean} [%]	L_m [Km]	T_c [h]
1826	0	1834	636	36	95	16

Table 2.3. Physiographic characteristics of the Flumendosa basin including area A_b, minimum (z_{min}), maximum (z_{max}) and mean (z_{mean}) elevation, mean slope (β_{mean}), length of the main reach (L_m), and concentration time (T_c), computed using the Giandotti [1934] formula.

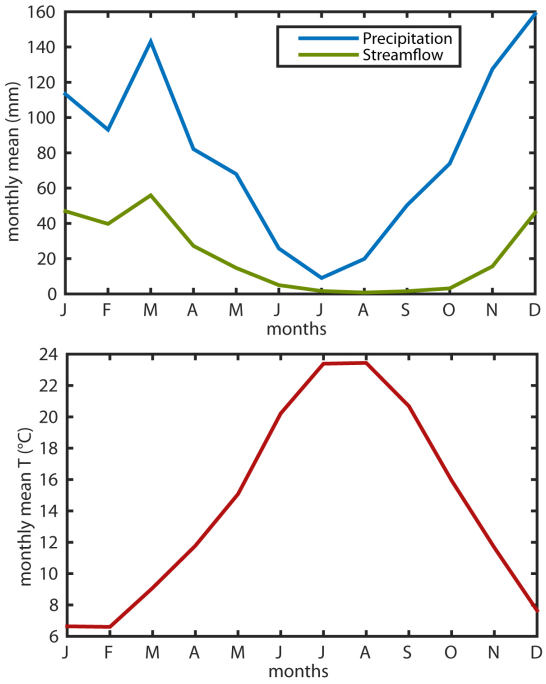

Figure 2.6. Mean monthly precipitation (P), discharge (Q), and temperature (T) for the Flumendosa basin during the period 1926-1937.

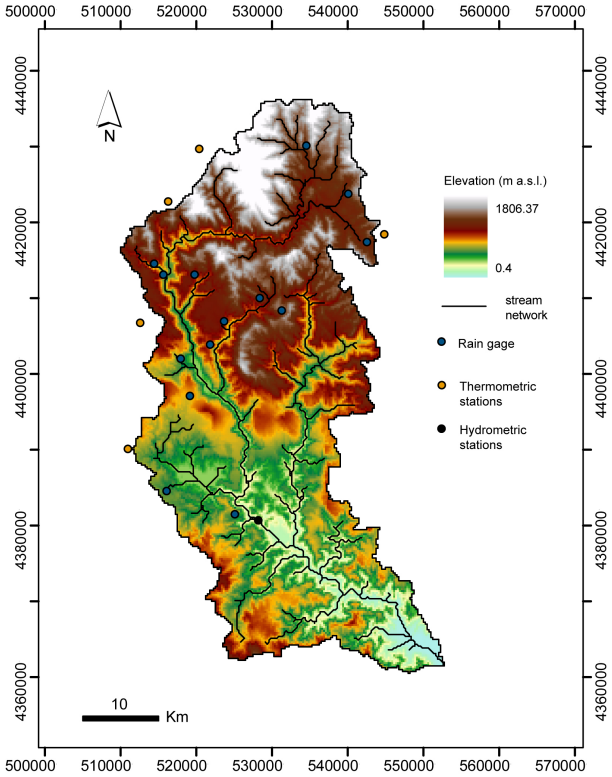

Figure 2.7. Location of the hydrometeorological stations inside or near the Flumendosa basin.

The geospatial data for the Flumendosa basin were provided by different agencies of the Sardinian Region Government and include the following: (i) a digital elevation model (DEM) at 10 m resolution (Figure 2.5c); (ii) the land cover (LC) map in digital format, derived from the COoRdination de l'INformation sur l'Environnement (CORINE) project of the European Environment Agency (EEA) for the year 2008; and (iii) a hard copy of a pedologic map of Sardinia at scale 1:250 000 [*Aru et al.*, 1992]. The LC and soil texture maps were pre-processed to be utilized as model inputs. The original CORINE LC classes were aggregated into 8 groups, based on land cover classes description and percentage of basin area occupied in the original map, obtaining the map shown in Figure 2.8a. According to this reclassification, the dominant classes are Mediterranean scrub (~ 38 %) and broad-leaved forests (~ 22 %). Other categories include agriculture, forests, pastures, and urban areas, with minor percentages as summarized in Table 2.4. The pedologic map was digitized and georeferenced resulting in 26 classes in the Flumendosa catchment. These data were then aggregated into 7 classes based on soil acronym and percentage of basin area occupied in the original map. The resulting map is shown in Figure 2.8b, while the percentage distribution of the classes is reported in Table 2.5.

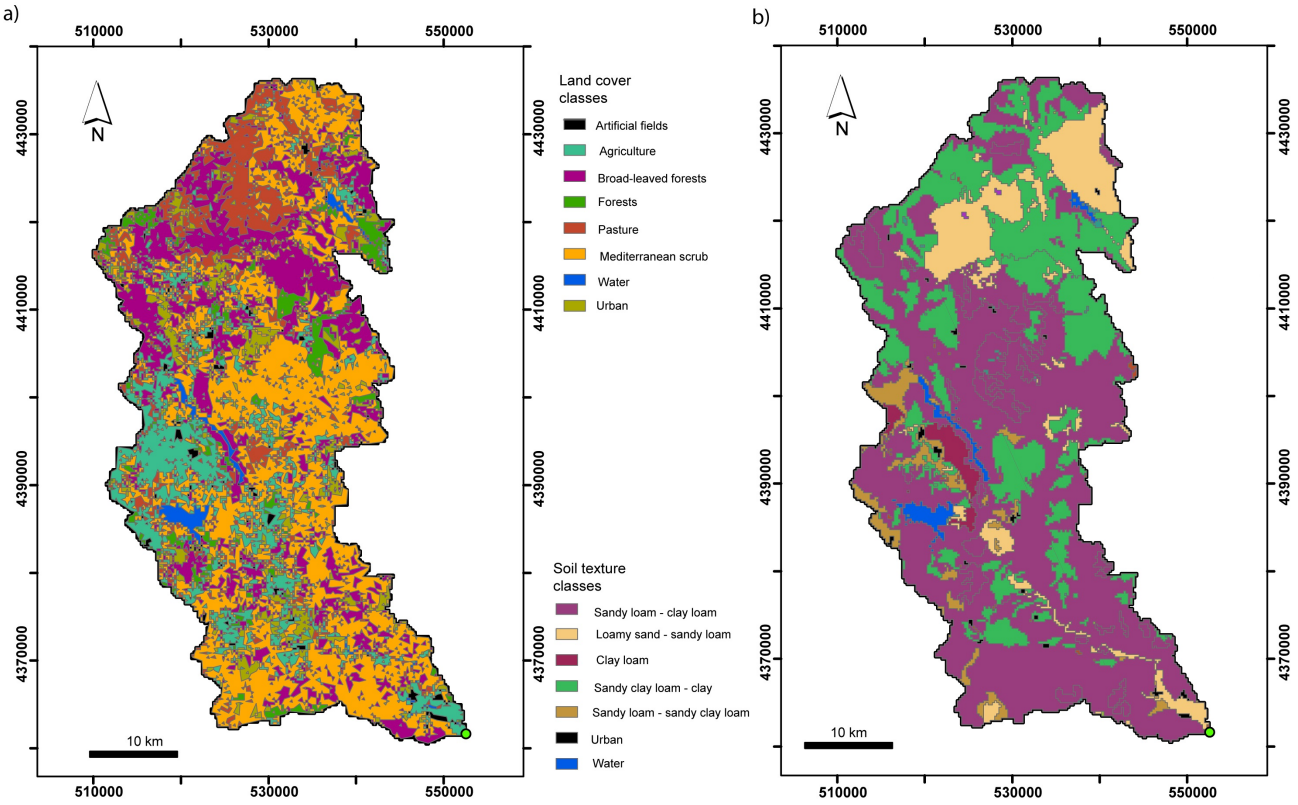

Figure 2.8. a) Land cover and b) soil texture maps for the Flumendosa basin.

ID	Description	Area (%)
1	Artificial fields	1.07
2	Agriculture	13.35
3	Broad-leaved forests	22.06
4	Forests	4.27
5	Pasture	12.60
6	Mediterranean scrub	38.38
7	Water	1.40
8	Urban	6.87

Table 2.4. Land cover and corresponding percentage of basin area for the Flumendosa basin.

ID	Description	Area (%)
1	Sandy loam – clay loam	67.99
2	Loamy sand – sandy loam	10.92
3	Clay loam	1.52
4	Sandy clay loam - clay	14.41
5	Sandy loam – Sandy clay loam	3.40
6	Urban	0.45
7	Water	1.33

Table 2.5. Soil texture and corresponding percentage of basin area for the Flumendosa basin.

3. Methodology

Some of the studies started during the CLIMB project are now completed and their outcomes are here analyzed to perform a multi-model assessment of hydrologic impacts of climate change. A detailed comparison of the responses obtained with the three physically based hydrologic models, Catchment Hydrology (CATHY), TIN-based Real Time Integrated Basin Simulator (tRIBS), Topographic Kinematic Approximation and Integration eXtended (TOPKAPI-X), is applied focusing in particular on the calibration and validation periods. Since the tRIBS model was previously implemented on the Rio Mannu basin during the CLIMB project, for the two other models the same datasets was adopted, including geospatial data of land surface properties and hydro-meteorological forcing, with the aim to test the transferability of parameters between the three physically based hydrologic models. The considered models represent physical processes and terrain features in a different way and this leads to different results, especially during the validation period, characterized by a much drier weather with respect to the calibration one.

The results of five different hydrologic models forced with the outputs of four climate models from the ENSEMBLE project (http://ensembles-eu.metoffice.com), after proper bias correction and downscaling, are compared on the Rio Mannu catchment. The examined models – CATHY, Soil and Water Assessment Tool (SWAT), TOPKAPI-X, tRIBS, and Water Flow and Balance Simulation (WASIM) – differ greatly in their representation of terrain features, physical processes, and numerical complexity, but can represent spatially distributed meteorological input, hydrologic variables, and catchment properties. The five hydrologic models, independently calibrated and validated, were applied in cascade with climate models in order to evaluate the effects of climate change for a reference (1971-2000) and a future (2041-2070)

period. Performances of both climate and hydrologic models are evaluated in terms of agreement and bias between model pairs using the Duveiller indices.

Finally, the TOPKAPI-X model is implemented on a complex system, the Flumendosa basin, to evaluate climate change impacts at a much larger scale. The hydrologic model was calibrated and validated, and then applied in cascade with climate models in order to evaluate the effects of climate change for five 30-year periods (1951-1980, 1981-2010, 2011-2040, 2041-2070, 2071-2100).

In the following, each hydrologic model used in this study is described, with Table 3.1 summarizing the characteristics of each model and their main differences, while the selection of the climate models is recalled in section 3.2.

3.1 Hydrologic models

3.1.1 CATHY

CATHY is a coupled physically based spatially distributed model that allows detailed description of subsurface and surface water and their interactions. CATHY couples two main solvers: FLOW3D, which simulates subsurface flow processes, and SURF_ROUTE, which describes surface flow. The subsurface module solves, using the finite element method, Richards equation (Eq. 3.1), that describes flow in variably saturated porous media [*Paniconi and Wood*, 1993; *Paniconi and Putti*, 1994].

$$S_W S_S \frac{\partial \psi}{\partial t} + \phi \frac{\partial S_W}{\partial t} = \nabla \cdot [K_r(\psi) K_s(\nabla \psi + \eta_Z)] + q_{ss} \qquad (3.1)$$

where $S_W = \vartheta / \vartheta_s$ is water saturation, ϑ[-] is the volumetric moisture content [-], ϑ_s is the saturated moisture content (generally equal to the porosity ϕ), S_S is the aquifer specific storage coefficient $[L^{-1}]$, ψ is pressure head $[L]$, t is time $[T]$, ∇ is the gradient operator $[L^{-1}]$, $K_r(\psi)$ is

the relative hydraulic conductivity [-], K_s is the saturated hydraulic conductivity [LT^{-1}], η_Z is the vertical coordinate directed upward [L], and q_{ss} is the surface to subsurface exchanges of water [L^3/L^3T]. The relation between pressure head and volumetric water content is defined via soil moisture characteristics, which can be specified by using different expressions [*Brooks et al.*, 1964; *Huyakorn et al*., 1984; *van Genuchten et al*., 1985]. The subsurface solver is based on Galerkin finite elements in space, a backward Euler scheme in time with adaptive time steps, and linearization via Newton or Picard iteration.

The surface module is based on resolution using the finite difference method of a one-dimensional diffusion wave equation for overland and channel routing [*Orlandini and Rosso*, 1996, 1998].

$$\frac{\partial Q}{\partial t} + C_k \frac{\partial Q}{\partial s} = D_h \frac{\partial^2 Q}{\partial s^2} + C_k q_s \qquad (3.2)$$

where Q is the discharge along the rivulet/stream channel network [L^3T^{-1}], t is time [T], C_k is the kinematic celerity [LT^{-1}], s is the 1-D coordinate system [L], D_h is the hydraulic diffusivity [L^2T^{-1}], and q_s is the subsurface to surface exchanges of water [L^3/LT]. The routing scheme derives from a discretization of the kinematic wave equation based on the Muskingum-Cunge method. Surface runoff is propagated through a 1-D drainage network of rivulets and channels automatically extracted by a digital elevation model (DEM)-based preprocessor and characterized using hydraulic geometry scaling relationships that relate water surface width and Gauckler-Strickler conductance coefficients to discharge [*Leopold and Maddock*, 1953]. Flow directions are assigned using the classical D8 scheme [*O'Callaghan and Mark*, 1984], the multiple-direction D1 method [*Tarboton*, 1997], or the more recent nondispersive D8-LTD scheme [*Orlandini et al.*, 2003, 2009]. The distinction between overland and channel flow regimes is made using threshold-type relationships based on, for instance, upstream drainage

area criteria [*Montgomery and Foufoula-Georgiou*, 1993]. Lakes and other topographic depressions are identified and specially treated as part of the DEM preprocessing procedure [*Mackay et al*., 1998].

The interaction between FLOW3D and SURF_ROUTE is controlled by the subsurface module that handles atmospheric forcing by implementing a special-case boundary condition. For any given surface node, the boundary condition can switch between a Dirichlet condition and a Neumann condition, depending on the saturation (or pressure) state of that node. A Neumann (or specified flux) boundary condition corresponds to atmosphere-controlled infiltration or exfiltration, with the flux equal to the rainfall or potential evaporation rate given by the atmospheric input data. When, during prolonged or intense periods of rainfall or evaporation the surface node reaches a threshold level of saturation or moisture deficit, the boundary condition is switched to a Dirichlet (specified head) condition, and the infiltration or exfiltration process becomes soil-limited. The boundary condition switching procedure is thus used to partition potential (atmospheric) fluxes into actual fluxes across the land surface (infiltration, exfiltration as evaporation, and exfiltration as return flow) and changes in surface storage (ponding heads) [*Camporese et al.*, 2010].

CATHY has been applied in past studies to real and artificial basins [*Camporese et al*., 2010] in order to illustrate the capability of the model to reproduce a variety of hydrologic processes, for instance the process of runoff generation of Horton [*Horton*, 1933] and Dunne [*Dunne*, 1978], re-infiltration and return flow processes, groundwater levels, and ponding heads dynamics. A modeling study of the impacts of subsurface heterogeneity on the hydrologic response of a small catchment was developed [*Gauthier et al*., 2009], showing that a significant level of heterogeneity is required to achieve appropriate results. The impact of different levels of

landscape representation on the hydrologic response of a medium size basin was also investigated [*Sulis et al*., 2011]: these analyses confirm that grid size significantly conditions land surface representation and therefore hydrologic simulations based on this representation. The more refined the grid is, the better is the land surface representation. CATHY has also been used to evaluate climate change impacts at the catchment scale [*Sulis et al*., 2011], showing that surface flow and evapotranspiration respond differently to precipitation variations. A comparison with another coupled physically based spatially distributed model (Parflow) [*Sulis et al.,* 2010] has been carried out: it shows that ParFlow and CATHY are both very sensitive to the vertical discretization in case of infiltration excess runoff scenario, with some differences between the two models due to the different discretizations used (finite difference for ParFlow, finite element method for CATHY). CATHY has been used for a modeling study of the seepage face boundary condition [*Scudeler et al.,* 2017], and also to study grassed buffer strips [*Gatel et al*., 2016] and the impact of subsurface drainage on watershed storage [*Muma et al.*, 2013, 2016]. The model has also been coupled with the NoahMP [*Niu et al*., 2014] land Surface Model (LSM), allowing for the development an ecohydrologic model, a useful tool to predict floods under climate change conditions.

3.1.2 SWAT

SWAT is a conceptual, continuous time model, capable of simulating long periods for computing the effects of management changes [*Arnold et al*., 1998]. It is designed to predict the impact of land use and management on water, sediment, and agricultural chemical yields in un-gauged basins and it operates on a daily time step. Major model components include weather, hydrology, soil temperature and properties, plant growth, nutrients, pesticides, bacteria and

pathogens, and land management. In SWAT, a watershed is divided into multiple sub watersheds, which are then further subdivided into hydrologic response units (HRUs) that consist of homogeneous land use, management, topographical, and soil characteristics. The HRUs are represented as a percentage of the sub watershed area and may not be contiguous or spatially identified. Alternatively, a watershed can be subdivided into only sub watersheds, whose components can be divided into the following: hydrology, weather, sedimentation, soil temperature, crop growth, nutrients, pesticides and agricultural management.

Water balance is the driving force behind all the processes in SWAT because it impacts plant growth and the movement of sediments, nutrients, pesticides, and pathogens. Simulation of the hydrology of a watershed can be separated into two major divisions. The first division is the land phase of the hydrologic cycle, which controls the amount of water, sediment, nutrient and pesticide loadings to the main channel in each sub basin. The second division is the water or routing phase of the hydrologic cycle, which can be defined as the movement of water, sediments, etc. through the channel network of the watershed to the outlet. Hydrology processes simulated include surface runoff estimated using the Soil Conservation Service (SCS) curve number procedure [*USDA-SCS*, 1972]:

$$Q = \frac{(R-0.2s)^2}{R+0.8s} \tag{3.3}$$

where Q is the daily surface runoff [mm], R is the daily rainfall [mm], and s is a retention parameter [mm], that varies spatially due to changes in soils, land use, management and slope and temporally due to changes in soil water content, and is related to curve number (CN) by the SCS equation [*USDA-SCS*, 1972]

$$s = 254\left(\frac{100}{CN} - 1\right) \tag{3.4}$$

Runoff will only occur when $R > 0.2s$. Percolation is calculated for each soil layer in the profile

and it is modeled with a layered storage routing technique combined with a crack flow model:

$$SW_i = SW_{oi}\, exp\left(\frac{-\Delta t}{TT_i}\right) \quad (3.5)$$

where SW_o and SW are the soil water content [mm] at the beginning and end of the day, respectively, Δt is the time interval (24h), and TT is the travel time (h) through layer *i.*

The movement of soil moisture vertically within the soil profile is simulated using a 1D "tipping bucket" approach where the effective precipitation fills the soil layer to field capacity starting with the top layer. Then, after the layer has reach field capacity, a fraction of the excess soil moisture is moved to the layer below [*Neitsch, Arnold et al*., 2005]. Lateral subsurface flow in the soil profile is calculated simultaneously with percolation. A kinematic storage model is used to predict lateral flow in each soil layer. Groundwater flow contribution to total streamflow in the main channel or reach of each sub basin is simulated by creating a shallow aquifer storage. Water that enters the deep aquifer is assumed to contribute to streamflow somewhere outside of the watershed. Potential evapotranspiration is computed using the Hargreaves, Priestley–Taylor, and Penman–Monteith methods. Actual soil water evaporation is estimated by using exponential functions of soil depth and water content. Plant water evaporation is simulated as a linear function of potential evapotranspiration and leaf area index. If snow is present a complex model of snow cover could be used, that allows non-uniform cover due to shading, drifting, topography, and land cover. Snow melt is controlled by the air and snow pack temperature, the melting rate, and the areal coverage of snow.

SWAT applications range from engineering/practical aims to research studies [*Arnold et al*., 1999a; *Mausbach and Dedrick*, 2004; *Volk et al*., 2007]. The model is used in many countries all over the world. SWAT has been applied to several projects in the USA dealing with the impact of climate change on water supplies and reservoir operations. Examples of climate

change studies include: regional impacts of climate change on groundwater recharge to the Ogallala aquifer [*Rosenberg et al*., 1999]; the impact of climate change on water yields in a high elevation, mountainous basin [*Stonefelt et al*., 2000]; the impact of climate change on Missouri River reservoir operation and water supply [*Hotchkiss et al*., 2000]; and surface water irrigation and riparian management influenced by climate change [*Wollmuth and Eheart*, 2000]. In Europe the model has been used in several ongoing major projects, often in the context of the suitability for the European Framework Directive: for example the BMW project (2004) aims at testing and demonstrating the use of integrated models such as SWAT for use in the implementation of the European Water Framework Directive. Within the CHESS project (2001), SWAT was used to explore the effects of climate change on water quality in European rivers. SWAT was also applied and modified within the Joint Research Project SFB 299 since 1997 to analyze the impact of land use change on water and nutrient cycles of low mountain range catchments in central Germany [*Fohrer et al*., 2002].

3.1.3 TOPKAPI-X

TOPKAPI-X is a physically based distributed rainfall-runoff model developed with the aim to improve the original model TOPKAPI [*Liu and Todini*, 2002]. The model consists of five main modules that simulate hydrologic processes that include subsurface flow, overland flow, channel flow, evapotranspiration, and snow, using user definable time steps (from few minutes to hourly or daily time steps). Four nonlinear reservoir differential equations, obtained by combining continuity of mass and momentum equations and solved using a 2D finite difference method, are used to describe the subsurface flow in the first and second layer, overland flow, and channel flow. The equation of mass continuity of each of the four reservoirs corresponding to

cell *i* at time *t* can be written as a classical differential equation of continuity [*Birsan*, 2013]:

$$\frac{dV_i}{dt} = Q_i^{in} - Q_i^{out} \quad (3.6)$$

where V_i is the total volume stored in the reservoir, $\frac{dV_i}{dt}$ is the rate of change of water storage, Q_i^{in} is the total inflow rate to the reservoir, Q_i^{out} is the total outflow rate from the reservoir. The kinematic wave approach used in TOPKAPI (by neglecting the acceleration terms in the St. Venant equation) leads to a nonlinear relationship between Q_i^{out} and V_i, transforming Eq.3 into an ordinary differential equation:

$$\frac{dV_i}{dt} = Q_i^{in} - b_i V_i^{\alpha} \quad (3.7)$$

where α e b_i are constants that depend on the characteristics and type of the reservoir [*Vischel et al.,* 2008].

The soil module is fundamental to determine flow in unsaturated conditions. TOPKAPI-X represents the soil zone by dividing it into two layers with different parameters, each represented as a nonlinear reservoir, whose interaction allows both Dunne and Horton runoff mechanisms. Therefore subsurface flow can occur in two layers, superficial and deep. The superficial layer is characterized by thin thickness and high hydraulic conductivity, because of the macroporosity, and it plays a key role in direct flow contributions to the drainage network and in the activation of the saturated area, which causes surface flow. The deep layer is characterized by a greater thickness and reduced hydraulic conductivity, due to the more compact soil, and plays a key role in determining infiltration and base flow. The flow paths and slopes are evaluated starting from a DEM, according to a relationship based on the principle of minimum energy cost [*Band*, 1986], or they can be evaluated externally, thanks to the compatibility of the model with any GIS software. In the new code TOPKAPI-X flow directions are assigned by using the classical D8 scheme. Potential evapotranspiration is estimated using

the Thornthwaite and Mather formula [*Thornthwaite and Mather*, 1955]. Actual evapotranspiration is computed with the radiation method [*Doorembos et al.,* 1984]. The snowmelt module is driven by a radiation estimate (the same used for computing the evapotranspiration) based on air temperature measurements.

The basic assumptions of the TOPKAPI-X model at the level of the grid cell are the following: 1) precipitation is assumed to be constant in space and time over the integration domain (namely the single grid cell and the basic time interval); 2) the slope of the water table is assumed to coincide with the slope of the ground; this constitutes the fundamental assumption of the approximation of the kinematic wave in the Saint Venant equations; 3) local transmissivity, like local horizontal flow, depends on the total water content of the soil, i.e., it depends on the integral of the water content profile in a vertical direction; 4) saturated hydraulic conductivity is constant with depth in a surface soil layer and much higher than that of the deeper layer.

TOPKAPI-X requires low computation time, compatible with times required for flood event forecasting in real time. It can be coupled with hydraulic and meteorological models. TOPKAPI-X has already been successfully implemented as a research and operational hydrologic model in several catchments in the world (Italy, Spain, France, Ukraine, China) [*Liu and Todini*, 2002; *Bartholomes and Todini*, 2005; *Liu et al.*, 2005; *Martina et al.*, 2006].

3.1.4 tRIBS

tRIBS is a process-based, distributed hydrologic model which is able to continuously represent the different hydrologic processes: canopy interception and transpiration, evaporation from bare and vegetated soils, infiltration and soil moisture redistribution, shallow subsurface transport, overland and channel flows. Hydrologic processes are simulated at high temporal

resolution (in most cases, 3.75 min). The model represents topography through triangulated irregular networks (TINs). This allows significant reduction of computational nodes as compared to grid-based models [*Vivoni et al.,* 2004, 2005], by representing the domain with multiple resolutions: larger number of nodes where the topography is complex and less details in flat homogenous areas. The use of TINs has also the advantage of preserving linear features such as stream networks and terrain breaklines. Voronoi polygons are the basic computational elements, in which the domain is discretized starting from TIN. In each element the governing equations are solved using a finite difference control-volume approach [*Ivanov et al.,* 2004a].

Considering local dynamics and lateral mass exchanges, the model can reproduce the spatially distributed hydrologic response of a catchment. In each element, the model explicitly simulates the different processes involved in the hydrologic cycle: 1) Rainfall interception is computed following the canopy water balance model [*Rutter at al.,* 1971]; 2) Radiation and surface balance are computed using the combination equation [*Penman*, 1948; *Monteith*, 1965], gradient method and force-restore [*Lin*, 1980; *Hu and Islam*, 1995]; 3) Evapotranspiration is estimated through three components [*Wigmosta et al*., 1994]: evaporation from wet canopy, canopy transpiration and bare soil evaporation [*Deardorff*, 1978]; 4) Infiltration scheme is based on the resolution of the two-dimensional modified Green-Ampt model in heterogeneous and anisotropic soils (Eq. 5) [*Cabral et al*., 1992; *Beven*, 1982, 1984]:

$$q_n(N_f) = -K_{eff}\left[\frac{h_f(N_f)}{N_f} - 1\right] \qquad (3.8)$$

where $q_n(N_f)$ is the normal component of the flow vector, N_f is the wetting front depth, h_f is the effective wetting front capillary pressure and K_{eff} is the harmonic mean of conductivities over the saturated depth. For the surface saturated conductivity K_{0n} exponentially decaying with depth at the rate f, K_{eff} can be expressed as

$$K_{eff}(N_f) = K_{0n} \frac{f(N_f)}{e^{f N_f - 1}} \quad (3.9)$$

Different saturation levels in the soil column are given by the evolution of moisture fronts (unsaturated zone) [*Morel- Seytoux et al*., 1974; *Neuman,* 1976] coupled with variable groundwater table depths (saturated zone). Topography and soil drive lateral fluxes in vadose zone and groundwater during storm and interstorm periods [*Smith et al*., 1993; *Childs and Bybordi*, 1969]. Accounting for these detailed processes, runoff generation is possible via four mechanisms: saturation excess, infiltration excess, perched subsurface stormflow, and groundwater exfiltration. 5) A kinematic wave routing model is used to simulate transport of water in the channel network [*Goodrich et al*., 1991; *Singh*, 1996]. The one-dimensional continuity equation for unsteady free surface flow is

$$\frac{\partial F}{\partial t} + \frac{\partial Q}{\partial x} = R_b \quad (3.10)$$

where F is the cross-sectional area, Q is the discharge along the x axis, R_b is the lateral influx of water into the channel per unit length. 6) The actual evapotranspiration (ET_a) losses are estimated as a fraction of the potential evapotranspiration (ETP) based on the soil moisture available in the upper soil layer, using a piecewise-linear equation with different parameterization if applied to bare soils or vegetated surfaces [*Mahfouf and Noilhan*, 1991; *Ivanov et al*., 2004a].

Model parameters can be divided into three groups: routing parameters, which are spatially uniform, and soil and vegetation parameters, which vary in space and are provided through maps and look-up tables. A detailed description of the physical processes simulated by the model and its parameterization is given by Ivanov et al. [2004a, b].

Applications of the tRIBS model to date have ranged from multiyear, continuous simulations using NEXRAD [*Ivanov et al.,* 2004a, 2004b], to event-based hydrograph

predictions based on radar now-casting fields [*Vivoni et al*., 2006] or short-lead-time NWP fields. tRIBS has been used to track hydrologic response to precipitation forcing and downscaled with different techniques [*Forman et al*., 2008; *Mascaro et al*., 2010]. Model applications in the academic field range from intercomparison projects [*Reed et al.*, 2004] to climate change impact assessment [*Liuzzo et al*., 2010] to eco-hydrology [*Vivoni et al*., 2014].

3.1.5 WASIM

WASIM is a process based and fully distributed hydrologic model [*Schulla*, 2015], originally developed to evaluate the influence of climate change on water balance and runoff regime in pre-alpine and alpine river catchments [*Shulla*, 1997]. The model can calculate water balances for catchments with the size of < 1 km^2 up to several 10000 km^2 where the spatial discretization is given by a regular or irregular raster (model grid). By using the raster format, interoperability with other software (e.g. GIS software) is guaranteed. The time discretization can be chosen variably, time steps of some minutes up to one day are possible.

The hydrologic processes are represented by different modules, which are processed for each time step and one by one for the entire catchment grid. The type of precipitation is calculated for each grid cell under consideration of the air temperature. The melting rate can be determined by use of the temperature- index-approach, temperature-wind-approach, or a combination approach. Snow accumulation and snowmelt are modeled according to Anderson [1973] and Braun [1985]. Surface runoff is created for each grid cell as the sum of infiltration excess and snowmelt along the topographic gradient towards the next river. It is assumed that saturated hydraulic conductivity decreases (depending on soil texture) with depth according to a recession constant. Discharge routing is performed by a kinematic wave approach using different

flow velocities for different water levels in the channel. After the translation of the wave a single linear storage is applied to the routed discharge considering diffusion and retention [*Schulla and Jasper*, 2001]. Vertical fluxes in the unsaturated soil zone are calculated by using the 1D Richards equation that is solved numerically using finite differences schemes. Therefore, the soil profile has to be discretized into numeric layers. Due to some differences in the notation used in the CATHY model, the Richards equation is repeated here:

$$\frac{\partial \vartheta}{\partial t} = \frac{\partial q}{\partial z} = \frac{\partial}{\partial z}\left(-k(\vartheta)\frac{\partial \psi}{\partial z}\right) \qquad (3.11)$$

where ϑ is the water content [m^3/m^3], t is time [s], k is the hydraulic conductivity [m/s], ψ is the hydraulic head, q is the specific flux [m/s], and z is the vertical coordinate [m].

The flux q between two layers is calculated with:

$$q = k_{eff}\left(\frac{h_h(\vartheta_u) - h_h(\vartheta_l)}{0.5(d_u + d_l)}\right) \qquad (3.12)$$

where q is the flux between two discrete layers [m/s], k_{eff} is the effective hydraulic conductivity calculated as an harmonic average of the layers, h_h is the hydraulic head, and d is the thickness of the layers under consideration.

A one-dimensional finite difference scheme is used – after extracting the amount of evaporating water – to solve equation (3.11). The dependence of the suction head and the hydraulic conductivity on soil moisture content is parameterized according to van Genuchten [1985].

The basics for the groundwater model is given by the flux equation that is obtained from the continuity equation and the Darcy equation [*Jasper et al*., 2002]. The change of the water storage in a control volume during time equals the difference between inflows and outflows. The calculation of the groundwater flow is independent of the unsaturated soil and uses an implicit finite-differences-scheme [*Rieger*, 2012]. WASIM calculates separately potential transpiration from plant leaves, evaporation from bare soil, and evaporation from interception surfaces.

Several approaches for calculating potential evapotranspiration are available: Penman-Monteith, Wending, Haude, and Hamon. Actual evapotranspiration is then determined by reducing the potential evapotranspiration using a relation between the soil water content and the actual capillary pressure.

Various model applications covering catchment sizes from 3 to 145000 km^2 have demonstrated its capabilities in addressing different hydrologic problems, such as the development of appropriate strategies for sustainable water management in arid and semi-arid regions [*Schulla et al*., 1999], the simulation of glacier melt and glacier runoff in partly and heavily glacierized high-alpine catchments [*Klok et al*., 2001], the validation of runoff and its components in mountainous watersheds [*Gurtz et al*., 2001; *Jasper et al*., 2002; *Kunstmann and Stadler*, 2005], and to assess the impact of climate change [*Schulla*, 1997; *Kunstmann et al*., 2004; *Cornelissen et al*., 2013; *Meyer et al*., 2016]. It is also possible to use WASIM for prediction of flood events [*Schulla*, 2015].

Model	Discretization scheme	Infiltration/Subsurface flow	Surface flow	Topographic representation
CATHY	Finite element	Richards' equation	Diffusive wave	Regular grid
SWAT	Subwatershed	Tipping bucket	Soil Conservation Service (SCS)	Homogeneous hydrologic units
TOPKAPI-X	Finite difference	Kinematic wave	Kinematic wave	Regular grid
tRIBS	Finite difference control volume	Modified Green-Ampt	Kinematic wave	Triangulated irregular network
WASIM	Finite difference	Richards' equation	Kinematic wave	Regular grid

Table 3.1. Summary and comparison of the structure and characteristics of the hydrologic models.

3.2 Climate models

Climate change impact assessments form the basis for the development of suitable climate change adaptation strategies [*Gädeke et al*., 2014]. Climate models are numerical tools to simulate the past, present, and future of Earth's climate [*Deidda et al*., 2013]. In general global climate models (GCMs) are suited to provide large-scale climate predictions (over the whole planet), but this scale is too large to allow a suitable assessment of the local impacts of climate change on the hydrological cycle and water resources availability at a river basin level, which can be of interest for local policymaking. The most common approach to refine GCM outputs is to use downscaling tools. Regional climate models (RCMs) are high-resolution models that take advantage of detailed representations of natural processes at high spatial resolutions. However, they are run on a limited domain and thus require boundary conditions from a driving GCM [*Giorgi and Mearns*, 1999; *Rummukainen*, 2010].

Climate change impacts at the catchment scale can be evaluated by coupling global and regional climate models (GCMs and RCMs) with distributed hydrologic models using downscaling techniques to bridge the scale mismatch between climate and hydrologic models [*Piras,* 2014].

Deidda et al. [2013] analyzed outputs of fourteen GCM-RCM combinations from the ENSEMBLES project in the seven study regions of CLIMB to identify those exhibiting the best performance in terms of representing the intra-annual variability of precipitation and temperature in the present climate. The models selected for the Rio Mannu catchment are listed in Table 3.2, including the acronyms used in this work (ECH-RCA, ECH-REM, ECH-RMO and HCH-RCA). The choice was constrained by the condition to keep at least one RCM forced by two GCMs (ECH-RCA and HCH-RCA) and more RCMs nested in the same GCM (ECH-RCA, ECH-REM, ECH-RMO), in order to explore a minimum degree of climate uncertainty in both GCM and

RCM representations. For these models, outputs were extracted on the Rio Mannu catchment for a reference (1971-2000) and a future (2041-2070) period under the A1B emission scenario [*Nakićeović et al*., 2000], which was considered one of the most realistic and provided the most complete dataset within the ENSEMBLES models. To limit the well-known discrepancies (especially in small basins) in reproducing climatological features and observed seasonality [*Lucarini et al*., 2007; 2008; *Hasson et al*., 2013; 2014], a large-scale bias correction was applied to precipitation and temperature fields using the daily translation method [*Wood et al*., 2004; *Maurer and Hildago*, 2008; *Sulis et al*., 2012] with the E-OBS dataset as reference [*Haylock et al*., 2008]. In addition, downscaling techniques were applied to disaggregate precipitation and temperature grids from the coarse resolution of the climate models (~25 km, 24 h) to finer resolutions (5 km, 1 h) suitable for hydrologic modeling. For precipitation, the multifractal downscaling model of Deidda et al. [1999] and Deidda [2000] was utilized, while temperature was interpolated in space through lapse rate corrections as in Liston and Elder [2006]. Lastly, the residual biases in precipitation due to the coarseness of the rain gage network used for E-OBS were corrected by a procedure of local-scale bias correction. More details on the bias correction and downscaling techniques are provided in Piras et al. [2014].

	Climatological center and model	Acronym
Global Climate Models, GCMs	Hadley Centre for Climate Prediction, Met Office, UK HadCM3 Model	HCH
	Max Planck Institute for Meteorology, Germany ECHAM5 / MPI Model	ECH
Regional Climate Models, RCMs	Swedish Meteorological and Hydrological Institute (SMHI), Sweden RCA Model	RCA
	Max Planck Institute for Meteorology, Hamburg, Germany REMO Model	REM
	Koninklijk Nederlands Meteorologisch Instituut (KNMI), Netherlands RACMO2 Model	RMO

Table 3.2. List of global climate models (GCMs) and regional climate models (RCMs) from the CLIMB project with corresponding climatological center and model and acronyms adopted in this work. The four GCM-RCM combinations used are ECH-RCA, ECH-REM, ECH-RMO and HCH-RCA.

Since climate projections of the CLIMB project do not cover also the Flumendosa basin, for the latter and the same climate models listed in Table 3.2 we used the precipitation fields obtained on the island of Sardinia at 1 km resolution during the period 1951-2100 from Mamalakis et al. [2017], that proposed a parametric approach for simultaneous bias correction and statistical downscaling, using (i) a two component theoretical distribution model (a generalized Pareto model for rainfall intensities above a specified threshold, and an exponential model for lower rainrates), and (ii) proper interpolation of the corresponding distribution parameters on the high-resolution grid, using kriging for uncertain data. For the temperature data instead, the hourly temperature grids obtained for the Rio Mannu catchment were used to derive the hourly temperature grid values on the Flumendosa basin adopting the same method described in Caracciolo et al. [2017]. In particular we first computed for each hour the spatial mean of

temperature grid values of the Rio Mannu catchment rescaled at sea level T_{mean}, using the following equation to scale each grid value of the Rio Mannu basin:

$$T_{sea} = T_j - (H_{sea} - H_j) \cdot \gamma \quad (3.13)$$

where T_{sea} is the temperature of each cell of the Rio Mannu catchment scaled at sea level, T_j is the temperature value of each cell of the Rio Mannu catchment, H_{sea}= 0 is the sea elevation, H_j is the elevation of each cell of the Rio Mannu catchment, and γ is the lapse rate (i.e., the temperature decrease per unit of elevation) that we assumed equal to 0.0057 °C/m, as in Caracciolo et al., [2017].

Then we obtained the temperature grid for the Flumendosa basin on the basis of the equation:

$$T_i = T_{mean} - (H_i - H_{sea}) \cdot \gamma \quad (3.14)$$

where T_i is the temperature of each cell of the Flumendosa basin, T_{mean} is the hourly mean temperature at the sea level for the Rio Mannu basin, and H_i is the elevation of each cell of the Flumendosa basin.

4. Results

4.1 An application of parameter transferability between three physically based distributed hydrologic models

In this section a detailed comparison of the responses obtained with the three physically based hydrologic models, CATHY, tRIBS, and TOPKAPI-X, implemented on a medium-sized Mediterranean catchment characterized by a semi-arid climate, the Rio Mannu, is shown.

Since the tRIBS model was previously implemented on the basin, for the two other models the same datasets were adopted, including geospatial data of land surface properties and hydrometeorological forcing, with the aim to test the transferability of parameters between the three physically based hydrologic models. The most prominent model distinction between the three models is that CATHY is fully integrated with 3D subsurface flow over the entire domain compared to the coupling between 1D unsaturated flow and 1D saturated flow in tRIBS and 1D unsaturated flow and 2D saturated flow in TOPKAPI-X. The soil and land cover parameters calibrated for the application of tRIBS were used to guide the calibration of the other two hydrologic models. The hypothesis of direct transferability of the parameters values was explored. While this led to satisfactory performances for TOPKAPI-X and CATHY during the calibration period, CATHY produced very low streamflow in the drier validation period. To circumvent this, for the CATHY model, an hypothesis of soil crusting was assumed and the first soil layer was modeled with a lower saturated hydraulic conductivity.

In the following a brief overview of the setup, calibration, and validation strategies adopted by Mascaro et al. [2013a] for the tRIBS model are first described. This effort was part of the CLIMB research project [*Mascaro et al., 2013b*; *Piras et al*., 2014]. Next, the approach implemented for the TOPKAPI-X and CATHY models is illustrated. The results during

calibration and validation periods for the three hydrologic models are then illustrated.

4.1.1 Model setups

4.1.1.1 tRIBS

The spatial domain for the tRIBS model was created by generating a TIN with an equivalent resolution of ~50 m from the 10-m resolution DEM [*Vivoni et al*., 2004; *Mascaro et al*., 2013]. In tRIBS only two layers are possible to schematize the soil: the unsaturated and the saturated zones, which are coupled accounting for the interaction of the moving infiltration front with a variable groundwater table. The model was calibrated against discharge observations at the outlet. The calibration was limited to the two most sensitive parameters, including saturated hydraulic conductivity at the surface (K_S) and the conductivity decay parameter (*f*), used to model the variation of K_S with soil depth [*Cabral et al*., 1992]. For each soil class (see Figure 2.3a) the values of K_S and *f* were selected within physically plausible ranges taken from Rawls et al. [1982]. Values from the literature [*Rawls et al*., 1982; *Noto et al*., 2008; *Montaldo et al*., 2008; *Vivoni et al*., 2010] were instead adopted for the other soil and vegetation parameters. The calibration was conducted manually to minimize the difference between observed and simulated discharge. Table 4.1 presents the parameter values for the main soil classes for the tRIBS model, which were assumed also for the two other models.

Soil Properties	Variable (unit)	Clay loam –Clay	Sandy loam – Loam	Sandy loam – Sandy clay loam
Area	A (%)	36.66	31.82	19.59
Saturated hydraulic conductivity	K_s (ms^{-1})	$1.67 \cdot 10^{-7}$	$3.67 \cdot 10^{-6}$	$8.33 \cdot 10^{-7}$
Conductivity decay	f (m^{-1})	0.51	0.96	0.96
Saturated soil moisture	θ_s (-)	0.385	0.434	0.330
Residual soil moisture	θ_r (-)	0.090	0.027	0.068
Stress soil moisture	θ^* (-)	0.308	0.347	0.264
Pore size distribution index	m (-)	0.165	0.252	0.319
Air entry pressure head	ψ_a (m)	-0.373	-0.112	-0.281

Table 4.1. Parameters values of the tRIBS model for the major soil classes of the Rio Mannu catchment, assumed also for the two other models, TOPKAPI-X and CATHY.

The tRIBS model was provided with precipitation grids obtained through the downscaling procedure explained in detail in Mascaro et al. [2013b]. In a basin with a semi-arid climate, the contrasts of climate conditions between different years could be important. Several authors proposed, adapted, or applied testing schemes to evaluate a model's ability to perform well under contrasted climate conditions [*Refsgaard and Knudsen*, 1996; *Xu*, 1999; *Donnelly-Makowecki and Moore*, 1999; *Seibert*, 2003*; Xu et al*., 2005; *Refsgaard et al., 2006*; *Gorgen et al*., 2010; *Vaze et al*., 2010; *Merz et al*., 2011]. All are inspired by the differential split-sample test (DSST), formulated by Klemes [1986], that recommends calibrating the model on data prior to a change (pre-change) and validate it on post-change data, so existing observations with dissimilar climatic characteristics can be used to calibrate and validate models on time periods [*Seiller et al*., 2012]. In particular, Klemes suggest using a wet period for calibration and a drier

period for validation, especially when the hydrologic model is used to evaluate the effects of climate change. To calibrate and validate the tRIBS models, among the daily discharge data available in the period 1925-1935, three consecutive years were chosen (1930-1932), during which the published rating curves did not vary significantly and problems were not reported. Among those three years, the year 1930 presented the major number of flood events and was then selected for the calibration, while 1931 and 1932 were used to validate the model performance.

4.1.1.2 TOPKAPI-X and CATHY

The spatial domain of TOPKAPI-X and CATHY consists of regular grids. These were obtained by aggregating the 10 m DEM at resolutions of 100 m and 250 m, respectively. These values were chosen as a compromise between accuracy and computational requirement of each model. Both models were calibrated and validated in the same period adopted for tRIBS, using the same soil texture and land cover maps, as well as hydrometeorological forcings.

For the TOPKAPI-X model only two layers are possible to discretize the soil, superficial and deep: the first thin layer is 0.5 m thick while the bottom layer is 1 m thick. To parameterize TOPKAPI-X the same values of of K_s, ϑ_s, ϑ_r, and air entry pressure head ψ_a used for the tRIBS model (see Table 4.1) were assumed. For the deep layer K_s, values were taken one order of magnitude lower.

For the CATHY model, on the basis of the 250 m resolution the 3-D subsurface grid was constructed by subdividing each DEM cell into two triangles and then projecting this 2-D surface mesh vertically for a depth handled for each cell from the assumed base map and 12 layers. The resulting 3-D grid contains 104819 nodes. The bottom and lateral boundaries of the domain were

assumed to be impermeable. The same range of values for $K_S, \vartheta_s, \vartheta_r$, air entry pressure head ψ_a, conductivity decay parameter (*f*), and van Genuchten parameters for soil moisture characteristics used for the tRIBS model for the different soil texture classes (Table 4.1) was assumed. The soil hydraulic properties were described by the van Genuchten and Nielsen [1985] relationships, using for the CATHY model equation (9) of Ghanbarian-Alavijeh et al. [2010] to convert the value of pore distribution index *m* used for tRIBS for each soil texture classes into the empirical parameter *n*. The threshold level of moisture deficit (in terms of pressure head) for the CATHY model was assumed at the value P_{min} = -3 m, according to the threshold in soil moisture θ^* used for the tRIBS model. The channel network was identified from the DEM of the catchment using an upstream drainage area threshold of 5 km^2 on the basis of visual similarity between the extracted network and the streamlines depicted on topographic maps. Structural parameters for the channel and overland flow networks were calibrated using values assumed for tRIBS (Manning coefficient for channel flow 0.04 $s/m^{1/3}$) and reported in literature studies as a basis [*Abrahams et al*., 1996; *Emmett*, 1970; *Orlandini*, 2002; *Weltz et al.,* 1992]. The values obtained are reported in Table 4.2.

For TOPKAPI-X and CATHY models we utilized the mean areal precipitation (MAP) series derived by the synthetic grids used for tRIBS at hourly resolution. For the two models, moreover, the same hourly time series of downscaled potential evapotranspiration basin-averaged used for tRIBS was assumed.

Parameter	Hillslope cells	Channel cells
Reference drainage area $A_s\ (m^2)$	0.1×10^6	48.5×10^6
Reference discharge $Q_f\ (m^3/s)$	0.007	2
Water surface width $W\ (A_s, Q_f)\ (m)$	0.3	10
Gauckler – Strickler conductance coefficient $k_s\ (m^{1/3}/s)$	0.5	25 (From tRIBS)
"At a station" scaling exponents [a], [b], b' and y'	0.26, 0	0.26, 0
"Downstream" scaling exponents [a], [b], b'' and y''	0.5, 0	0.5, 0

$For\ [a]\ W(A,Q) = W(A_s,Q_f)Q_f(A/A_s)^{(b''-b')}Q^{b'}$; $For\ [b]\ k_s(A,Q) = (A_s,Q_f)Q_f(A_s)^{-y'}(A/A_s)^{(y''-y')}Q^{y'}$

Table 4.2. Hydraulic geometry parameters for the surface routing module of the CATHY model.

4.1.2 Discussion during calibration and validation periods

Different sets of simulations using as atmospheric input the ensemble of 50 downscaled precipitation series which were assumed as forcing for the tRIBS model, each representing a statistically possible scenario, were carried out also with the hydrologic models TOPKAPI-X and CATHY during calibration (year 1930) and validation (years 1931 and 1932) periods. For each member of this ensemble, generated with the STRAIN multifractal model [*Deidda*, 2000], the total daily precipitation volume is the same, whereas the disaggregation in time and space changes [*Mascaro et al.*, 2013b]. A spin-up interval of 2 years prior to the start of the calibration period was used for the tRIBS model, following the approach of Vivoni et al. [2005], and for the

TOPKAPI-X model. For the CATHY model, initial conditions, in terms of pressure heads in each node of the domain, were defined with the drainage of the basin, starting from saturated condition, with a zero value atmospheric input, until the runoff attained the value observed at the beginning of 1930. The setting of this initial condition required several tests according to the ability of the basin to reach steady state conditions that depend essentially on the K_S values. In this case 100 days drainage with zero value atmospheric input was used, using the same range of saturated hydraulic conductivity values of tRIBS for the different soil texture classes.

Figure 4.1 shows the comparison of simulated and observed discharge for the calibration year 1930 with the three models tRIBS, TOPKAPI-X, and CATHY, using the ensemble of 50 downscaled precipitation series. The two insets allow to better visualize the comparison over two time periods with significant flood events. The difference between the downscaled ensemble average (MAP_D) and observed (MAP_O) mean areal precipitation at the daily scale is also plotted for each inset. Observed series of mean areal precipitation were derived applying the Thiessen polygon method to the observations of the twelve rain gages. We can notice that globally the three hydrologic models reproduce the shape and time of the major flood events, with some differences. In particular, the three models are not able to reproduce the peaks labeled as M (missed), due to a previous period of underestimated precipitation (negative MAP_D - MAP_O), but with different degree of underestimation. In fact, CATHY and TOPKAPI-X simulate quite well the recession curves, while tRIBS has a tendency to simulate steeper recession limbs. Moreover the timing of flood peaks can be also affected by the differences in observed and simulated MAP, as illustrated by the label D (delayed). These discrepancies may not be entirely attributed to a failure of the downscaling procedure. In fact the sub-hourly resolution of tRIBS and CATHY outputs and hourly resolution of TOPKAPI-X allow to better represent the hydrograph

dynamics with respect to the coarse sampling of stage levels (daily) that is not sufficient to capture the high frequency of the discharge variability. However since the downscaling tool redistributes in stochastic fashion the daily rainfall volumes from large to smaller domain and times, it may be possible that on some days the exact spatial localization of the storms is not captured by the multifractal model [*Mascaro et al*., 2013b].

We can also note that the CATHY model is not able to reproduce the final pick of discharge during 1930: in fact since the soil dries out after the warm months, the model allows water to infiltrate into the soil, so it is not able to reproduce the observed Horton runoff. Table 4.3 reports the Nash-Sutcliffe index (NS) [*Nash and Sutcliffe*, 1970] for the calibration year evaluated using the observed and simulated water volume for the three hydrologic models. This parameter can vary from -∞ to 1, with better performance closer to 1. The minimum, mean, and maximum values of the 50 ensemble members are reported for different aggregation times (daily, weekly, and monthly).

The lowest values of NS were obtained at daily resolution because at this scale the direct correspondence between observations and simulations was more affected by the different sampling time step and by mismatching in the disaggregated forcing [*Piras*, 2014]. When larger time scales were considered, NS increased and reached a mean value of 0.55 at monthly resolution for the tRIBS model, 0.61 for TOPKAPI-X, and 0.62 for CATHY. In terms of total runoff volume, the ensemble mean for the three hydrologic models together with the standard deviation across the 50 members is reported in Table 4.4. To better illustrate the model performance, Figure 4.2 shows the comparison between the observed flow duration curve (FDC) and the 90% confidence intervals from the 50 ensemble simulations for the three hydrologic models. We can notice that the shape of the observed FDC is well reproduced for the three

hydrologic models. The tRIBS model notably underestimates the discharge values corresponding to the percentage of exceedance of 5 to 10 %, due to a tendency to simulate steeper recession limbs.

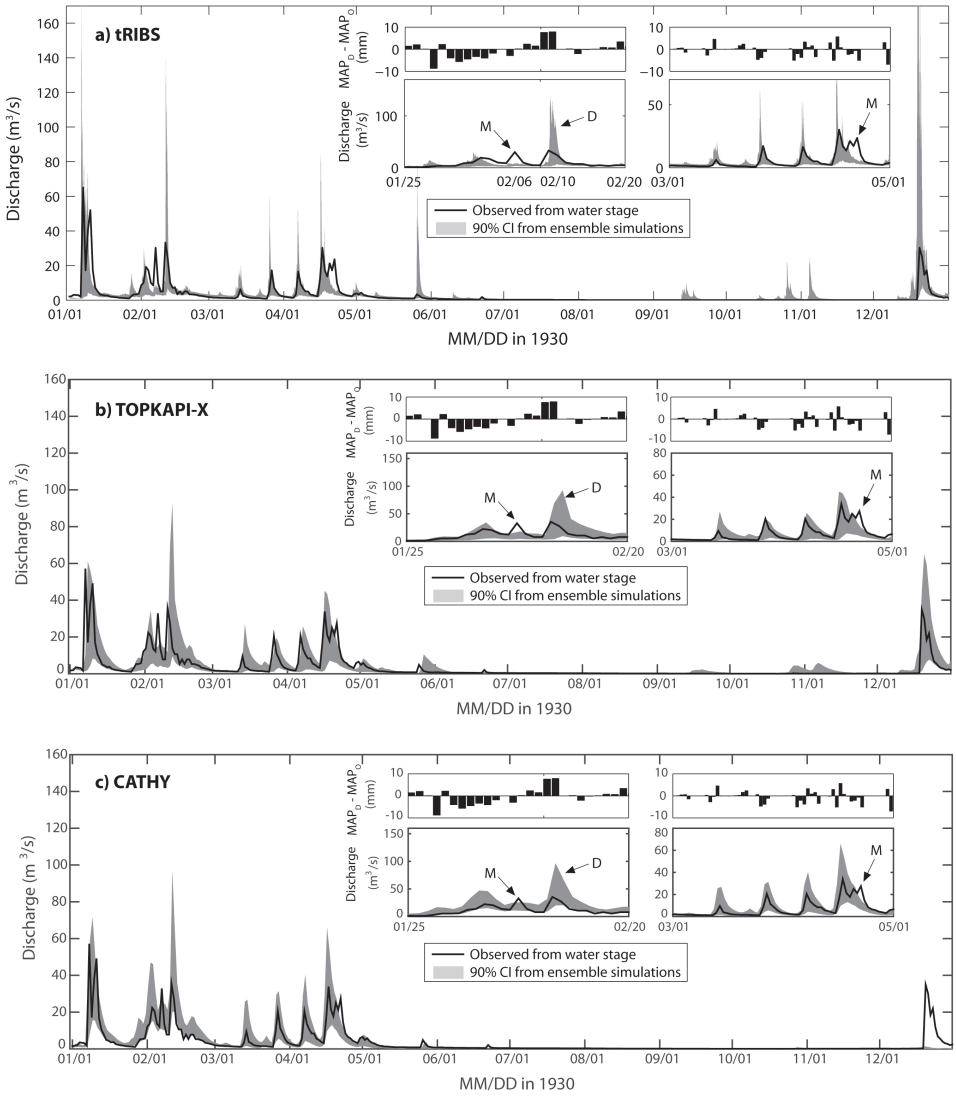

Figure 4.1. Calibration simulation for the tRIBS (a), TOPKAPI-X (b), and CATHY (c) hydrologic models applied to the Rio Mannu catchment. Observed discharge is compared against 90% confidence intervals (CI) derived from 50 ensemble simulations for each of the models. In the insets, a zoom on two periods with significant flood events is shown in order to better

highlight the differences between the daily downscaled ensemble average (MAP_D) and observed (MAP_O) mean areal precipitation time series. Peaks labeled as M (missed) and D (delayed) are also reported.

	tRIBS	**TOPKAPI-X**	**CATHY**
Time scale	**Calibration NS Min, Mean, Max**	**Calibration NS Min, Mean, Max**	**Calibration NS Min, Mean, Max**
Daily	-3.53, 0.07, 0.61	-2.77, 0.27, 0.63	-0.20, 0.40, 0.66
Weekly	-5.50, 0.46, 0.83	-1.85, 0.48, 0.81	-0.07, 0.56, 0.80
Monthly	-0.06, 0.55, 0.89	-1.59, 0.61, 0.95	0.08, 0.62, 0.85

Table 4.3. Nash-Sutcliffe index (NS) for the calibration year 1930, evaluated using the observed and simulated water volume at daily, weekly, and monthly time scales, for the three hydrologic models.

		Total runoff volume (mm)	
		Calibration period	**Validation period**
tRIBS	μ	170	103
	σ	70	17
TOPKAPI-X	μ	200	75
	σ	124	53
CATHY	μ	205	78
	σ	86	55
Observed	μ	183	147

Table 4.4. Total runoff volume (mm) observed and computed as ensemble mean and standard deviation across the 50 members with the three hydrologic models, during the calibration and validation periods.

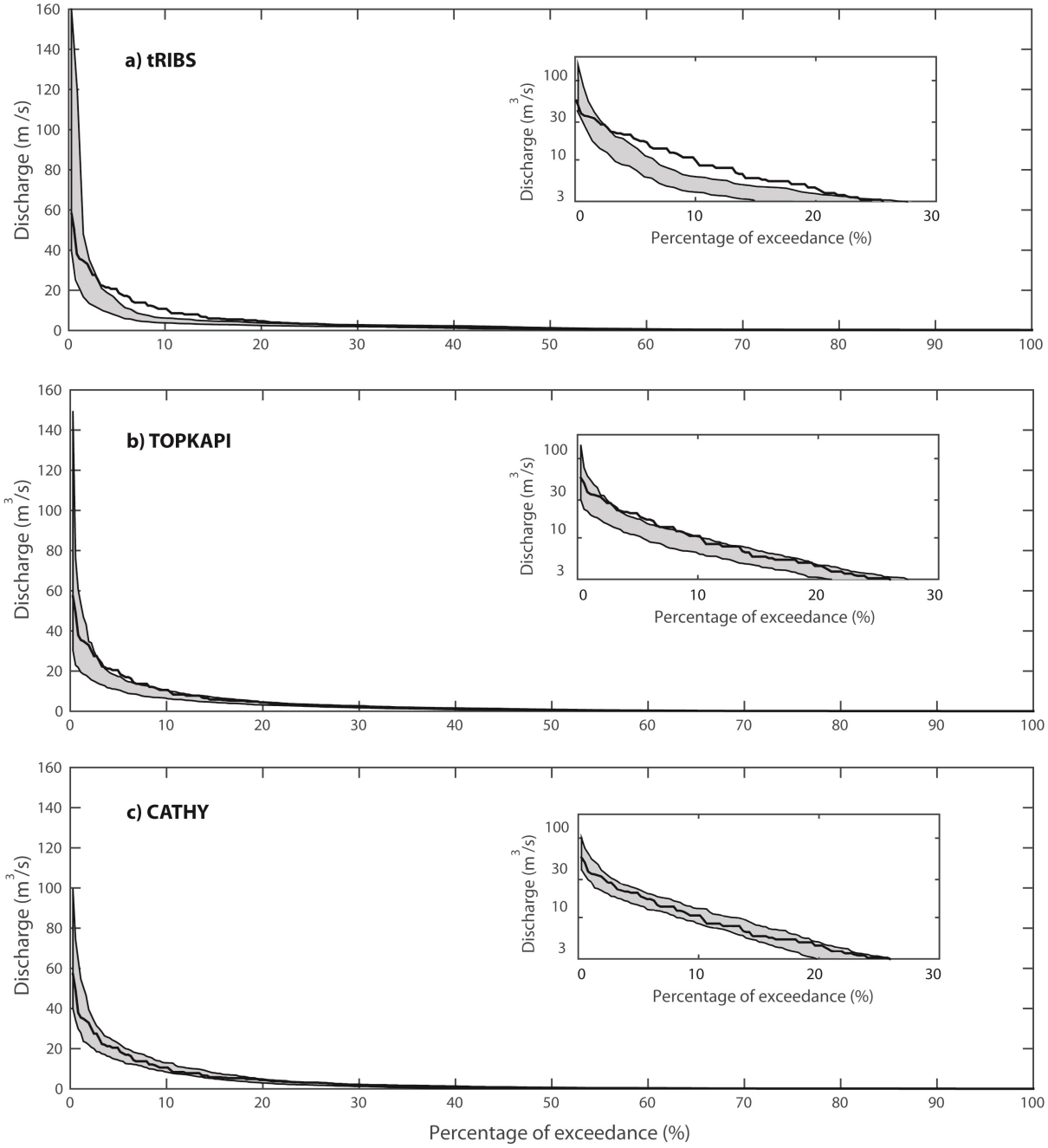

Figure 4.2. Comparison between the observed flow duration curve (FDC) and the 90% confidence intervals from the 50 ensemble simulations for the tRIBS (a), TOPKAPI-X (b), and CATHY (c) hydrologic models, during the calibration period (year 1930).

Results for the validation period, characterized by a very dry climate (years 1931 and 1932), are shown in Figure 4.3. We can notice the good performances in reproducing the discharge time series over year 1931 and most of 1932 for tRIBS and TOPKAPI-X. In the period from October to December 1932, the two models simulate a number of peaks that were not observed, while sometimes underestimating the discharge, due to the same reasons discussed for the calibration period. CATHY is not able to generate any discharge except at the beginning of 1931. This is due to the same reason discussed for the final peak missed at the end of 1930. For this reason for the CATHY model during the validation period an hypothesis of soil crusting was assumed, on the basis of which the first thin layer is modeled with a lower saturated hydraulic conductivity. Assouline [2013] provided a review of the approaches proposed to model infiltration into sealed soils. Hillel and Gardner [1969, 1970] were the first to hypothesize that a sealed soil could be modeled as a uniform soil profile capped with a saturated thin layer of low permeability. This was applied in different studies [*Ahuja*, 1974, 1983; *Moore*, 1981a; *Parlange et al*., 1984b]. Variations and extensions of this basic approach included the simulation of infiltration with time-dependent seal [*Farrell and Larson*, 1972; *Whisler et al*., 1979; *Moore*, 1981b; *Ahuja*, 1983; *Brakensiek and Rawls*, 1983; *Chu et al*., 1986; *Vandervaere et al*., 1998]. Where the soil is sealed (soil crusted), rainfall cannot penetrate and runs off, so we model this mechanism by using for the first thin layer a low hydraulic conductivity. The validation period is characterized by a very dry climate, but there is an observed Hortonian runoff, characterized by a hydrograph peak and the absence of a baseflow recession curve, so we assumed the hypothesis of a time-dependent mechanism of soil crusting. Figure 4.4 shows the comparison of simulated and observed discharge for the validation period for the CATHY model with the assumption of soil crusting, while Table 4.4 summarizes the total simulated runoff volume for the three hydrologic

models. Table 4.5 reports the Nash- Sutcliffe index (NS) for the three hydrologic models. With the assumption of soil crusting the Nash- Sutcliffe index (NS) values obtained with the CATHY model are comparable to those of the other models: even if there are some differences, they are of the same order of magnitude. Finally, Figure 4.5 shows the comparison between the observed flow duration curve (FDC) and the 90% confidence intervals from the 50 ensemble simulations for the three hydrologic models. This Figure also confirms the presence during the validation period of an observed Hortonian runoff, characterized by the absence of a baseflow recession curve, which CATHY overestimates for the percentage of exceedance of 2 to 7%, due to the structure of the model with a detailed subsurface schematization allowing the representation of accurate runoff and baseflow, tRIBS underestimates due to the tendency to simulate steeper recession limbs discussed above, and TOPKAPI-X reproduces quite well.

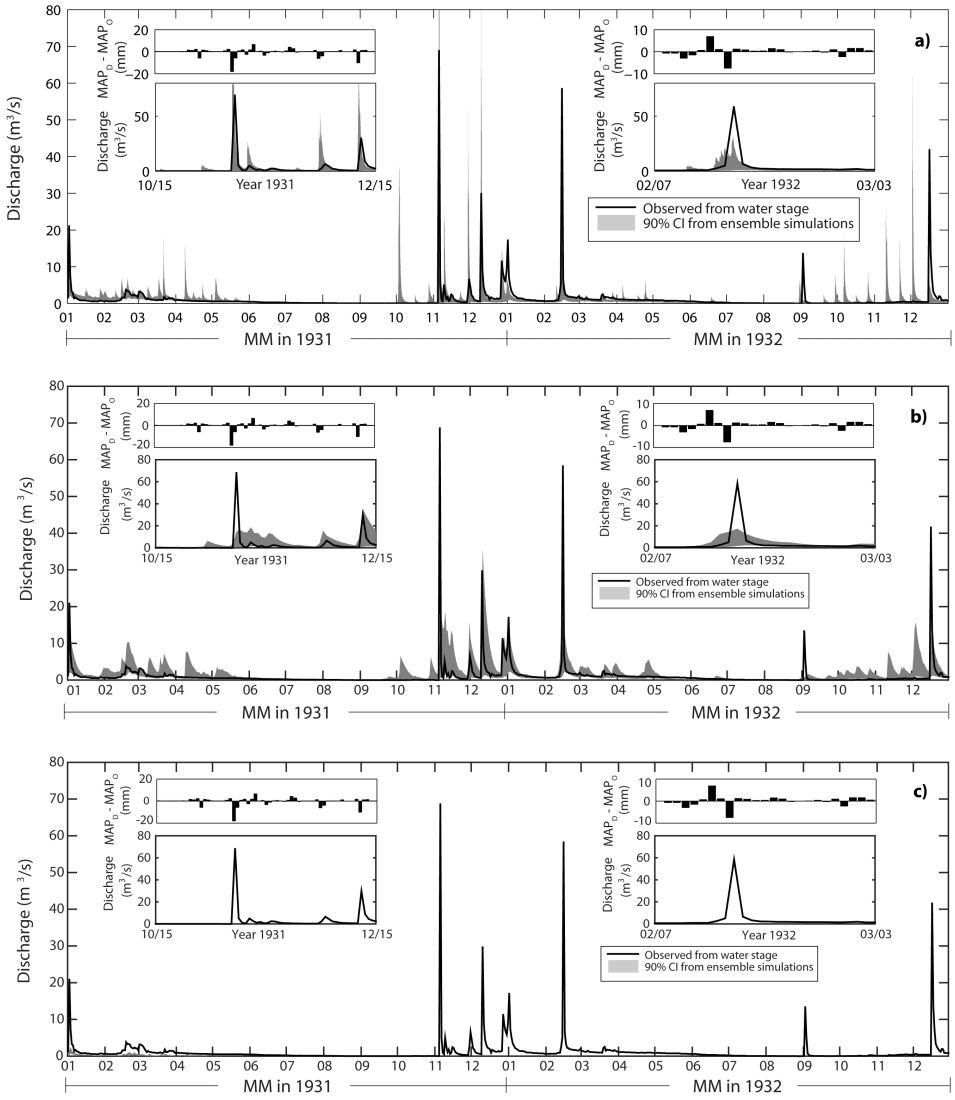

Figure 4.3. Validation simulation for the tRIBS (a), TOPKAPI-X (b), and CATHY (c) hydrologic models applied to the Rio Mannu catchment. Observed discharge is compared against 90% confidence intervals (CI) derived from 50 ensemble simulations for each of the models. In the insets, a zoom on two periods with significant flood events is shown in order to better highlight the differences between the daily downscaled ensemble average (MAP_D) and observed (MAP_O) mean areal precipitation time series.

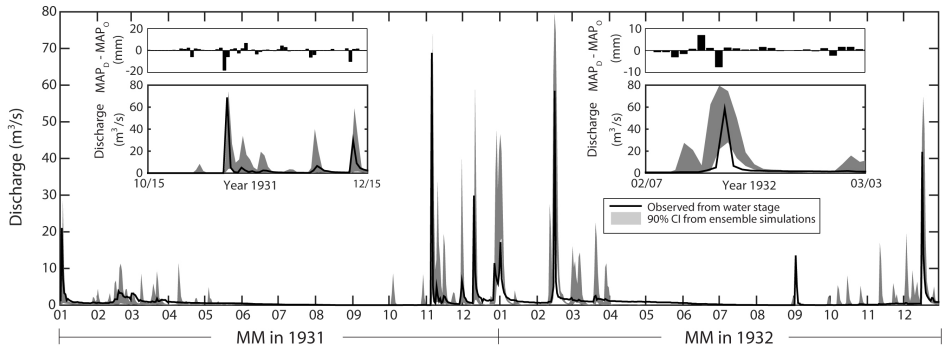

Figure 4.4. Results for the CATHY model during validation years 1931-1932 with a soil crusting assumption.

	tRIBS	TOPKAPI-X	CATHY
Time scale	**Calibration NS Min, Mean, Max**	**Calibration NS Min, Mean, Max**	**Calibration NS Min,Mean,Max**
Daily	-0.99, 0.02, 0.42	-1.92, -0.03, 0.23	-1.37, -0.37, -0.01
Weekly	-0.72, 0.13, 0.47	-1.89, 0.09, 0.56	-0.64, 0.06, 0.54
Monthly	0.03, 0.25, 0.74	-1.45, 0.40, 0.84	-0.38, 0.26, 0.62

Table 4.5. Nash-Sutcliffe (NS) index for the validation years 1931-1932, evaluated using the observed and simulated water volume at daily, weekly, and monthly time scales, for the three hydrologic models. For the CATHY model an hyphotesis of soil crusting was assumed.

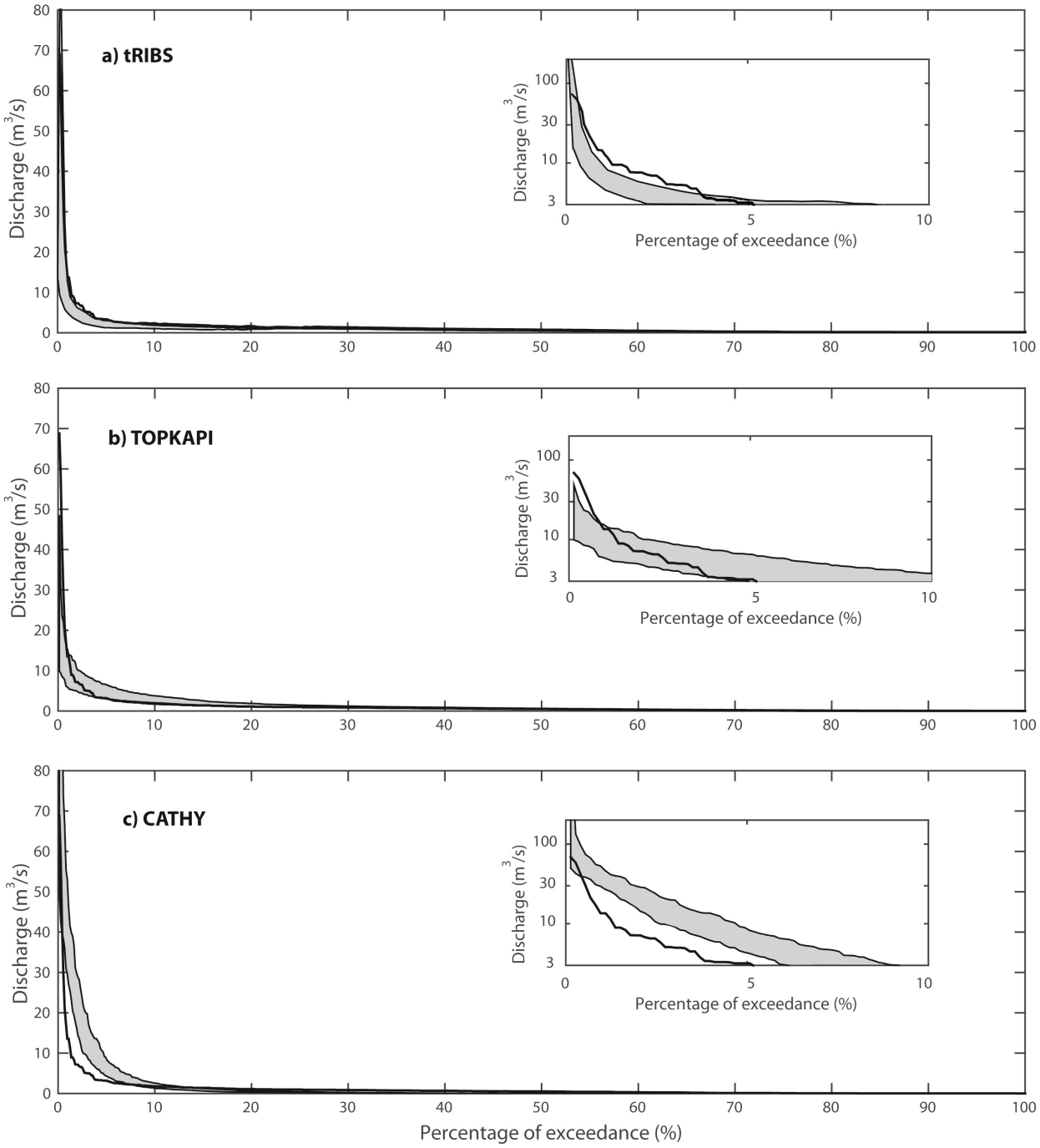

Figure 4.5. Comparison between the observed flow duration curve (FDC) and the 90% confidence intervals from the 50 ensemble simulations for the tRIBS (a), TOPKAPI-X (b), and CATHY (c) hydrologic models during the validation period (years 1931-1932).

4.1.3 Summary and concluding remarks

The response obtained with three hydrologic models tRIBS, TOPKAPI-X, and CATHY, were compared on a medium-sized basin (area of 473 km^2) in the Mediterranean island of Sardinia, Italy, with a semi-arid climate, the Rio Mannu catchment. In the considered basin precipitation, discharge, and meteorological data were collected in different historical periods and at different temporal resolutions. For this reason, Mascaro et al. [2013b] developed two downscaling tools that are able to create hourly precipitation forcing from daily observations and estimate the hourly potential evapotranspiration for applying the tRIBS model during the CLIMB project. The model was calibrated against discharge records over a one-year period and, then, validated over a drier period of two years. In this study two additional distributed hydrologic models, TOPKAPI-X and CATHY, were applied in the Rio Mannu catchment using the same datasets adopted for the tRIBS model, including geospatial data of land surface properties and hydrometeorological forcings.

The hypothesis of direct transferability of the parameters values was explored. While the three hydrologic models responded similarly during the calibration year, significant differences were found for the drier validation period for the CATHY model, which produced very low streamflow. To obtain satisfactory results for the CATHY model, an hypothesis of soil crusting was assumed and the first soil layer was modeled with a lower saturated hydraulic conductivity. This study provides insights on parameter transferability across distributed hydrologic models characterized by different structures and levels of sophistication in their process descriptions.

4.2 Multimodel assessment of climate change-induced hydrologic impacts for the Rio Mannu catchment

During the CLIMB project, an impact assessment framework was developed wherein the best performing four GCM-RCM combinations from the ENSEMBLE project [*van der Linden et al.*, 2009] were selected for each of the seven study sites. The daily GCM-RCM outputs at 25 km resolution for a reference (1971-2000) and a future (2041-2070) period were bias corrected and statistically downscaled. For the Rio Mannu site, the downscaled data were then used to force five hydrologic models – CATHY, SWAT, TOPKAPI-X, tRIBS, WASIM –for the reference and future periods. The hydrologic models were independently calibrated and validated against observed data, with each modeling group using the type of data most suitable to that model, such as field-scale soil moisture, evapotranspiration patterns, and discharge [*Cau et al*., 2005; *Mascaro et al*., 2013b; *Meyer et al*., 2016; *Perra et al*., in preparation].

After illustrating the metrics used to compare both climate and hydrologic models, the main meteorological forcing, precipitation, and temperature, projected by the four climate models are presented and analyzed first in terms of variations between the future (2041-2070) and reference (1971-2000) periods, in order to establish the expected climate change trends for the Rio Mannu catchment, and then in terms of level of agreement between climate models for the reference and future periods using Pearson correlation values and Duveiller biases. Subsequently, the impact of projected climate change is investigated through application of the five hydrologic models. Water availability and fluxes in terms of discharge, soil water content, and actual evapotranspiration are analyzed for trends and inter-model agreement [*Perra et al*., 2018].

4.2.1 Metrics to compare climate and hydrologic models

To compare the outputs of (i) the four climate models and (ii) the five hydrologic models forced by the four climate models in the reference (1971-2000) and future (2041-2070) periods, the climatological monthly means were first derived. Next, the difference between each pair of climate or hydrologic models is quantified by using the Pearson correlation coefficient *r* and the bias coefficient α, proposed by Duveiller et al. [2016], defined as:

$$r = \frac{\sum_{i=1}^{n}(X_i - \bar{X})(Y_i - \bar{Y})}{n\sigma_X\sigma_Y} \tag{4.1}$$

$$\alpha = \begin{cases} \frac{2}{\frac{\sigma_X}{\sigma_Y} + \frac{\sigma_Y}{\sigma_X} + \frac{(\bar{X}-\bar{Y})^2}{\sigma_X\sigma_Y}} & , \ r > 0 \\ 0 & , \ r \leq 0 \end{cases} \tag{4.2}$$

where X_i and Y_i are the 30-year mean monthly values of a given response variable simulated by a pair of models, $\bar{X}$ and $\bar{Y}$ are their means, σ_X and σ_Y are their standard deviations, and $n = 12$ is the number of months per year.

The Pearson coefficient, which can range between -1 and 1, is a widely used measure of the degree of linear dependence between two datasets, but it does not give any indication of how similar they are in magnitude. In contrast, the bias coefficient, ranging from 0 (full bias, no agreement) to 1 (no bias, perfect agreement), evaluates possible additive or multiplicative biases between the model outputs. These two indices were recently used in a hydrologic model intercomparison study [*Kollet et al*., 2017] to evaluate the agreement between seven integrated surface-subsurface models for a series of benchmark test cases. Here, the two indices *r* and α were computed for all pairs of both climate and hydrologic representative variables. The results are presented in matrix pictures where each element represents the index value for a single model pair, thus allowing easy comparison of each combination of model pairs with all the others. In Figure 4.6, an example of a matrix picture between two models A and B is shown: the circles

represent correlation r and the squares bias α, with the color and size of the markers proportional to the value of the metric. Three possible levels of model agreement are reported: high, medium, and low.

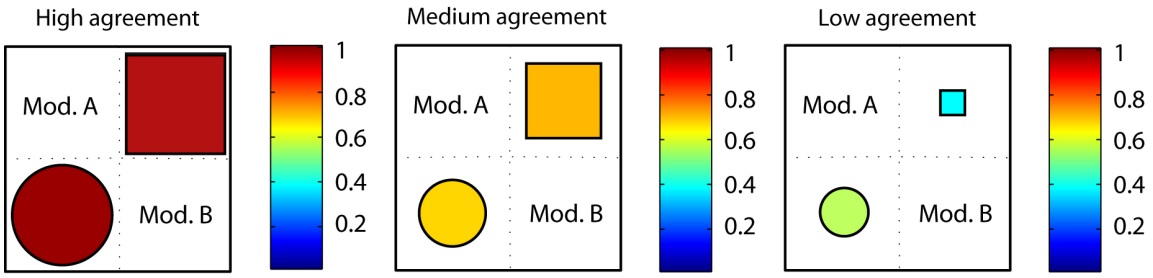

Figure 4.6. Example of matrix picture between two models A and B. Correlation values ($-1 \le r \le 1$) are represented with circles below the diagonal, while bias ($0 \le \alpha \le 1$) is plotted as squares above the diagonal. The size and color of symbols are proportional to the coefficient values. White (blank) matrix entries correspond to $r = 0$ or $\alpha = 0$.

4.2.2 Climate models: projected changes and comparison/agreement analysis

For each climate model, the climatological means of precipitation (P) and temperature (T) averaged over the catchment were computed at annual and monthly scales. Figure 4.7 compares results for the reference and future periods. All models predict a decrease of mean annual P, with percent changes ranging from -7% to -21%, and an increase of T from 1.9ºC to 3ºC. All models predict negative changes in P for all months except winter (December–February), where the models simulated an increase in P, and also June for ECH-REM and October for ECH-RMO. T is projected to rise in all months for all models, with the RCMs forced by ECH predicting comparable magnitudes in change, and HCH-RCA simulating the largest increment.

To quantify the agreement of the monthly climatologies of P and T predicted by the models, the correlation coefficient, r, and the bias, α, are plotted in Figure 4.8. The left and right panels show the results for, respectively, P and T for the reference (top) and future (bottom) periods, and in the bottom panels there is also the comparison between the reference and future periods. In each panel, circles represent r and squares α, while color and size of the markers are proportional to the metric value. The metrics indicate a general high level of agreement of the climatologies simulated by all models, with r and α for each pair of models always larger than 0.9 for both variables and in both periods. Comparing the same climate model for the reference and future periods, the values of r and α (last row and last column, respectively, of the bottom panels) are also high for both variables: for P and the HCH-RCA model, which is the model that slightly differs from the others, both Pearson and bias coefficients are close to 1 (r = 0.918 and α = 0.912). As a result, the agreement of seasonal cycles is high, especially in the case of temperature, suggesting that the uncertainty due to climate models can be considered low, although a small bias is found when comparing the three climate models forced by ECH with HCH-RCA, as expected since it is recognized that GCMs exert the major influence on the projected climate change [*Graham et al*., 2007; *Kay et al*., 2009].

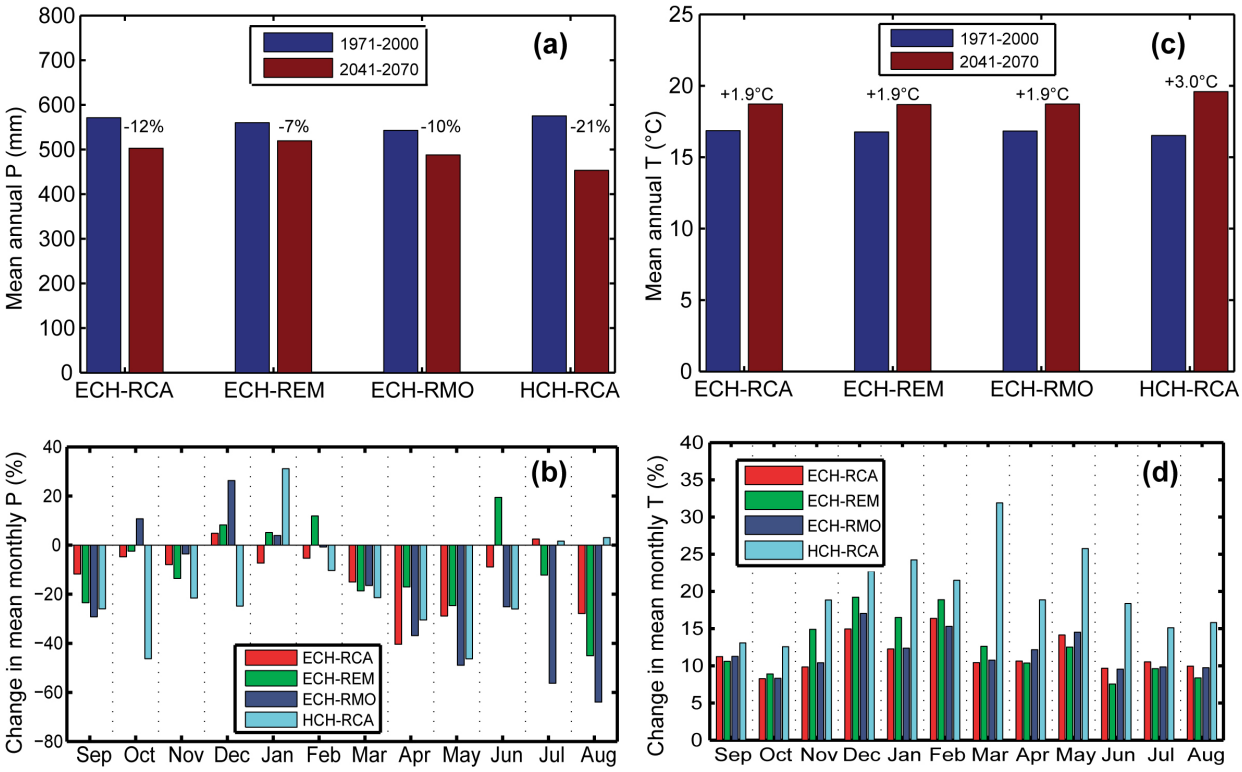

Figure 4.7. Mean annual precipitation P (a) and temperature T (c) predicted by the four climate models for the reference (1971-2000), blue bars, and future (2041-2070), red bars, periods. Relative change in mean monthly precipitation P (b) and temperature T (d) between the reference and future periods for the four climate models.

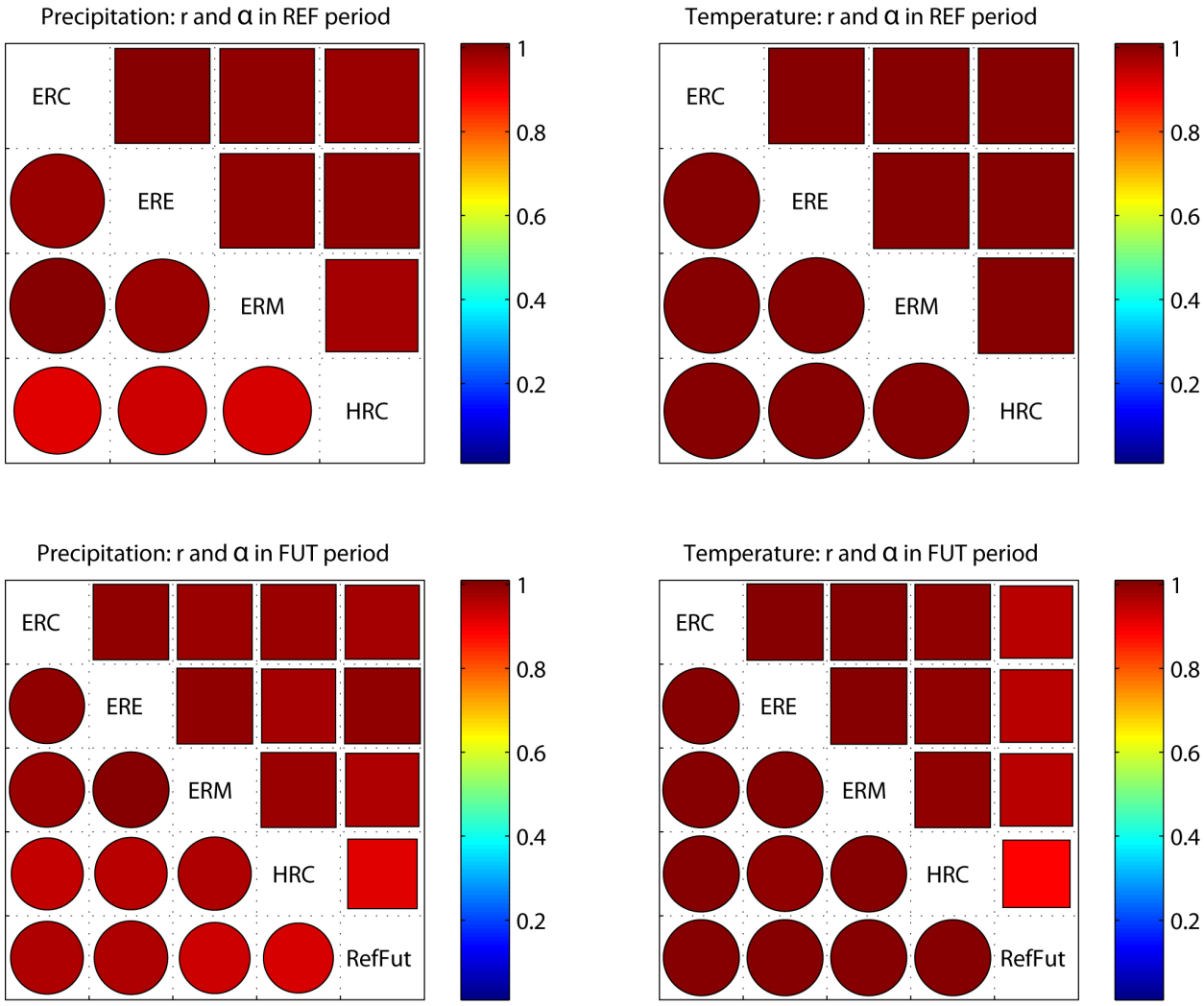

Figure 4.8. Results of the analysis of agreement for mean monthly precipitation (left) and temperature (right) among the four climate models (ERC = ECH-RCA, ERE = ECH-REM, ERM = ECH-RMO, HRC = HCH-RCA) for the reference (REF, 1971-2000, top) and future (FUT, 2041-2070, bottom) periods. In the bottom panels the comparison between the reference and future periods (labeled RefFut) is also shown.

4.2.3 Hydrologic impact

A summary of the annual and monthly climatologies of basin-averaged potential evapotranspiration (ETP), runoff (Q), soil water content (SWC), and actual evapotranspiration (ET_a) simulated by the five hydrologic models, forced by four climate models, is reported in Figures 4.9-4.12. Each figure shows: the annual simulated variable in each period, including the percent change from reference to future (panel a); the relative change in mean annual values between reference and future periods forced by the four climate models (panel b); the seasonal distribution of mean monthly values of each variable during reference and future periods and corresponding standard deviations (panel c); and the seasonal distribution of relative change of mean monthly values between reference and future periods (panel d).

ETP is predicted to rise by all models on an annual basis (Figure 4.9a), mostly due to the projected increment of T. The values of annual and monthly (Figure 4.9c) ETP differ among the hydrologic models, due to the different computation methods adopted. For SWAT and WASIM, ETP was computed at a daily time scale by internal routines based on Hargreaves [*Hargreaves, 1994; Hargreaves and Allen*, 2003] and Penman-Monteith [*Penman*, 1948; *Monteith*, 1965] formulas, respectively, producing an annual mean of about 1100 mm for SWAT and 1400 mm for WASIM. For CATHY, TOPKAPI-X, and tRIBS, a common reliable diurnal cycle for ETP was derived at hourly time scale using an approach based on Penman-Monteith and Hargreaves formulas, detailed in Mascaro el al. [2013b], producing an annual mean of about 650 mm, which is consistent with previous estimates for this region [*Pulina et al*., 1986]. From Figure 4.9c we can also observe the slight increase of ETP predicted by all hydrologic models in the future period, except for the WASIM model and especially during summer and spring months. Furthermore, notice that the highest increase of ETP is predicted with all hydrologic models

under HCH-RCA forcing (Figure 4.9b), as expected since this GCM-RCM combination also projects the highest increase in temperature, as already discussed. Among the hydrologic models, WASIM is the one that predicts the higher increase. We can observe also from Figure 4.9d that relative changes in potential evapotranspiration are predicted to increase much more during summer and spring.

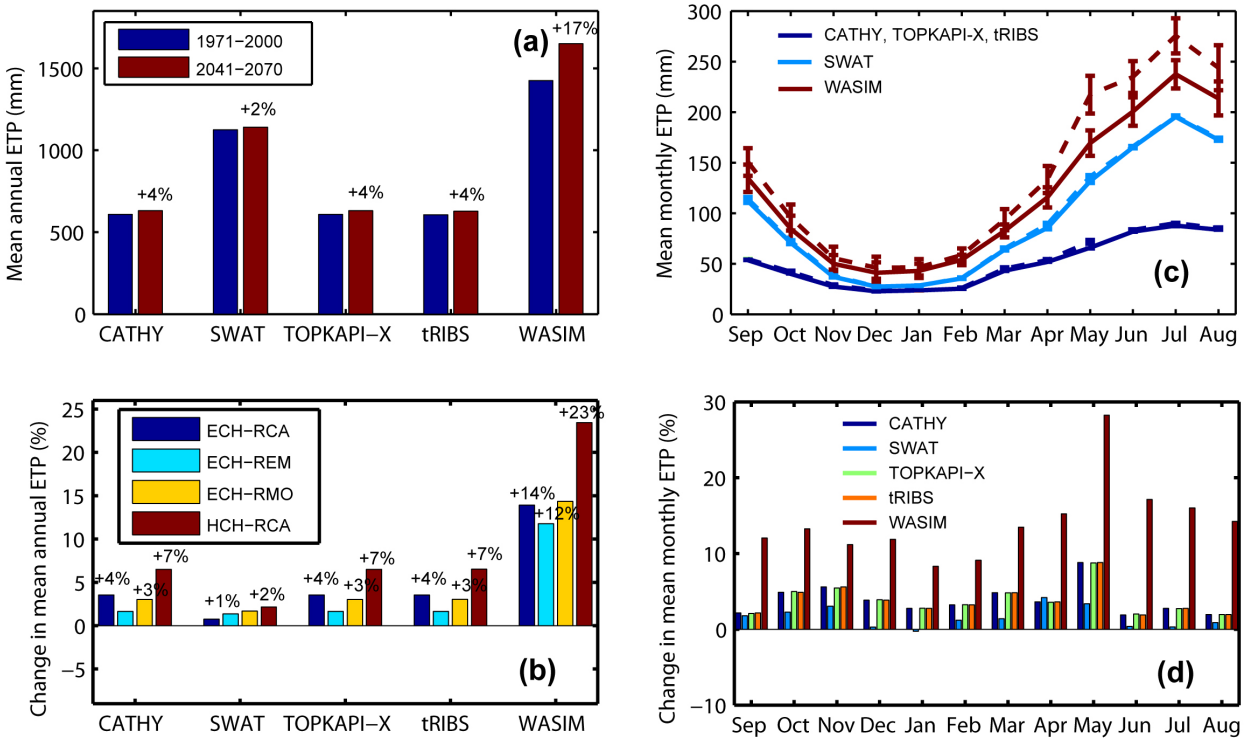

Figure 4.9. Potential evapotranspiration (ETP) for each hydrologic model forced by the four selected climate models for the reference (REF, 1971-2000) and future (FUT, 2041-2070) periods. (a) Mean annual ETP during REF and FUT periods, obtained as an average among the four climate models. (b) Relative change in mean annual ETP between REF and FUT periods forced by the four climate models. (c) Seasonal distribution of mean monthly ETP during REF (solid line) and FUT (dotted line) periods and corresponding standard deviations (vertical bars), obtained as an average among the four climate models. (d) Seasonal distribution of relative

change in mean monthly ETP between REF and FUT periods, obtained as an average among the four climate models.

Results in terms of Q are analyzed in Figure 4.10: it is apparent that all models predict decreasing values in the future. Figure 4.10a, reporting mean annual Q obtained for each hydrologic model in the reference and future periods obtained as an average among the four climate models, shows a reduction that ranges from -12% according to SWAT to -69% according to CATHY. Figure 4.10b reports the relative change between future and reference periods computed for each climate model configuration: we can observe that the reduction varies within the same hydrologic model considering different climate forcing. The largest decrease is always given by configurations forced with HCH-RCA, ranging from -23% for the SWAT model to -91% for the CATHY model, followed by the climate model ECH-RCA, for which the reduction varies from -16% for SWAT to -67% for CATHY. A summary in terms of change (%) between reference and future periods for mean annual Q, simulated by the five hydrologic models and the four climate models, is provided in Table 4.6. Figure 4.10c refers to mean monthly Q, showing the mean seasonality in reference (solid line) and future (dotted line) periods with bars indicating the standard deviations within each model. Figure 4.10d details the monthly variations during the two periods according to the five hydrologic models: the seasonality is quite similar among them even if some differences hold also in this case. The five hydrologic models predict diminished mean monthly Q in the future period throughout the year with the exception of January and February, when SWAT and WASIM simulate a slight increase.

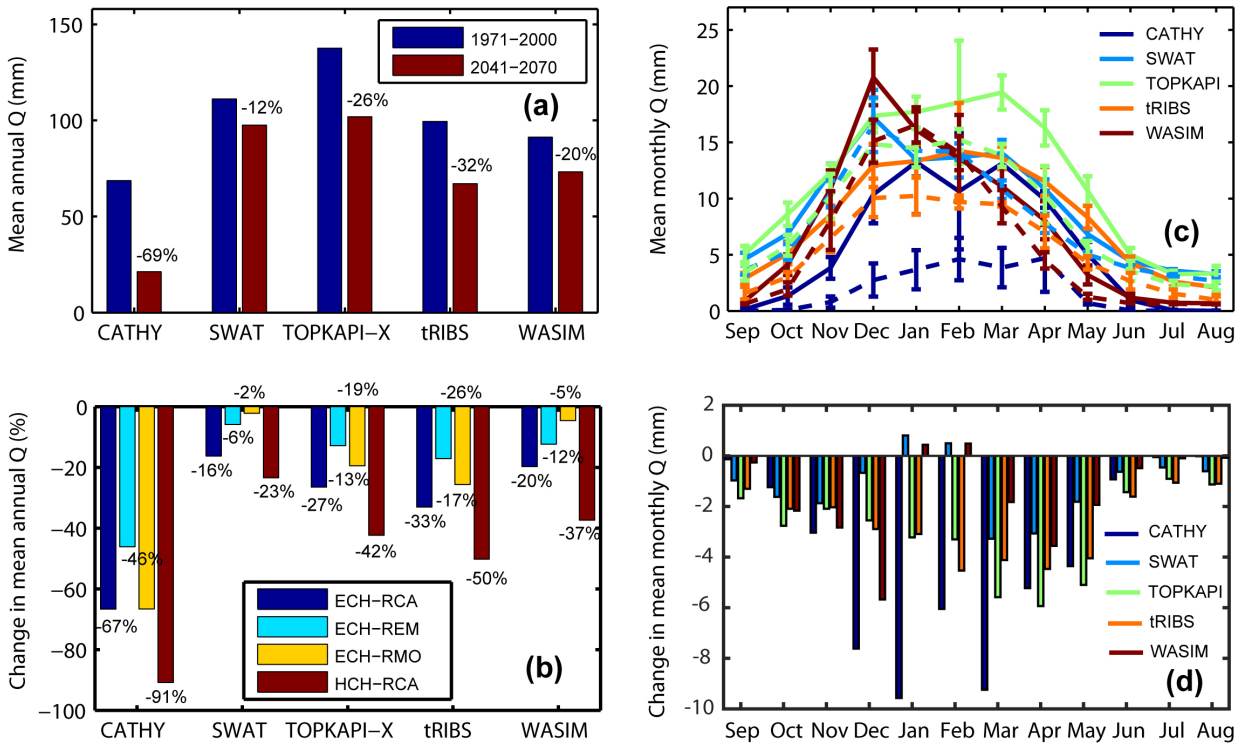

Figure 4.10. As Figure 4.9, but for discharge (Q) simulated by each hydrologic model forced by the four selected climate models for the reference (REF, 1971-2000) and future (FUT, 2041-2070) periods.

		Overall tendencies considering all climate models						Overall tendencies Overall tendencies considering all hydrologic models				
		CAT (%)	**SWA (%)**	**TOP (%)**	**TRI (%)**	**WAS (%)**	**ALL H.M. (%)**	**ERC (%)**	**ERE (%)**	**ERM (%)**	**HRC (%)**	**ALL C.M. (%)**
Q	μ	-68	-12	-25	-32	-19	-31	-32	-19	-24	-49	-31
	σ	18	10	13	14	14	14	20	16	26	25	22
SWC	μ	-10	-8	-13	-5	-10	-9	-8	-6	-6	-16	-9
	σ	5	5	6	3	4	5	2	2	3	5	3
ET_a	μ	10	-12	-8	-2	-11	-5	-3	-3	-5	-7	-5
	σ	4	5	3	1	5	3	7	6	9	14	9

Table 4.6. Change (%) between future and reference periods of mean annual discharge (Q), soil water content (SWC), and actual evapotranspiration (ET_a) for the five hydrologic models (CAT = CATHY, SWA = SWAT, TOP = TOPKAPI-X, TRI = tRIBS, WAS = WASIM), expressed as mean (μ) and standard deviation (σ) calculated for each and then all hydrologic models (H.M.) considering all climate models (ERC = ECH-RCA, ERE = ECH-REM, ERM = ECH-RMO, HRC = HCH-RCA), and for each and then all climate models (C.M.) considering all hydrologic models.

Figure 4.11 shows mean values and changes of SWC in the first meter depth of soil. All simulations predict a decreasing trend of SWC, but again we can notice some differences among the hydrologic models. For instance Figure 4.11a clearly shows that CATHY presents the highest soil humidity (35%) and WASIM the lowest (17%), while the highest and lowest decrements in the future are observed, respectively, for TOPKAPI-X (-13%) and tRIBS (-5%). Figure 4.11b details the relative change between future and reference periods for each configuration of

hydrologic and climate models. As for Q, each hydrologic model simulates the maximum SWC reduction under the HCH-RCA configuration. The reduction with this climate forcing, ranging from -9% for tRIBS to -22% for TOPKAPI-X, can in fact be double with respect to the one obtained with the other climate models. A summary in terms of change (%) between reference and future periods of mean annual SWC, simulated by the five hydrologic models and the four climate models, is provided in Table 4.6. The mean monthly seasonal distribution of SWC reported in Figure 4.11c is quite different among the five hydrologic models. SWAT presents the highest variations from winter/spring to summer month values, while the annual range is more limited in the CATHY and tRIBS simulations. The mean monthly relative changes between reference and future periods represented in Figure 4.11d are always negative. CATHY simulates a quite constant diminution (of about 0.035) throughout the year, which is always larger than the other models. The changes exceed 0.03 in May for TOPKAPI-X and SWAT, which instead predict the lowest reduction in winter months. These reductions during spring months can be related to the higher vegetation activity combined with moderate values of temperature and potential evapotranspiration.

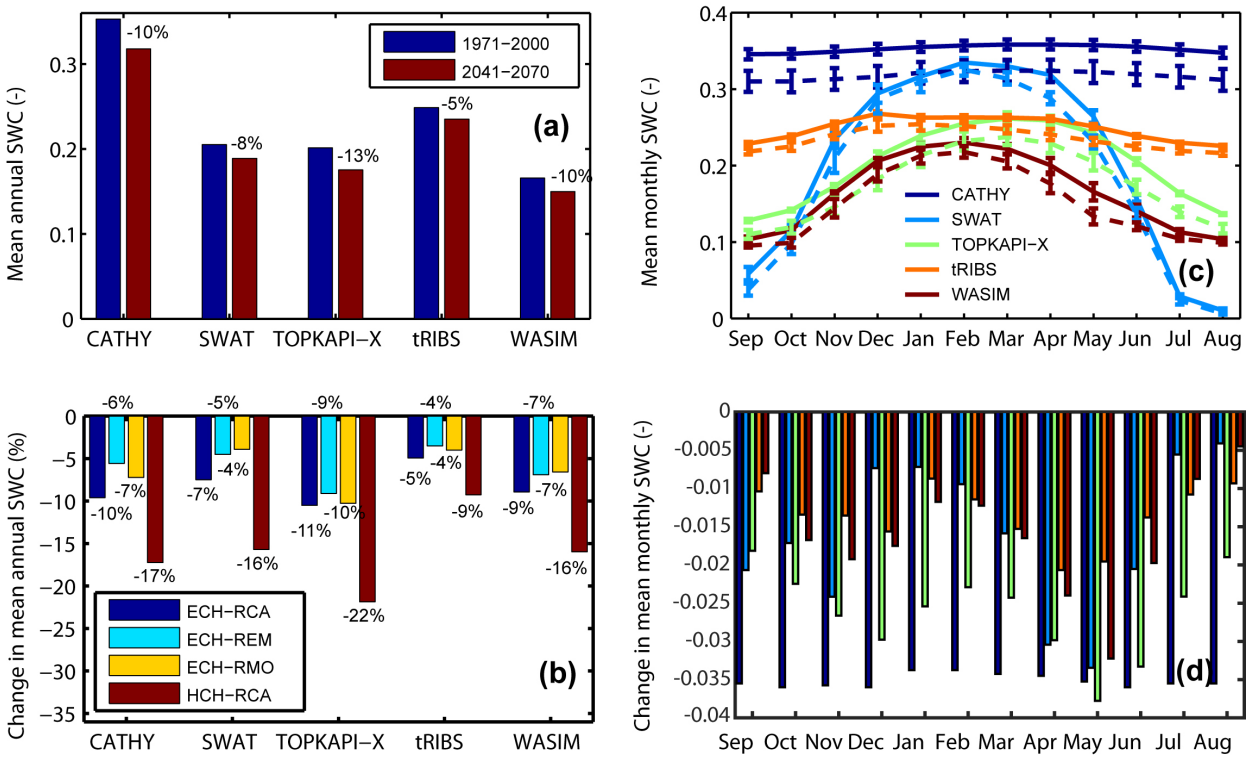

Figure 4.11. As Figure 4.9, but for soil water content (SWC) simulated by each hydrologic model forced by the four selected climate models for the reference (REF, 1971-2000) and future (FUT, 2041-2070) periods. For panel d) colors for each model are the same as panel c).

The differences among the hydrologic models in representing soil–vegetation–atmosphere transfers are reflected also in simulations of ET_a processes (Figure 4.12). The mean annual values reported in Figure 4.12a are predicted to decrease in the future by four models (tRIBS presents the lowest reduction, -2% on average, SWAT the highest, -12% on average), with CATHY being the only one projecting a slight increase. The reason for this is that CATHY simulates the highest soil water content in the first meter depth, as can be appreciated in Figure 4.11a and 4.11c, and it is the model that simulates the minimum discharge (Figure 4.10a and 4.10c), thus it retains more water within the soil zone available for evaporation. Figure 4.12b shows that the highest variations (both positive and negative) in actual evapotranspiration are

again reached in simulations forced by the HCH-RCA model, ranging from -17% for SWAT and WASIM and +16% for CATHY. A summary in terms of change (%) between reference and future periods of mean annual ET_a, simulated by the five hydrologic models and the four climate models, is provided in Table 4.6. Mean monthly ET_a reported in Figure 4.12c presents different patterns, with the hydrologic models divided into two groups: CATHY, TOPKAPI-X, and tRIBS reach the highest values during summer months, when temperature and potential evapotranspiration are higher; SWAT and WASIM anticipate the seasonal peak in spring when moderate temperatures coincide with vegetation activity. Figure 4.12d, reporting relative changes in monthly values, shows that the increase predicted by CATHY is highest in spring; in fact relative changes in monthly temperatures (Figure 4.7d) and potential evapotranspiration (Figure 4.9d) during spring are predicted to increase much more than during summer months. The other four models predict instead a future diminution more pronounced in summer, exceeding -10mm for the WASIM model. This can be related to the fact that these models in the future simulate during summer months lower soil water content with respect to the reference period (Figure 4.11d). In winter months the future evapotranspiration reduces negligibly, or even increases slightly in the case of WASIM.

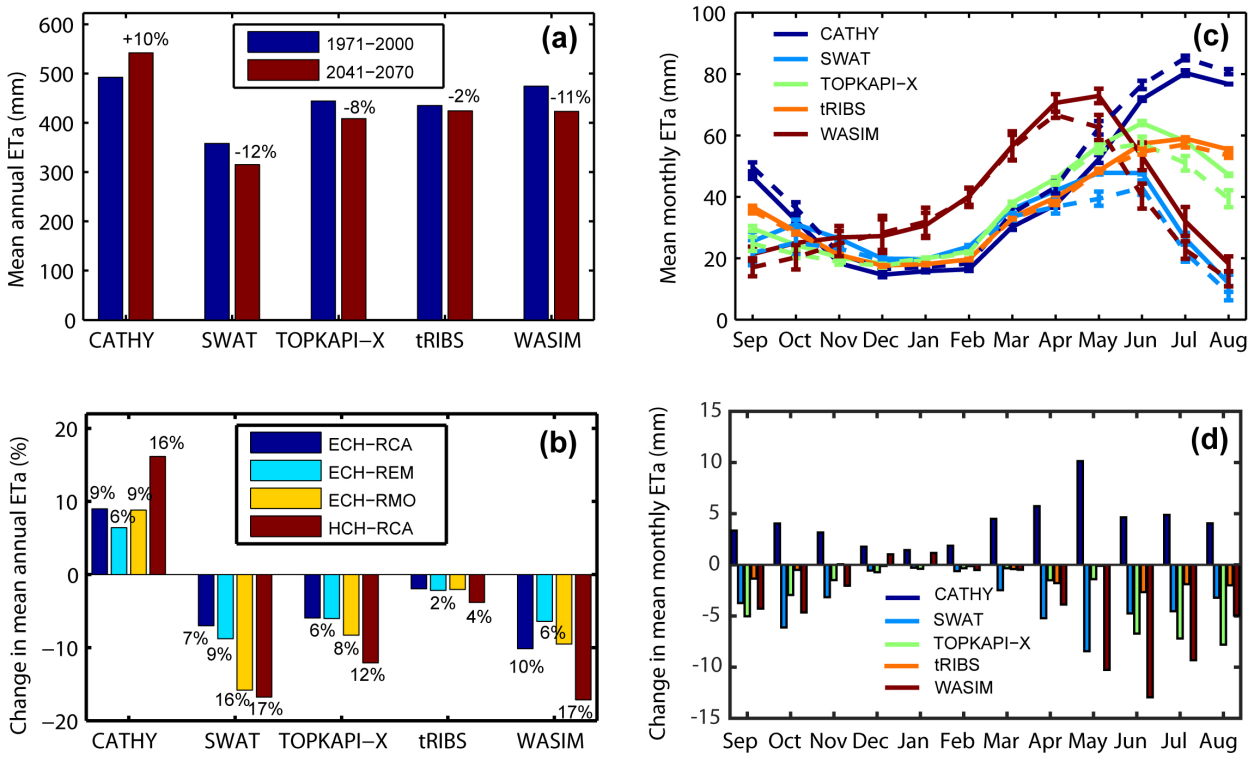

Figure 4.12. As Figure 4.9, but for actual evapotranspiration (ET_a) simulated by each hydrologic model forced by the four selected climate models for the reference (REF, 1971-2000) and future (FUT, 2041-2070) periods.

4.2.4 Agreement analysis

The agreement among the hydrologic models forced with the different climate configurations is evaluated using the Pearson correlation and Duveiller bias coefficients in Figures 4.13-4.15. Figure 4.13 shows the results for Q, and each panel summarizes the agreement among hydrologic models forced by a specific GCM-RCM configuration for the reference (top panels) and future (bottom panels) periods. Following the same graphical representation of Figure 4.6, Pearson coefficients are displayed as circles in the lower-left part of each panel, while the bias coefficients are represented with squares in the upper-right part. In both cases the size of symbols is proportional to the magnitude of the corresponding coefficient.

We can notice that during the reference period the agreement in terms of both indices between any pair of hydrologic models is high, with the HCH-RCA performance slightly better than for the other climate forcing configurations. The values of the Pearson coefficient *r*, comparing the hydrologic models in pairs, range from 0.70 (CATHY-WASIM under ECH-RMO forcing) to 0.99 (TOPKAPI-X-tRIBS under ECH-RMO forcing) for the reference period and from 0.67 (CATHY-WASIM and CATHY-SWAT under ECH-REM forcing) to 0.99 (SWAT-TOPKAPI-X under HCH-RCA forcing) for the future period. Looking at the bias coefficient we can observe a general agreement ($\alpha > 0.7$) regardless of the climate forcing among the hydrologic models, except for CATHY, which shows in the future period the highest differences with the other models, as expected from Figure 4.10, with the lowest agreement occurring for the HCH-RCA configuration. CATHY generates the lowest Q in the future, and this result is reflected in the values of the bias parameter α, which exceeds the value of 0.7 only when CATHY is compared under ECH-REM with tRIBS and WASIM, which use the same equations as CATHY to represent subsurface and surface dynamics, albeit simplified in some way (e.g., lower dimensionality). Bias parameters values range from 0.53 (CATHY-TOPKAPI-X forced by ECH-RMO) to 0.99 (SWAT-tRIBS forced by ECH-RMO) for the reference period and from 0.09 (CATHY-SWAT under HCH-RCA forcing) to 0.99 (SWAT-TOPKAPI-X under ECH-RMO forcing) for the future period.

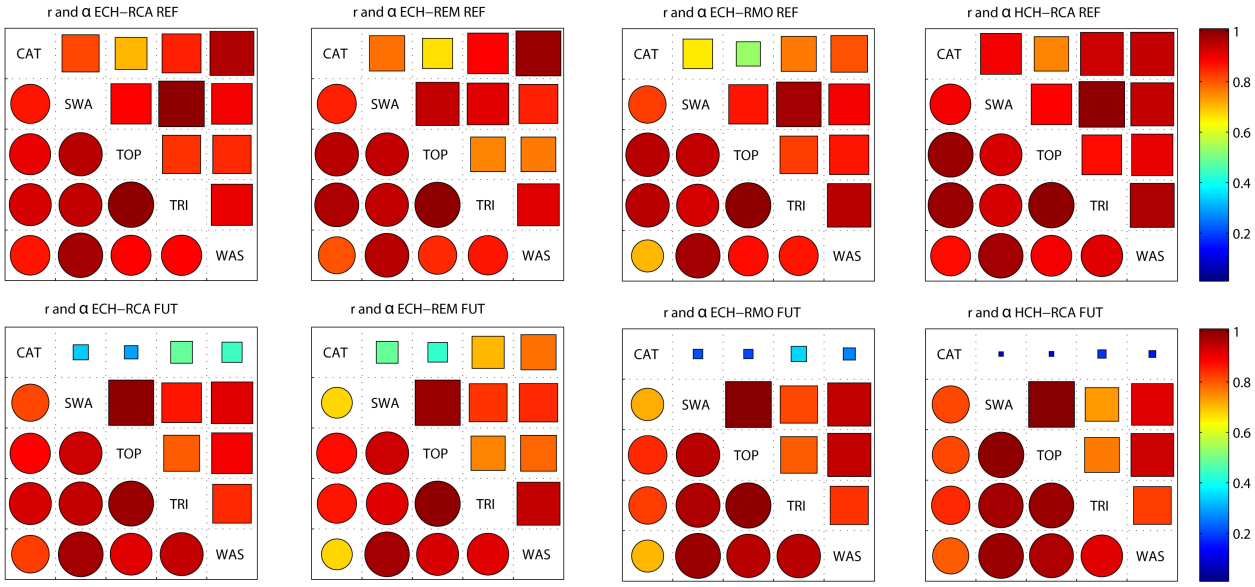

Figure 4.13. Same as Figure 4.6, but for mean monthly discharge agreement between the five hydrologic models (CAT = CATHY, SWA = SWAT, TOP = TOPKAPI-X, TRI = tRIBS, WAS = WASIM). Each panel displays the agreement under a specific GCM-RCM forcing, for the reference (REF, top) and future (FUT, bottom) periods.

Figure 4.14 shows a similar comparison for SWC. The agreement among the hydrologic models generally diminishes with respect to the discharge intercomparison. Again the CATHY model presents the lowest correlation with the others, followed by tRIBS. CATHY and tRIBS are in fact the two models that show limited variations of SWC from winter/spring to summer month values with respect to the others, as shown in Figure 4.11b. The values of the Pearson coefficient r range from 0.65 (CATHY-tRIBS in HCH-RCA configuration) to 0.98 (SWAT-tRIBS forced by ECH-RCA) for the reference period and from 0.57 (CATHY-tRIBS in ECH-RCA simulations) to 0.97 (CATHY-TOPKAPI-X forced by HCH-RCA) for the future period. The value of the bias coefficient α is near zero when the models are compared with CATHY and also quite low (about 0.2) when compared with tRIBS. The values of α range from 0.01

(CATHY versus tRIBS and WASIM in both ECH-RCA and ECH-REM configurations) to 0.86 (TOPKAPI-X versus WASIM forced by ECH-RMO) for the reference period and from 0.01 (CATHY-WASIM in ECH-REM simulations) to 0.94 (TOPKAPI-X versus WASIM forced by ECH-RMO) for the future period.

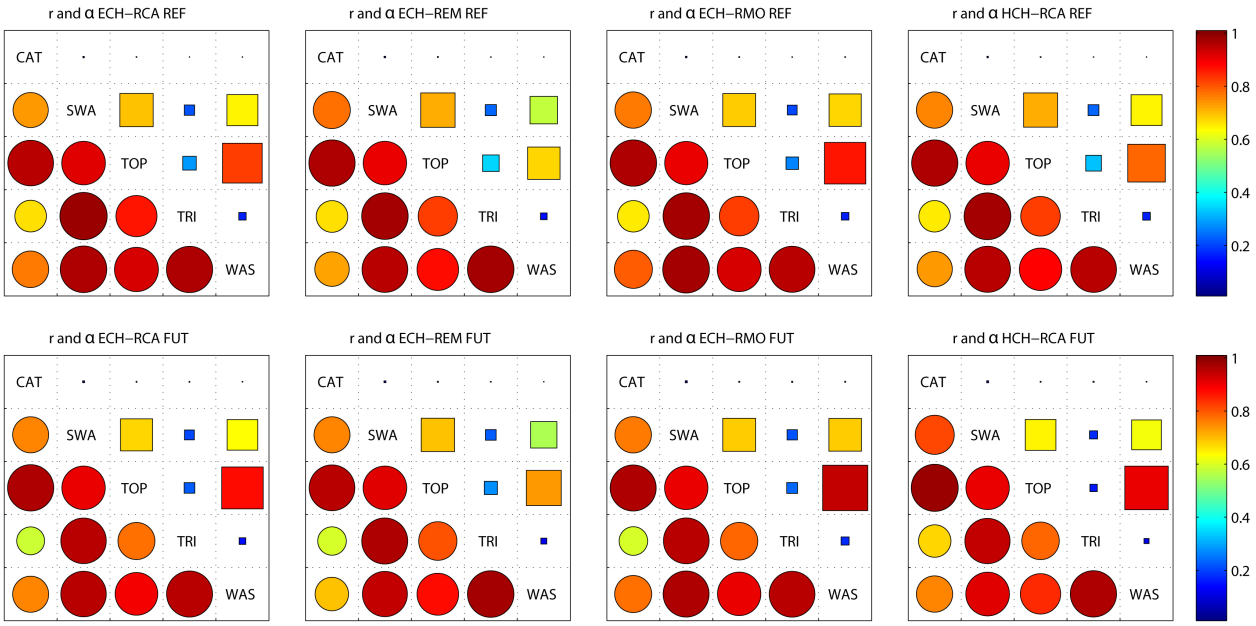

Figure 4.14. Same as Figure 4.13, but for mean monthly soil water content agreement between the five hydrologic models (CAT = CATHY, SWA = SWAT, TOP = TOPKAPI-X, TRI = tRIBS, WAS = WASIM) for the reference (REF, top) and future (FUT, bottom) periods.

The analysis of agreement presents the lowest Pearson correlation values in the case of ET_a (Figure 4.15). The values of *r* range from -0.21 (CATHY-WASIM in ECH-REM configuration) to 0.98 (CATHY-tRIBS for all climate model configurations) for the reference period and from -0.29 (CATHY-WASIM in ECH-REM simulations) to 0.99 (CATHY-tRIBS for all configurations) for the future period. Despite the high values of the Pearson coefficient

between CATHY and tRIBS for both the reference and future periods regardless of the GCM-RCM forcing, the Duveiller index displays a worsening ($\alpha \approx 0.6 - 0.8$). Considering overall results, the values of the bias coefficient α range from 0 (CATHY and tRIBS versus WASIM in ECH-REM configuration) to 0.99 (TOPKAPI-X versus tRIBS for all configurations) for the reference period and from 0 (CATHY-WASIM in ECH-RMO simulations) to 0.99 (TOPKAPI-X versus tRIBS for all configurations) for the future period. From this figure it can be noted that, notwithstanding the differences, Pearson and bias indices for the reference period are similar for CATHY, tRIBS, and TOPKAPI-X (which are forced with the same ETP values). Furthermore, these models reach the highest values of ET_a during the summer months (Figure 4.12c), when the temperature is highest. For the future period this agreement is maintained, with a strong correlation between tRIBS and TOPKAPI-X. Referring to the pair SWAT-WASIM, they anticipate the peak of ET_a in spring when moderate temperatures coincide with vegetation activity (Figure 4.12c). This can be seen for the reference period and to a lesser extent for the future one, when α is slightly lower.

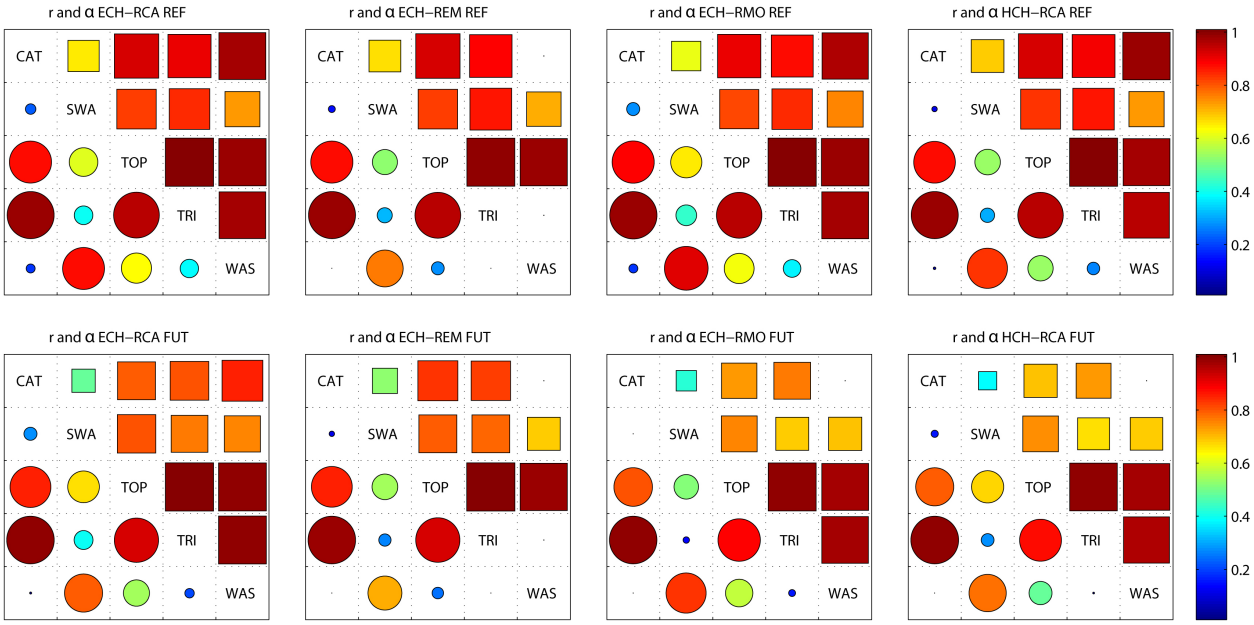

Figure 4.15. Same as Figure 4.13, but for mean monthly actual evapotranspiration agreement between the five hydrologic models (CAT = CATHY, SWA = SWAT, TOP = TOPKAPI-X, TRI = tRIBS, WAS = WASIM) for the reference (REF, top) and future (FUT, bottom) periods.

4.2.5 Summary and concluding remarks

Five hydrologic models forced with the outputs of four combinations of global and regional climate models were compared to evaluate climate change consequences on the response of a medium-sized Mediterranean basin, the Rio Mannu catchment. In order to evaluate the agreement between model pairs, a new metric based on Pearson correlation and Duveiller bias coefficients has been used. The hydrologic models, independently calibrated and validated, were applied in cascade with climate models for a reference (1971-2000) and a future (2041-2070) period. Temporal series of different response variables simulated by the hydrologic models were used to evaluate the impacts on the basin of the predicted climate change in terms of water resource availability.

In a first step, climate model outputs, suitably bias corrected and downscaled, were analyzed for the reference and future periods by comparing mean monthly and annual values of precipitation and temperature and by examining the agreement metrics. All of the GCM-RCM combinations agree that in the future period there will be decreasing mean annual precipitation (average differences of about -12%), whereas on a monthly basis the sign of the variation depends on the month and the model. As regards the temperature trend, all of the GCM-RCM combinations predict increasing mean annual T values that vary from 11% (1.9°C) to 19% (3°C) depending on the model. A similar behavior for the four GCM-RCM combinations is also found for the mean monthly temperature trend, with positive variations in every season for the future period, from about 7% (ECH-REM in June) to 30% (HCH-RCA in March). The correlation and bias coefficients show favorable agreement when analyzing mean monthly precipitation and temperature for the reference and future periods. The uncertainty due to climate models can thus be considered low and is due principally to the GCM component that is recognized to exert the major influence on projected climate change.

In a second step, hydrologic model outputs related to water availability (namely discharge, soil water content, and actual evapotranspiration) were analyzed. Simulation results show decreasing mean annual runoff and a reduction of the soil water content at 1 m depth for the future period (average decreases of 31% and 9%, respectively). Actual mean annual evapotranspiration in the future will diminish according to four of the five hydrologic models due to drier soil conditions (average decrease of 8%), while it will rise (by 10%) in the prediction of the CATHY model, which retains the highest water content in its soil profile. For all response variables the biggest decrease is always predicted with the HCH-RCA model. Analyzing hydrologic model outputs at monthly scale, we can observe variations not perceptible at the

annual scale. Discharge for instance is predicted to decrease in the future period in all months except for January and February.

In terms of model agreement, for the reference period we can observe a good concordance between each pair of hydrologic models, while more significant differences emerge for the future period. The model that most differs from the others is CATHY, which generates the lowest discharge in the future, and this result is reflected in the values of the bias parameter. The five hydrologic models confirm the reduction of soil water content throughout the year, and the magnitude of variation depends on the hydrologic model considered. Again the CATHY model yields the lowest correlation with the other models, followed by tRIBS. Both models, in fact, show limited variation of soil water content from winter/spring to summer months with respect to the others, and this as well is reflected in the bias value. Actual evapotranspiration could rise in the future period according to the CATHY model and, during January and February, also according to WASIM, which instead predicts the strongest reductions in summer months. As regards the analysis of agreement for actual evapotranspiration, Pearson and bias indices are similar for CATHY, tRIBS, and TOPKAPI-X (which are forced with the same values of potential evapotranspiration). Moreover, these models reach the highest values of actual evapotranspiration during summer months. For the future period this agreement is maintained, with a strong correlation between tRIBS and TOPKAPI-X. The model pair SWAT-WASIM anticipates the peak of actual evapotranspiration in spring when moderate temperatures coincide with vegetation activity. This behavior is more pronounced for the reference period than for the future one, due to the higher bias.

The differences that emerge from the analysis of agreement are consistent with the key structural differences between the hydrologic models. CATHY, for instance, has the most

detailed subsurface representation of the five models (fully three-dimensional Richards equation; soil and aquifer zones), and as such will tend to retain more water in subsurface storage, making some of this water available for subsequent evaporation. In the agreement metrics CATHY tends to align most with TOPKAPI-X and tRIBS, which, although with a more simplified representation, also account for both vertical and lateral subsurface flow, unlike SWAT and WASIM, which resolve flow only in the vertical direction. These latter two models, on the other hand, show strong agreement, to the exclusion of the other models, for some of the evapotranspiration responses, consistent with the fact that both these models include a quite detailed representation of vegetation processes. Notwithstanding these differences, overall the five hydrologic models show good agreement, and they responded similarly to the reduced precipitation and increased temperatures predicted by the climate models, lending strong support to a future scenario of increased water shortages for this region of the Mediterranean, with negative consequences especially for the agricultural sector.

4.3 Preliminary climate change impact assessment on the Flumendosa basin

In this section a preliminary application of the TOPKAPI-X model on a large Sardinian basin prone to extreme flood events, the Flumendosa basin, is presented. In the following the calibration and validation of the model is illustrated, then the hydrologic impact of climate change is evaluated for five 30-year periods (1951-1980, 1981-2010, 2011-2040, 2041-2070, 2071-2100).

4.3.1. TOPKAPI-X calibration and validation

To run the TOPKAPI-X model on the Flumendosa basin we focus on the period before the reservoir construction, from 1926 to 1936. In this period daily precipitation from 14 rain gages, daily minimum and maximum temperature from 5 thermometric stations, and daily discharge data from one hydrometric station were published in annual technical reports of the Italian Hydrologic Survey (called "Annali idrologici). Since the TOPKAPI-X model runs at hourly time step, the daily precipitation was split equally during the 24 hours, while to obtain hourly temperature data the daily minimum and maximum temperature were linearly interpolated. Moreover, because the model needs the same number of meteorological stations for precipitation and temperature, we applied a procedure similar of that described above in section 3.2 to compute the temperature data for the 14 rain gage stations, based on the temperature data of the 5 thermometric stations, following the approach described in Caracciolo et al. [2017]. In particular, among the 5 thermometric stations we chose the nearest station to the basin centroid, we rescaled the hourly values for this station at the sea level using the Eq. 3.13, and then we obtained the hourly temperatures for the 14 rain gage stations by using the Eq. 3.14.

A resolution of 250 m was chosen to delineate the Flumendosa basin, as a compromise between computational time and accuracy. The calibration of the model was performed using the hydrometeorological data described above during the years 1927-1931, while potential evapotranspiration data are estimated in TOPKAPI-X using the Thornthwaite and Mather formula [*Thornthwaite and Mather*, 1955]. A spin-up interval of 1 year was used prior to the start of the calibration period. The available data during the period 1932-1936 were used to validate the model performance. An initial guess for the model parameters was derived from the available map of soil types (Figure 2.8b), by assuming parameter values taken from the literature

[*Rawls et al*., 1982]. Following Ciarapica et al. [2002] and results of a sensitivity analysis, the most influential parameters were found to be the saturated hydraulic conductivity at the surface (K_S) and the Manning coefficient (n). The values of K_S were modified within the ranges typical for the corresponding soil texture classes (Figure. 2.8b). For the Manning coefficient of the drainage network we assumed literature values ranging from 0.03 to 0.04 $m/s^{1/3}$ [*Chow*, 1959], while for other parameters we adopted literature values for similar soil properties [*Rawls et al*., 1983]. The values reported in Table 4.6 were assumed for the main soil texture classes. For the TOPKAPI-X model only two layers are possible to discretize the soil, superficial and deep: the first thin layer is taken 0.4 m depth, the deep soil layer 0.7 m depth. For the deep layer K_S values were taken one order of magnitude lower.

The model performance is quantified using the Nash-Sutcliffe index, evaluated on the basis of the daily observed and simulated water volume. Figure 4.16 shows the comparison between observed and simulated discharges for the calibration years, producing a performance measure of NS = 0.79. Despite some disagreements in the peaks probably due to the disaggregation of daily precipitation during the day equally, the model is able to capture quite well the dynamics of the catchment in both the rising and recession limbs of the hydrograph. In Figure 4.17 a comparison of the cumulated observed and simulated volume is shown. We can notice that the simulated volumes underestimate the observed volumes during the calibration period.

With the parameter values obtained from the calibration, the model was applied using the input data of the validation period. Figure 4.18 shows the results for the validation years, that confirm a good model performance with NS = 0.75. In Figure 4.19 a comparison of the

cumulated observed and simulated volume is reported. We can notice that during the validation period the simulated volumes overestimate the observed volumes.

Soil Properties	**Variable (unit)**	**Sandy loam – Clay loam**	**Sandy clay loam – Clay**	**Loamy sand – Sandy loam**
Saturated hydraulic conductivity	K_s (m/s)	$1.86 \cdot 10^{-4}$	$3.79 \cdot 10^{-5}$	$9.53 \cdot 10^{-4}$
Saturated soil moisture	θ_s (-)	0.458	0.436	0.445
Residual soil moisture	θ_r (-)	0.058	0.079	0.038
Head suction	ψ_a (m)	0.159	0.267	0.087
Exponent of the horizontal flow	α	2.5	2.5	2.5

Table 4.6. Parameters values of the TOPKAPI-X model for the major soil classes of the Flumendosa basin.

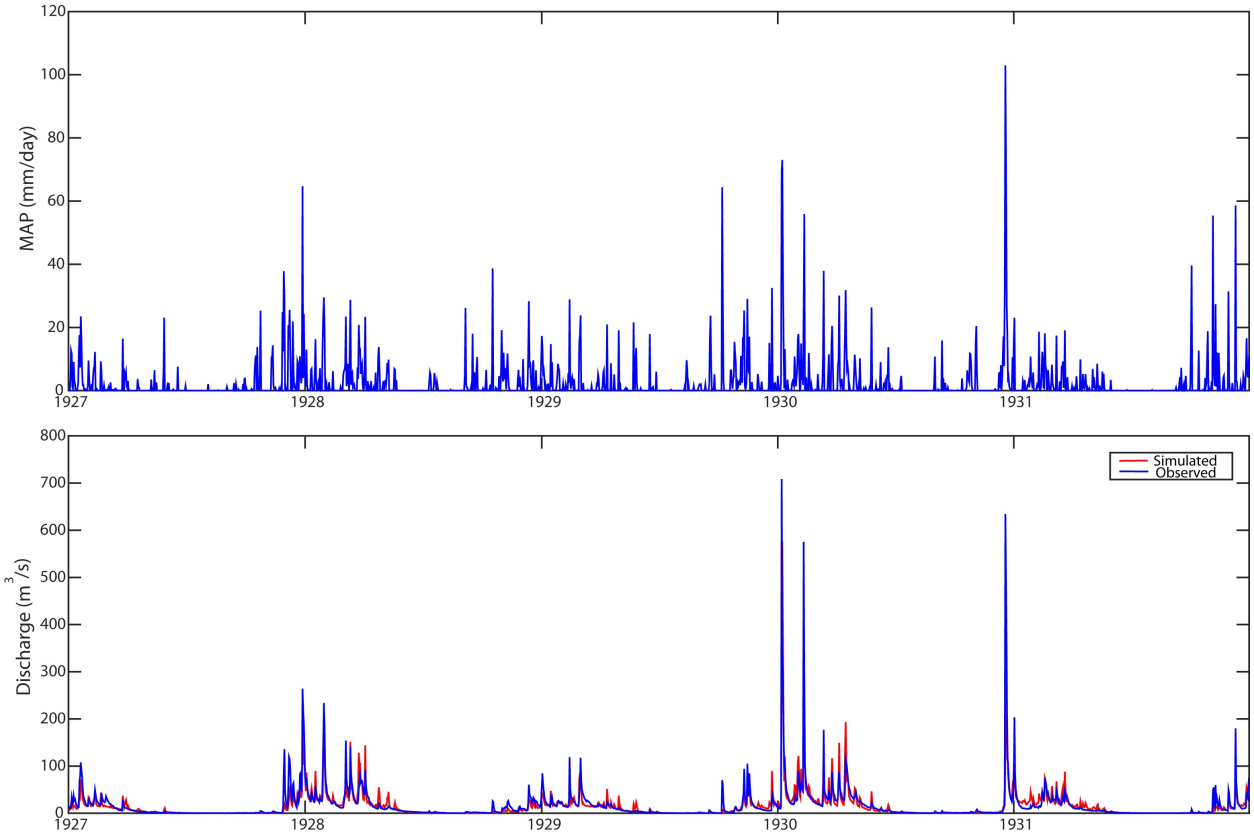

Figure 4.16. Calibration simulation for the TOPKAPI-X hydrologic model applied to the Flumendosa basin. Observed discharge is compared against simulated one. In the top panel the mean areal precipitation time series computed from the 14 rain gages during the period 1927-1931 is reported.

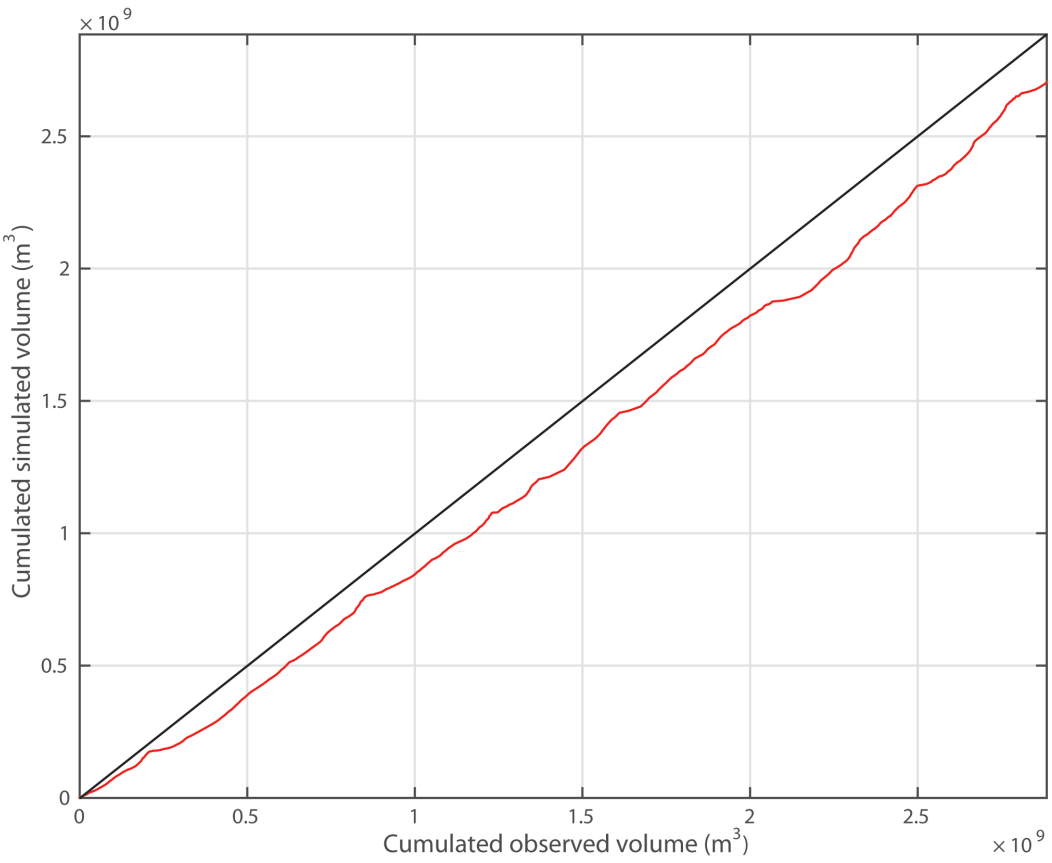

Figure 4.17. Cumulated simulated volume versus observed volume during the calibration period.

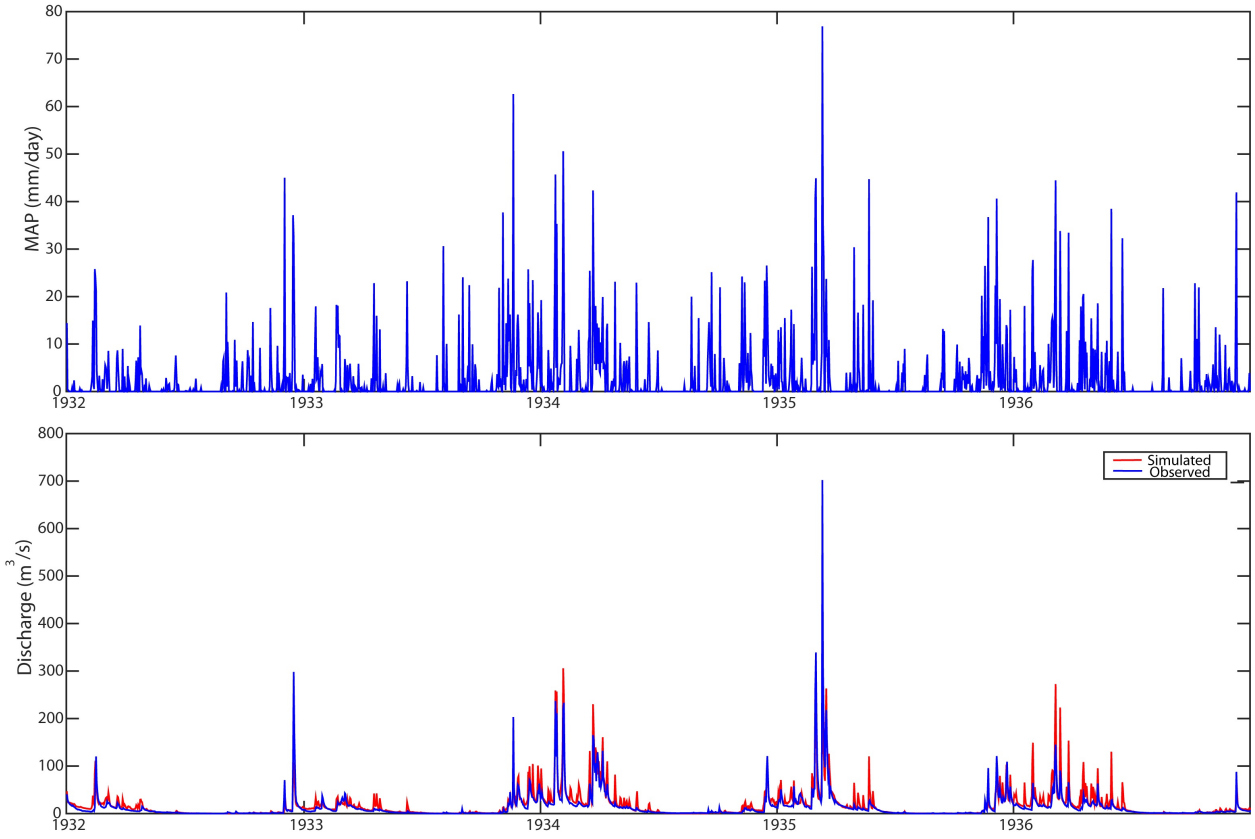

Figure 4.18. Validation simulation for the TOPKAPI-X hydrologic model applied to the Flumendosa basin. Observed discharge is compared against simulated one. In the top panel the mean areal precipitation time series computed from the 14 rain gages during the period 1932-1936 is reported.

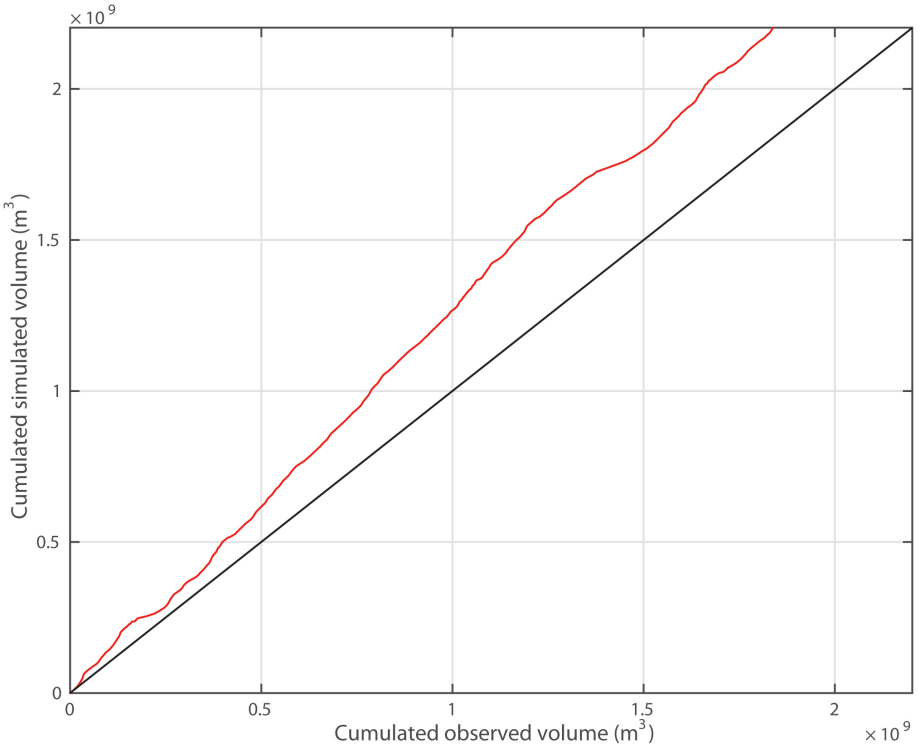

Figure 4.19. Cumulated simulated volume versus observed volume during the validation period.

4.3.2. Hydrologic impact of climate change

In this section the climatological means of precipitation (P) and temperature (T) averaged over the catchment and among the four climate models were computed at annual and monthly scales. Figure 4.20 compares results for the five 30-year periods (1951-1980, 1981-2010, 2011-2040, 2041-2070, 2071-2100). The models predict a decrease of mean annual P from the period 2011-2040 until the period 2071-2100, with percent changes of about -27%, and an increase of +2% in the second period 1981-2010 (Figure 4.20a). As regards the seasonal distribution of precipitation we can notice a peak during October (Figure 4.20b). The model predicts also an increase of T among all the five periods of about 3.4ºC (Figure 4.20c) and for all months (Figure 4.30d).

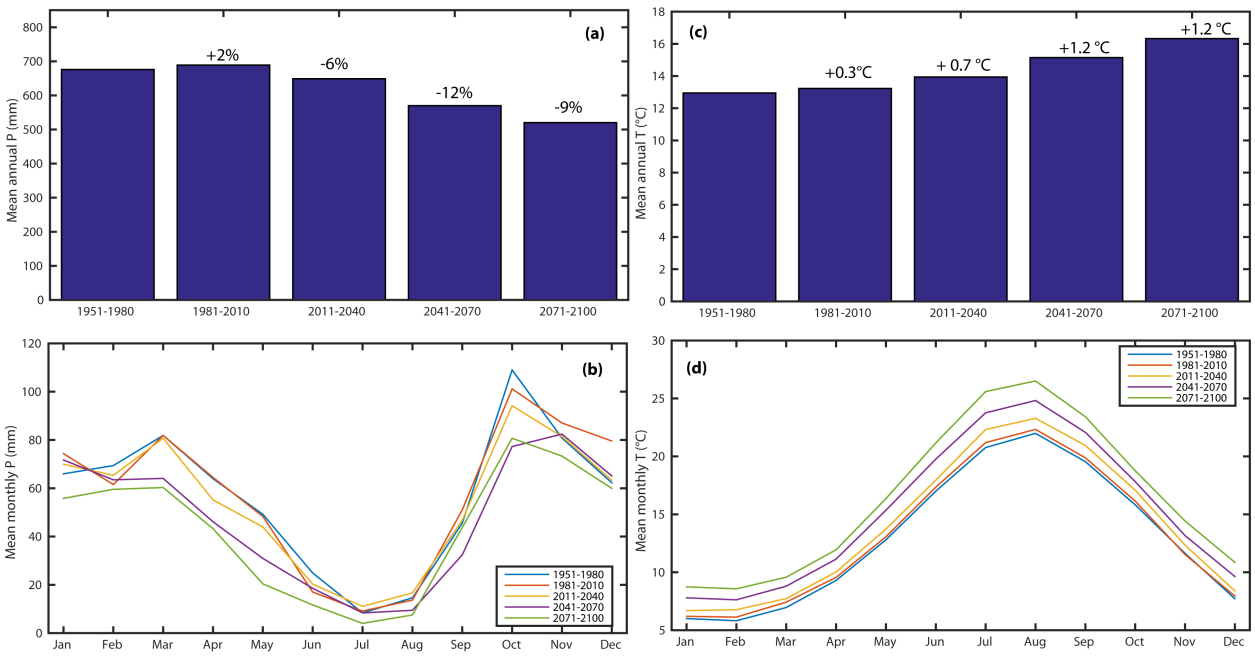

Figure 4.20. Mean annual precipitation P (a) and temperature T (c) obtained as an average among the four climate models during the five 30-year periods (1951-1980, 1981-2010, 2011-2040, 2041-2070, 2071-2100). Seasonal distribution of mean monthly precipitation P (b) and temperature T (d) during the five considered 30-year periods.

A summary of the annual and monthly climatologies of basin-averaged potential evapotranspiration (ETP), runoff (Q), soil water content (SWC), and actual evapotranspiration (ET_a) simulated by the TOPKAPI-X model, obtained as an average among the four climate models, is reported in Figures 4.21-4.24. Each figure shows: the annual simulated variable in each period, including percent change from each one (panel a); the seasonal distribution of mean monthly values of each variable during the five periods (panel b).

ETP is computed in TOPKAPI-X using the Thornthwaite and Mather formula, producing an annual mean of about 650 mm during the period 1951-1980, which is consistent with previous estimates for this region [*Pulina et al*., 1986]. ETP is predicted to rise during all the considered

periods on annual (Figure 4.21a) and monthly basis (Figure 4.21b), mostly due to the projected increment of T.

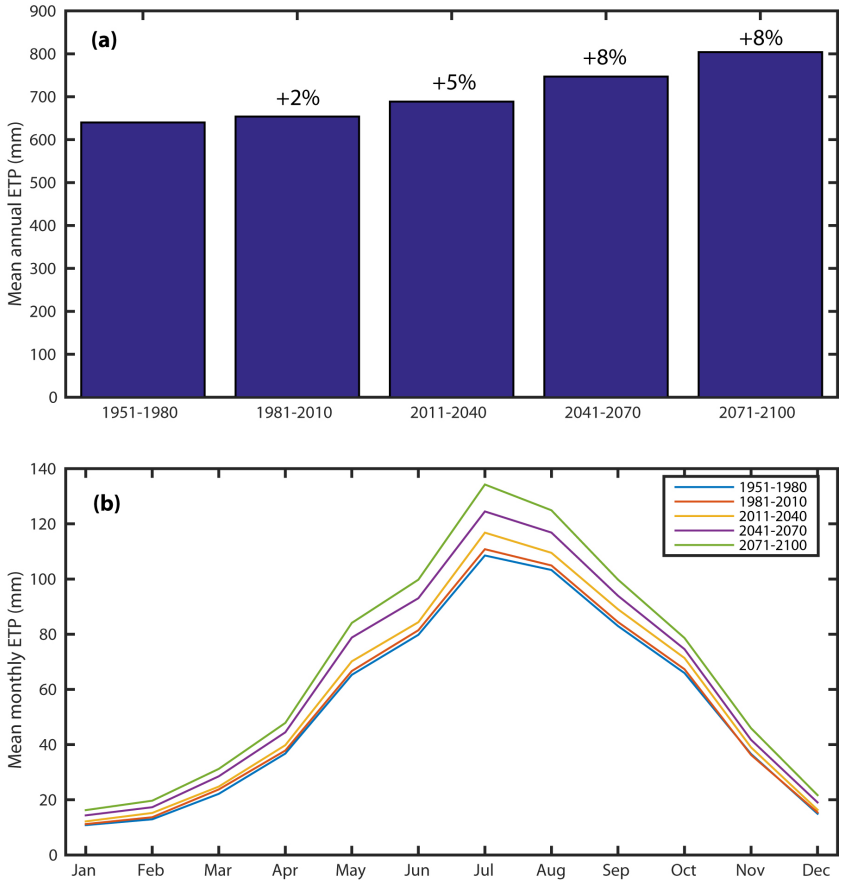

Figure 4.21. Potential evapotranspiration (ETP) for the TOPKAPI-X model obtained as an average among the four climate models during the five 30-year periods (1951-1980, 1981-2010, 2011-2040, 2041-2070, 2071-2100). (a) Mean annual ETP during the five 30-year periods. (b) Seasonal distribution of mean monthly ETP during the five 30-year periods.

Results in terms of Q are analyzed in Figure 4.22: the discharge is predicted to decrease from the period 2011-2040 until the period 2071-2100, with percent changes of about -60%, following the precipitation trend, and to increase by +3% in the second period 1981-2010 (Figure

4.22a). Figure 4.22b refers to mean monthly Q, showing the mean seasonality during the five considered periods.

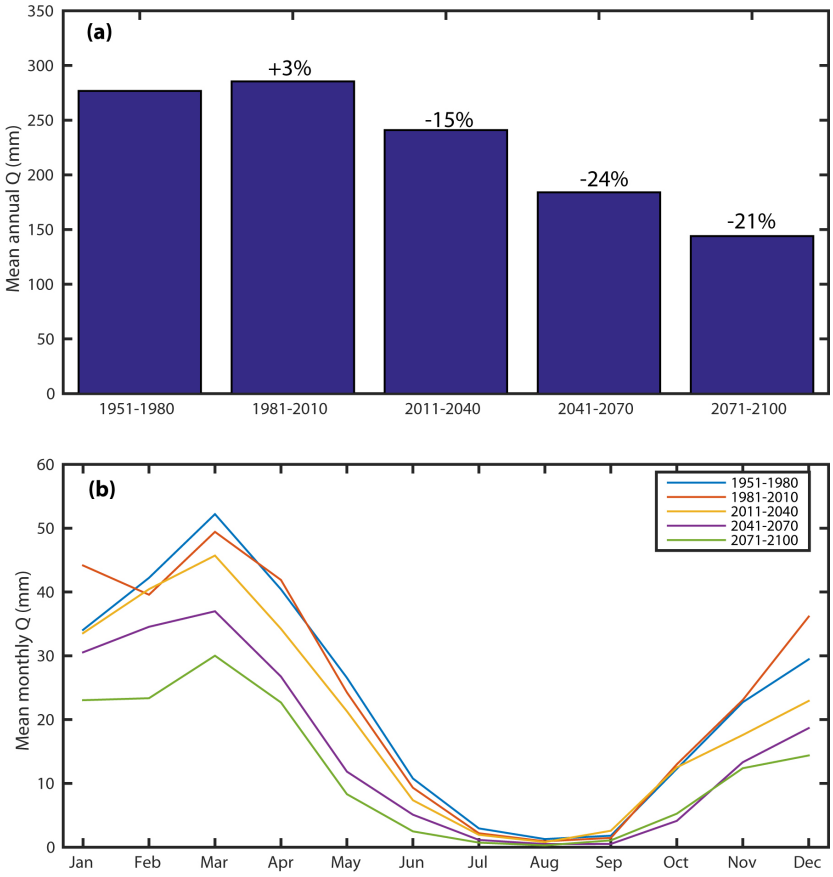

Figure 4.22. As Figure 4.21, but for discharge (Q).

Figure 4.23 shows mean values of SWC: again we can notice decreasing values of the soil water content from the period 2011-2040 until the period 2071-2100, with percent changes of about -20%, following the precipitation trend, and slight increasing values (+0.3%) in the second period 1981-2010 (Figure 4.23a). The mean monthly seasonal distribution of SWC is reported in Figure 4.23b: we can observe increasing values of SWC in the second considered period in winter months, as for precipitation and discharge values.

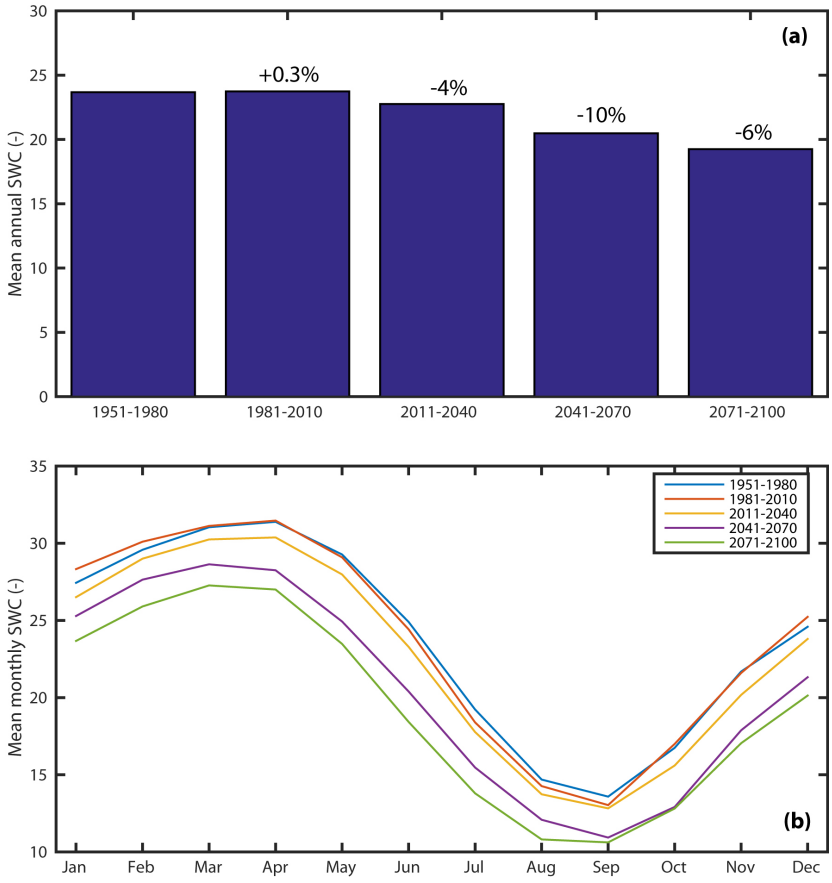

Figure 4.23. As Figure 4.21, but for soil water content (SWC).

The simulation results in terms of ET_a are reported in Figure 4.24. The mean annual values are predicted to decrease from the period 2011-2040 until the period 2071-2100, with percent changes of about -5%, following the soil water content trend, and to slightly increase (+0.02%) in the second period 1981-2010 (Figure 4.24a). Figure 4.24b refers to mean monthly ET_a, showing the mean seasonality during the five considered periods. We can notice the highest values during summer months, when temperature and potential evapotranspiration are higher, and an increase also during October, probably due to water available in the surface because of the increase in precipitation.

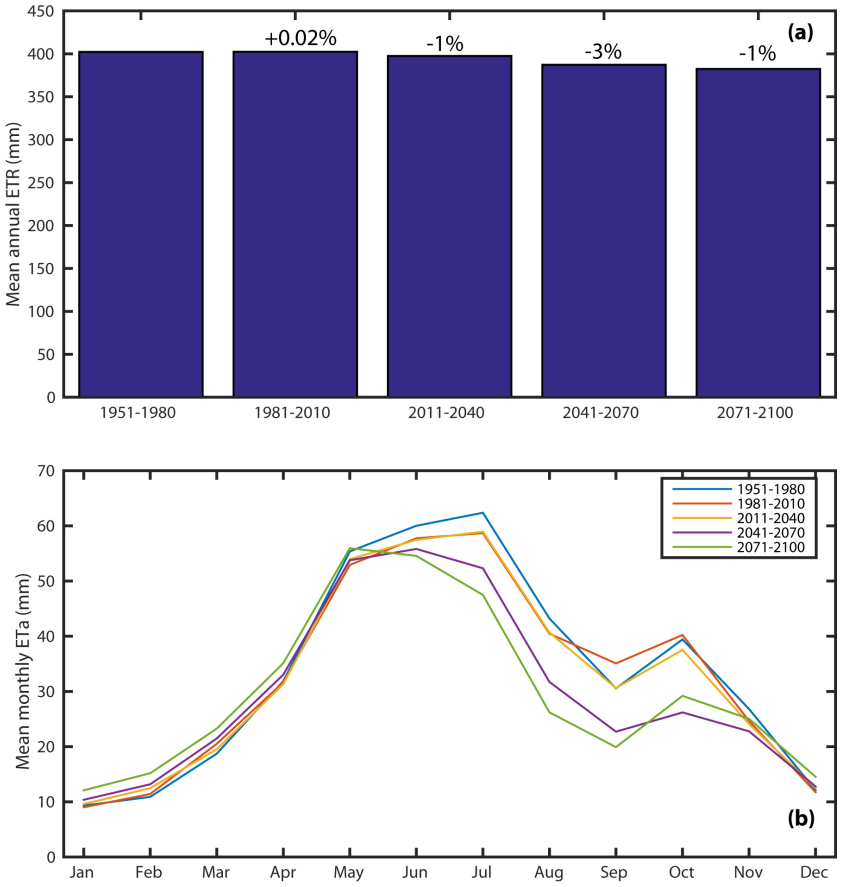

Figure 4.24. As Figure 4.21, but for actual evapotranspiration (ET_a).

4.3.3. Summary and concluding remarks

A preliminary implementation of the TOPKAPI-X model on a complex system, the Flumendosa basin, is presented, with the aim to evaluate climate change impacts at a much larger scale. This region was prone to prolonged periods of drought, together with social and economic problems created by conflicts amongst different water uses. In addition, some villages within the basin (for instance Ballao, St. Vito, Muravera, and Villaputzu) have suffered extreme flood episodes that required the intervention of the civil protection agency and that caused loss of human lives. Hydrometeorological data from the Italian Hydrologic Survey were collected within and around the Flumendosa basin at a daily time scale from 1926 to 1936, and were used

to calibrate and validate the hydrologic model, leading to satisfactory results. The model performance was evaluated using the Nash-Sutcliffe index. After calibration and validation, TOPKAPI-X is applied in cascade with climate models in order to evaluate the effects of climate change for five 30-year periods (1951-1980, 1981-2010, 2011-2040, 2041-2070, 2071-2100). Climate model output, suitably bias corrected and downscaled, were analyzed for the five considered periods by comparing mean monthly and annual values of precipitation and temperature averaged among the four climate models. The models predict decreasing mean annual precipitation from the period 2011-2040 until the period 2071-2100, with percent changes of about -27%, and an increase of +2% in the second period 1981-2010. The seasonal distribution of precipitation reported a peak during the month of October. The models predict also an increase of T among all the five periods of about 3ºC (Figure 4.20c) and for all months. Hydrologic model outputs were analyzed in terms of discharge, soil water content, and actual evapotranspiration. Simulation results show decreasing mean annual value of discharge, soil water content, and actual evapotranspiration from the period 2011-2040 until the period 2071-2100, with percent changes of about, respectively, -60%, -20%, and -5%, and slightly increasing values of the same variables during the second period 1981-2010.

These results lend strong support to a future scenario of increased water shortages also in this region of the Mediterranean basin.

5. Conclusions

The main contributions of this research work are summarized in this final chapter. The main objective of this thesis is to develop a modeling approach to assess local hydrologic impacts of climate change in two Mediterranean basins, located in Sardinia, Italy. The work to achieve this general objective is elaborated into three stages. A detailed comparison of the responses obtained with three physically based hydrologic models but to varying degrees as regards physical processes and terrain features representation – CATchment HYdrology (CATHY), TIN-based Real time Integrated Basin Simulator (tRIBS), and TOPographic Kinematic APproximation and Integration-eXtended (TOPKAPI-X) – on a semi-arid Mediterranean catchment located in Sardinia, the Rio Mannu, is carried out, with the aim to test the parameter transferability among them, focusing in particular on the calibration and validation difficulties. While the three hydrologic models responded similarly during the calibration year, significant differences were found for the drier validation period for the CATHY model, which produced very low streamflow. To obtain satisfactory results for the CATHY model, an hypothesis of soil crusting was assumed and the first soil layer was modeled with a lower saturated hydraulic conductivity.

The effects of climate change are then evaluated on the Rio Mannu catchment through comparison of the results from five hydrologic models, CATHY, Soil and Water Assessment Tool (SWAT), TOPKAPI-X, tRIBS, and Water flow and balance Simulation Model (WASIM), and using as atmospheric input outputs of four global (GCM) and regional (RCM) climate model combinations. In order to evaluate uncertainties a new metric, proposed by Duveiller et al. (2016), is used: climate and hydrologic models results are compared in terms of agreement with each other in reference (1971-2000) and future (2041-2070) periods using Pearson correlation

values and Duveiller bias as in Kollet et al. (2017). Notwithstanding some differences, overall the five hydrologic models show good agreement, and they responded similarly to the reduced precipitation and increased temperatures predicted by the climate models, lending strong support to a future scenario of increased water shortages for this region of the Mediterranean, with negative consequences especially for the agricultural sector.

Finally, a preliminary implementation of the TOPKAPI-X model on a large Sardinian basin prone to extreme flood events, the Flumendosa, is shown with the aim to test the hydrologic impact of climate change at much larger scale for five 30-year periods (1951-1980, 1981-2010, 2011-2040, 2041-2070, 2071-2100) using as atmospheric input the outputs of four global (GCM) and regional (RCM) climate model combinations. The TOPKAPI-X model responds with decreasing value of discharge, soil water content, and actual evapotranspiration to the reduced precipitation and increased temperature predicted by the climate models from the period 2011-2040 to the period 2071-2100, lending strong support to a future scenario of increased water shortages also in this basin of the Mediterranean region.

References

Abbaspour, K.C., M. Faramarzi, S.S Ghasemi, and H. Yang, Assessing the impact of climate change on water resources in Iran, Water Resources Research, 45, W10434, 2009.

Abbott, M.B., J.C. Bathurst, J.A. Cunge, P.E. O'Connell, and J. Rasmussen, An introduction to the European Hydrological System — Systeme Hydrologique Europeen, "SHE", 1: History and philosophy of a physically-based, distributed modelling system, Journal of Hydrology, 87(1-2), 45-59, doi: 10.1016/0022-1694(86)90114-9, 1986.

Abrahams, A.D., G. Li, and A.J. Parsons, Rill hydraulics on a semi- arid hillslope, southern Arizona, Earth Surf. Processes Landforms, 21(1), 35–47, doi:10.1002/(SICI)1096-9837(199601), 1994.

Acero, F.J., J.A. García, M.C. Gallego, S. Parey, and D. Dacunha-Castelle, Trends in summer extreme temperatures over the Iberian Peninsula using nonurban station data, Journal of Geophysical Research Atmospheres, 119 (1), 39–53, 2014.

Adamovic, M., F. Branger, I. Braud, and S. Kralisch, Development of a data-driven semi-distributed hydrological model for regional scale catchments prone to Mediterranean flash floods, Journal of Hydrology 541, 173–189, 2016.

Ahuja, L.R., Applicability of the Green-Ampt approach to water infiltration through surface crusts, Soil Science, 118, 283–288, 1974.

Ahuja, L.R., Modeling infiltration into crusted soils by the Green- Ampt approach, Soil Science Society of America Journal, 47, 412–418, 1983.

Anderson, E., National Weather River Forecast System – Snow Accumulation and Ablation Model, NOAA, Tech. Mem., NWS-Hydro-17, U.S. Department of Commerce, USA, 1973.

Arnold, J.R., R. Srinivasan, R.S. Muttiah, and J.R. Williams, Large area hydrologic modeling and assessment. Part 1: Model development, Journal of the American Water Resources Association, 34(1), 73-89, 1998.

Arnold, J.G., R. Srinivasan, R.S. Muttiah, P.M. Allen, and C. Walker, Continental-scale simulation of the hydrologic balance, Journal of the American Water Resources Association, 35(5): 1037-1052, 1999a.

Artan, G., J. Verdin, and K. Asante, A wide-area flood risk monitoring model, Proc. 5th Int. Workshop on Application of Remote Sensing in Hydrology, Montpellier, France, 2001.

Aru, A., Baldaccini, P., and A. Vacca, Carta dei suoli della Sardegna 1:250,000. Regione Autonoma della Sardegna, Assessorato Programmazione, Bilancio ed Assetto del Territorio, 1992.

Assouline, S., Infiltration into soils: Conceptual approaches and solutions, Water Resources Research, 49, 1755–1772, doi:10.1002/wrcr.20155, 2013.

Bae, D.H., I.W. Jung, and D.P. Lettenmaier, Hydrologic uncertainties in climate change from IPCC AR4 GCM simulations of the Chungju Basin, Korea, Journal of Hydrology, 401, 90–105, 2011.

Band, L.E., Topographic partition of watersheds with digital elevation models, Water Resources Research, 22, 15–24, 1986.

Bartholomes, J. and E. Todini, Coupling meteorological and hydrological model for flood forecasting, Hydrology and Earth System Sciences, 9, 333-346, 2005.

Bastola, S., C. Murphy, and J. Sweeney, The role of hydrological modelling uncertainties in climate change impact assessments of Irish river catchments, Advances in Water Resources, 34, 562–576. http://dx.doi.org/10.1016/j.advwatres.2011.01.008, 2011.

Bathurst, J.C., Physically-based distributed modelling of an upland catchment using the Système Hydrologique Europèen, Journal of Hydrology, 87(1-2), 79–102, doi:10.1016/0022-1694(86)90116-2, 1986.

Bathurst, J.C., Flow resistance through the channel network, in Channel Network Hydrology, edited by K. Beven and M. J. Kirkby, pp. 69 – 98, John Wiley, New York, 1993.

Beven, K.J., On subsurface stormflow: An analysis of response times, Hydrological Sciences Journal, 27, 505–521, 1982.

Beven, K.J., Infiltration into a class of vertically non-uniform soils, Hydrological Sciences Journal, 29, 425–434, 1984.

Birsan, M.V., Application of a distributed physically-based hydrological model on the upper river basin of Somesul Mare (Northern Romania), Romanian Reports in Physics, 65(4), 1469–1478, 2013.

Bosshard, T., M. Carambia, K. Goergen, S. Kotlarski, P. Krahe, M. Zappa, C. Schär, Quantifying uncertainty sources in an ensemble of hydrological climate- impact projections, Water Resources Research, 49, 1523–1536. http://dx.doi.org/ 10.1029/2011WR011533, 2013.

Brakensiek, D.L., and W.J. Rawls, Agricultural management effects on water processes: II. Green and Ampt parameters for crusting soils, Trans. ASAE, 26, 1753–1757, 1983.

Breuer, L., J.A. Huisman, P. Willems, H. Bormann, A. Bronstert, B.F.W. Croke, H.G. Frede, T. Graeff, L. Hubrechts, A.J. Jakeman, G. Kite, J. Lanini, G. Leavesley, D.P. Lettenmaier, G. Lindstroem, J. Seibert, M. Sivapalan, and N.R. Viney, Assessing the impact of land use change on hydrology by ensemble modeling (LUCHEM). I: Model intercomparison with current land

use, Advances in Water Resources, 32 (2), 129–146, http://dx.doi.org/10.1016/j.advwatres.2008.10.003, 2009.

Braun, L.N., Simulation of snowmelt-runoff in lowland and lower alpine regions of Switzerland, Zürcher Gegraphische Schriften, ETH Zürich, 21, 166 pp, 1985.

Brooks, R.H., and A.T. Corey, Hydraulic properties of porous media, Hydrology Papers 3, Colorado State University, Fort Collins, 1964.

Cabral, M.C., L. Garrote, R.L. Bras, and D. Entekhabi, A kinematic model of infiltration and runoff generation in layered and sloped soils, Advances in Water Resources, 15, 311–324, 1992.

Camporese, M., C. Paniconi, M. Putti, and S. Orlandini, Surface-subsurface flow modeling with path-based runoff routing, boundary condition-based coupling, and assimilation of multisource observation data, Water Resources Research, 46, W02512, doi:10.1029/2008WR007536, 2010.

Caracciolo, D., R. Deidda, and F. Viola, Analytical estimation of annual runoff distribution in ungauged seasonally dry basins based on a first order Taylor expansion of the Fu's equation, Advances in Water Resources 109, 320-332, https://doi.org/10.1016/j.advwatres.2017.09.019, 2017.

Cassiani, G., N. Ursino, R. Deiana, G. Vignoli, J. Boaga, M. Rossi, M.T. Perri, M. Blaschek, R. Duttmann, S. Meyer, R. Ludwig, A. Soddu, P. Dietrich, and U. Werban, Noninvasive monitoring of soil static characteristics and dynamic states: a case study highlighting vegetation effects on agricultural land, Vadose Zone Journal 11(3), 2012.

Cau, P., A. Cadeddu, C. Gallo, G. Lecca, and M. Marrocu, Estimating the water balance of the Sardinian island using the SWAT model, L'Acqua, 5, 29-38, 2005.

Chessa, P.A., G. Ficca, M. Marrocu, and R. Buizza, Application of a limited-area short-range ensemble forecast system to a case of heavy rainfall in the Mediterranean region, Weather and Forecasting, 19, 566–581, 2004.

Chiew, F., M. Stewardson, and T. McMahon, Comparison of six rainfall-runoff modelling approaches, Journal of Hydrology, 147, 1–36, 1993.

Childs, E.C., and M. Bybordi, The vertical movement of water in stratified porous material: 1. Infiltration, Water Resources Research, 5, 446 – 459, 1969.

Chow, V.T., Open-Channel Hydraulics, McGraw-Hill, New York, 1959.

Chu, S.T., C.A. Onstad, and W. J. Rawls, Field evaluation of layered Green-Ampt model for transient crust conditions, Trans. ASAE, 29, 1268–1272, 1277, 1986.

Ciarapica, L., and E. Todini, TOPKAPI: a model for the representation of the rainfall-runoff process at different scales, Hydrological processes, 16, 207-229, 2002.

Clark, M., A. Slater, D. Rupp, R. Woods, J. Vrugt, H. Gupta, T. Wagener, L. Hay, Framework for understanding structural errors (FUSE): a modular framework to diagnose differences between hydrological models, Water Resources Research, 44. http://dx.doi.org/10.1029/2007WR006735 W00B02, 2008.

Clark, M.P., D. Kavetski, and F. Fenicia, Pursuing the method of multiple working hypotheses for hydrological modeling, Water Resources Research, 47 (9), W09301, 2011.

Clarke, R.T., A review of some mathematical models used in hydrology, with observations on their calibration and use, Journal of Hydrology, 19, 1–20, 1973.

Cornelissen, T., B. Diekkrüger, and S. Giertz, A comparison of hydrological models for assessing the impact of land use and climate change on discharge in a tropical catchment, Journal of Hydrology, 498, 221-236, 2013.

Cudennec, C., C. Leduc, and D. Koutsoyiannis, Dryland hydrology in Mediterranean regions – a review, Hydrological Sciences Journal, 52, 1077-1087, 2007.

Dams, J., J. Nossent, T.B. Senbeta, P. Willems, and O. Batelaan, Multi-model approach to assess the impact of climate change on runoff, Journal of Hydrology 529, 1601–1616, 2015.

Deardorff, J.W., Efficient prediction of ground surface temperature and moisture with inclusion of a layer of vegetation, Journal of Geophysical Research, 82, 1889–1903, 1978.

Deidda, R., Rainfall downscaling in a space-time multifractal framework, Water Resources Research, 36(7), 1779–1784, 2000.

Deidda, R., R. Benzi, and F. Siccardi, Multifractal modeling of anomalous scaling laws in rainfall, Water Resources Research, 35, 1853–1867, 1999.

Deidda, R., M. Marroccu, G. Caroletti, G. Pusceddu, A. Langousis, V. Lucarini, M. Puliga, and A. Speranza, Climate model validation and selection for hydrological applications in representative Mediterranean catchments, Hydrology and Earth System Sciences, 17, 5041-5059, 2013.

Del Río, S., L. Herrero, R. Fraile, A. Penas, Spatial distribution of recent rainfall trends in Spain (1961–2006), International Journal of Climatology, 31 (5), 656–667, 2011.

Dingman, S.L., Physical Hydrology – Waveland Press, Inc. Long Grove, Illinois, 2008.

Donnelly-Makowecki, L. and R. Moore, Hierarchical testing of three rainfall–runoff models in small forested catchments, Journal of Hydrology, 219, 136–152, 1999.

Dooge, J., Looking for hydrologic laws, Water Resources Research, 22, 46-58, 1986.

Doorembos, J., W.O. Pruitt, A. Aboukhaled, J. Damagnez, N.G. Dastane, C. van den Berg, P.E. Rijtema, O.M. Ashford, and M. Frere, Guidelines for predicting crop water requirements, FAO Irrigation and Drainage Paper, No. 24, 1984.

Duan, Q., J. Schaake, V. Andréassian, S. Franks, G. Goteti, G. Gupta, Y.M. Gusev, F. Habets, A. Hall, L. Hay, T. Hogue, M. Huang, G. Leavesley, X. Liang, O.N. Nasonova, J. Noilhan, L. Oudin, S. Sorooshian, T. Wagener, E.F. Wood, Model Parameter Estimation Experiment (MOPEX): an overview of science strategy and major results from the second and third workshops, Journal of Hydrology, 320, 3–17, http://dx.doi.org/10.1016/j.jhydrol.2005.07.031, 2006.

Dunne, T., Field studies of hillslope flow process, Hillslope Hydrology, M. J. Kirkby (Ed.), Wiley, Chichester, UK, 227–293, 1978.

Duveiller, G., D. Fasbender, and M. Meroni, Revisiting the concept of a symmetric index of agreement for continuous datasets, Scientific Reports, 6:9401, doi: 10.1038/srep19401, 2016.

El Kenawy, A., J.I. López-Moreno, and S.M. Vicente-Serrano, Recent trends in daily temperature extremes over northeastern Spain (1960–2006), Natural Hazards and Earth System Sciences, 11 (9), 2583–2603, 2011.

Emmett, W.W., Overland flow, in Hillslope Hydrology, edited by M. J. Kirkby, p. 145 – 176, John Wiley, New York, 1978.

Farrell, D.A., and W.E. Larson, Dynamics of the soil-water system during a rainstorm, Soil Science, 113, 88–96, 1972.

Fatichi, S., E.R. Vivoni, F.L. Ogden, V.Y. Ivanov, B. Mirus, D. Gochis, C.W. Downer, M. Camporese, J.H. Davison, B. Ebel, and N. Jones, An overview of current applications, challenges, and future trends in distributed process-based models in hydrology, Journal of Hydrology, 537, 45-60, 2016.

Filion, R., M. Bernier, C. Paniconi, K. Chokmani, M. Melis, A. Soddu, M. Talazac, and F.-X. Lafortune, Remote sensing for mapping soil moisture and drainage potential in semi-arid regions: Applications to the Campidano plain of Sardinia, Italy, Science of the Total Environment 543, 862–876 , 2016.

Fleckenstein, J.H., S. Krause, D.M. Hannah, and F. Boano, Groundwater-surface water interactions: New methods and models to improve understanding of processes and dynamics, Advances in Water Resources, 33, 1291–1295, 2010.

Fohrer, N., D. Möller, and N. Steiner, An interdisciplinary modelling approach to evaluate the effects of land use change. Phys. Chem. Earth 27(9-10): 655-662, 2002.

Forman, B.A., E.R. Vivoni, and S.A. Margulis, Evaluation of ensemble-based distributed hydrologic model response with disaggregated precipitation products, Water Resources Research, 44, 1–18, doi:10.1029/2008WR006827, 2008.

Fowler, H.J., S. Blenkinsop, and C. Tebaldi, Review Linking climate change modelling to impacts studies: recent advances in downscaling techniques for hydrological modelling. International Journal of Climatology 27, 1547– 1578, 2007.

Gädeke, A., H. Hölzel, H. Koch, I. Pohle, and U. Grünewald, Analysis of uncertainties in the hydrological response of a model-based climate change impact assessment in a subcatchment of the Spree River, Germany, Hydrological Processes, 28, 3978–3998, 2014.

Gatel, L., C. Lauvernet, N. Carluer, C. Paniconi, Effect of surface and subsurface heterogeneity on the hydrological response of a grassed buffer zone, Journal of Hydrology 542, 637-64, 2016.

Gaume, E., V. Bain, P. Bernardara, O. Newinger, M. Barbuc, A. Bateman, L. Blaškovicová, G. Blöschl, M. Borga, A. Dumitrescu, I. Daliakopoulos, J. Garcia, A. Irimescu, S. Kohnova, A. Koutroulis, L. Marchi, S. Matreata, V. Medina, E. Preciso, D. Sempere-Torres, G. Stancalie, J. Szolgay, I. Tsanis, D. Velasco, A. Viglione, A compilation of data on European flash floods. J. Hydrol. 367, 70–78, 2009.

Gauthier, M.J., M. Camporese, C. Rivard, C. Paniconi, and M. Larocque, A modeling study of heterogeneity and surface water-groundwater interactions in the Thomas Brook catchment, Annapolis Valley (Nova Scotia, Canada), Hydrology and Earth System Sciences, 13, 1583-1596, 2009.

Ghanbarian-Alavijeh, B., A. Liaghat, G.H. Huang, and M.Th. van Genuchten, Estimation of the van Genuchten soil water retention properties from soil textural data, Pedosphere, 20(4): 456–465, 2010.

Giandotti, M., Previsione delle piene e delle magre dei corsi d'acqua. Istituto Poligrafico dello Stato, 8, 107-117, 1934.

Giorgi, F., Climate change hot-spots, Geophysical Research Letters, 33, L08707, doi:10.1029/2006GL025734, 2006.

Giorgi, F., and P. Lionello, Climate change projections for the Mediterranean region, Global and Planetary Change, 63 (2–3), 90–104. http://dx.doi.org/10.1016/j.gloplacha.2007. 09.005, 2008.

Giorgi, F. and L.O. Mearns, Introduction to special section: regional climate modeling revisited, Journal of Geophysical Research, 104, 6335–6352, doi:10.1029/98JD02072, 1999.

Giorgi, F., and L.O. Mearns, Calculation of average, uncertainty range, and reliability of regional climate changes from AOGCM simulations via the ''Reliability Ensemble Averaging (REA)'' method, Journal of Climate, 15 (10), 1141–1158, 2002.

Goodrich, D.C., D.A. Woolhiser, and T.O. Keefer, Kinematic routing using finite elements on a triangular irregular network, Water Resources Research, 27, 995–1003, 1991.

Gorgen, K., J. Beersma, G. Brahmer, H. Buiteveld, M. Carambia, O. de Keizer, P. Krahe, E. Nilson, R. Lammersen, C. Perrin, and D. Volken, Assessment of climate change impacts on discharge in the Rhine river basin?: Results of the Rhein- Blick2050 project, International Commission for the Hydrology of the Rhine Basin Secretariat, Lelystad, p. 211, 2010.

Gosling, S.N., R.G. Taylor, N.W. Arnell, and M.C. Todd, A comparative analysis of projected impacts of climate change on river runoff from global and catchment- scale hydrological models, Hydrology and Earth System Sciences, 15, 279–294. http://dx.doi. org/10.5194/hess-15-279-2011, 2011.

Gottardi, G, and M. Venutelli, A control-volume finite element model for two-dimensional overland flow, Advances in Water Resources, 16, 227–84, 1993.

Graham, L.P., Hagemann, preting hydrological change from regional climate models, Climatic Change, 81, 97–122, 2007.

Grouillet, B, Fabre, J., Ruelland, D., and A. Dezetter, Historical reconstruction and 2050 projections of water demand under anthropogenic and climate changes in two contrasted Mediterranean catchments, Journal of Hydrology, 522, 684–696, 2015.

Gunduz, O., and M.M. Aral, River networks and groundwater flow: a simultaneous solution of a coupled system, Journal of Hydrology, 301, 216–34, 2005.

Gurtz, J., M. Zappa, K. Jasper, M. Verbunt, A. Badoux, T. Vitvar, and H. Lang, Modelling of runoff and its components and model validation in Swiss pre-alpine and alpine catchments. In: Freiburger Schriften zur Hydrologie, Band 13: 206–220, 2001.

Hargreaves, G.H., Defining and using reference evapotranspiration, Journal of Irrigation and Drainage Engineering, 120(6), 1132–1139, 1994.

Hargreaves, G.H., and R.G. Allen, History and evaluation of Hargreaves evapotraspiration equation, Journal of Irrigation and Drainage Engineering, 129(1), 53–63, 2003.

Hasson, S., V. Lucarini, and S. Pascale, Hydrological cycle over South and Southeast Asian river basins as simulated by PCMDI/CMIP3 experiments, Earth System Dynamics, 4, 199–217, doi:10.5194/esd-4-199-2013, 2013.

Hasson, S., V. Lucarini, S. Pascale, and J. Böhner, Seasonality of the hydrological cycle in major South and Southeast Asian river basins as simulated by PCMDI/CMIP3 experiments, Earth System Dynamics, 5, 67–87, doi:10.5194/esd-5-67-2014, 2014.

Haylock, M.R., Hofstra, N., Klein Tank, A.M.G., Klok, E.J., Jones, P.D., and M. New, A European daily high-resolution gridded dataset of surface temperature and precipitation, Journal of Geophysical Researchv, 113, D20119, doi:10.1029/2008JD010201, 2008.

Hillel, D., and W.R. Gardner, Steady infiltration into crust topped profiles, Soil Science, 108, 137–142, 1969.

Hillel, D., and W.R. Gardner, Transient infiltration into crust topped profiles, Soil Science, 109, 69–76, 1970.

Hogue, T. S., L. A. Bastidas, H. V. Gupta, S. Sorooshian, K. Mitchell, and W. Emmerich, Evaluation and transferability of the Noah land surface model in semiarid environments, Journal of Hydrometeorology, 6, 68–84, doi:10.1175/JHM-402.1, 2005.

Horton, R.E., The role of infiltration in the hydrologic cycle, Earth and Space Science news, 14(1), 446-460, doi: 10.1029/TR014i001p00446, 1933.

Hotchkiss, R.H., S. F. Jorgensen, M.C. Stone, and T.A. Fontaine. Regulated river modeling for climate change impact assessment: The Missouri River, Journal of the American Water Resource Association, 36(2): 375-386, 2000.

Hu, Z., and S. Islam, Prediction of ground surface temperature and soil moisture content by the force-restore method, Water Resources Research, 31, 2531 – 2539, 1995.

Huyakorn, P. S., S. D. Thomas, and B. M. Thompson, Techniques for making finite elements competitive in modeling flow in variably saturated porous media, Water Resources Research, 20(8), 1099-1115, 1984.

Huyakorn, P.S, E.P. Springer, V. Guvanasen, and T.D. Wadsworth, A three-dimensional finite element model for simulating water flow in variably saturated porous media, Water Resources Research, 22(12), 1790–808, 1986.

Im, E.S., I.W. Jung, H. Chang, D.H. Bae, W.T. Kwon, Hydroclimatological response to dynamically downscaled climate change simulations for Korean basins, Climatic Change 100 (3), 485–508. doi:10.1007/s10584-009-9691-2, 2010.

IPCC, Climate Change 2014: Impacts, Adaptation, and Vulnerability. Part A: Global and Sectoral Aspects. Contribution of Working Group II to the Fifth Assessment Report of the Intergovernmental Panel on Climate Change [Field, C.B., V.R. Barros, D.J. Dokken, K.J. Mach, M.D. Mastrandrea, T.E. Bilir, M. Chatterjee, K.L. Ebi, Y.O. Estrada, R.C. Genova, B. Girma, E.S. Kissel, A.N. Levy, S. MacCracken, P.R. Mastrandrea, and L.L. White (eds.)], Cambridge University Press, Cambridge, United Kingdom and New York, NY, USA, 1132 pp., 2014.

Ivanov, V.Y., E.R. Vivoni, R.L. Bras, and D. Entekhabi, Catchment hydrologic response with a fully-distributed triangulated irregular network model, Water Resources Research, 40(11), doi:10.1029/2004WR003218, 1–23, 2004a.

Ivanov, V.Y., E.R. Vivoni, R.L. Bras, and D. Entekhabi, Preserving high-resolution surface and rainfall data in operational-scale basin hydrology: A fully-distributed physically-based approach, Journal of Hydrology, 298, 80–111, doi:10.1016/j.jhydrol.2004.03.041, 2004b.

Jaber, F.H., and R.H. Mohtar, Stability and accuracy of two-dimensional kinematic wave overland flow modeling, Advances in Water Resources, 26, 1189–98, 2003.

Jang et al., Comparison of hydrological impacts of climate change simulated by six hydrological models in the Dongjiang Basin, South China, Journal of Hydrology, 336, 316-333, doi:10.1016/j.jhydrol.2007.01.010, 2007.

Jasper, K., Gurtz, J., and Lang, H.: Advanced flood forecasting in Alpine watersheds by coupling meteorological observations and forecasts with a distributed hydrological model Journal of Hydrology, 267, 40–52, 2002.

Johnson, M., Don D. Ratnayaka, M.J. Brandt, Twort's Water Supply, 6th edition, Elsevier, 2009.

Jones, J.E., and C.S. Woodward, Newton–Krylov-multigrid solvers for large-scale, highly heterogeneous, variably saturated flow problems, Advances in Water Resources, 24,763–74, 2001.

Kampf, S.K. and S.J. Burgess, A framework for classifying and comparing distributed hillslope and catchment hydrologic models, Water Resources Research, 43, W05423, doi:10.1029/2006WR005370, 2007.

Kay, A.L., H.N. Davies, V.A. Bell, and R.G. Jones, Comparison of uncertainty sources for climate change impacts: flood frequency in England, Climatic Change, 92, 41–63, 2009.

Kite, G.W., The SLURP model (Chapter 15), Computer models of watershed hydrology, V.P. Singh (Ed.), Water Resources Publications, Colorado, USA, 521-562, 1995.

Klemes, V., Operational testing of hydrological simulation models, Hydrological Science Journal, 31, 13-24, 1986.

Klok, E.J., Jasper, K., Roelofsma, K.P., Badoux, A., Gurtz, J., Distributed hydrological modelling of a glaciated Alpine river basin, Hydrological Science Journal, 46 (4), 553–570, 2001.

Koch, J., T. Cornelissen, Z. Fang, H. Bogena, B. Diekkruger, S. Kollet, and S. Stisen, Inter-comparison of three distributed hydrological models with respect to seasonal variability of soil moisture patterns at a small forested catchment, Journal of Hydrology 533, 234–249, 2016.

Kollet, S.J., and R.M. Maxwell, Integrated surface-groundwater flow modeling: A free-surface overland flow boundary condition in a parallel groundwater flow model, Advances in Water Resources, 29(7), 945-958, 2006.

Kollet, S., et al., The integrated hydrologic model intercomparison project, IH-MIP2: A second set of benchmark results to diagnose integrated hydrology and feedbacks, Water Resources Research, 53, doi:10.1002/ 2016WR019191, 2017.

Kirkland, M.R, R.G. Hills, and P.J. Wierenga, Algorithms for solving Richards equation for nonuniform porous media, Water Resources Research, 28, 2049–58, 1992.

Kunstmann, H. and Stadler, C.: High Resolution Distributed Atmospheric-Hydrological Modelling for Alpine Catchments, Journal of Hydrology, 314, 105–124, 2005.

Kunstmann, H., Schneider, K., Forkel, R., and Knoche, R.: Impact analysis of climate change for an Alpine catchment using high resolution dynamic downscaling of ECHAM 4 time slices, Hydrology and Earth System Sciences, 8, 1030–1044, 2004.

Leopold, L.B., and T. Maddock Jr., The hydraulic geometry of stream channels and some physiographic implications, Professional Paper 252, U.S. Geological Survey, Washington, D.C, 1953.

Lin, J.D., On the force-restore method for prediction of ground surface temperature, Journal of Geophysical Research, 85, 3251–3254, 1980.

Liston, G.E. and K. Elder, A meteorological distribution system for high-resolution terrestrial modeling (Micro Met), Journal of Hydrometeorology, 7, 217–234, 2006.

Liu, Z., and E. Todini, Towards a comprehensive physically-based rainfall-runoff model, Hydrology and Earth System Sciences, 6(5), 859-881, 2002.

Liu, Z., L.V. Mario and E. Todini, Flood forecasting using a fully distributed model: application of the TOPKAPI model to the Upper Xixian catchment, Hydrology and Earth System Sciences, 9, 347-364, 2005.

Liuzzo, L., L.V. Noto, E.R. Vivoni, and G. La Loggia, Basin-scale water resources assessment in Oklahoma under synthetic climate change scenarios using a fully distributed hydrological model, Journal of Hydrologic Engineering, 15(2), 107–122, 2010.

Lucarini, V., Validation of climate models, in: Encyclopaedia of Global Warming and Climate Change, edited by: Philander, G., SAGE, Thousand Oaks, USA, 1053–1057, 2008.

Lucarini, V., R. Danihlik, I. Kriegerova, and A. Speranza, Does the Danube exist? Versions of reality given by various regional climate models and climatological data sets, Journal of Geophysical Research, 112, D13103, doi:10.1029/2006JD008360, 2007.

Ludwig, R., The role of hydrological model complexity and uncertainty in climate change impact assessment, Advances in Geosciences, 21, 63–71, 2009.

Ludwig, R., et al., Climate-induced changes on the hydrology of Mediterranean basins - A research concept to reduce uncertainty and quantify risk, Fresenius Environmental Bulletin, 19 (10 A), 2379–2384, 2010.

Mackay, D.S., and L.E. Band, Extraction and representation of nested catchment areas from digital elevation models in lake-dominated topography, Water Resources Research, 34(4), 897-901, 1998.

Mamalakis, A., A. Langousis, R. Deidda, and M. Marrocu, A parametric approach for simultaneous bias correction and high-resolution downscaling of climate model rainfall, Water Resources Research, 53, 2149–2170, doi:10.1002/2016WR019578, 2017.

Mahfouf, J.F., and J. Noilhan, Comparative study of various formulations from bare soil using in situ data, Journal of Applied Meteorology and Climatology, 30, 1354–1365, 1991.

Majone, B., F. Villa, R. Deidda, and A. Bellin, Impact of climate change and water use policies on hydropower potential in the south-eastern Alpine region, Science of The Total Environment, 543, 965-980, 2016.

Marras, P., D. Muroni, S. Manca, C. Soru, G. Pusceddu, M. Marrocu, and P. Cau, (2014), The SWAT model and a web-based information system to assess the water balance of Sardinia (Italy), SWAT International Conference 2014.

Martina, M.L.V, E. Todini E and A. Libralon, A Bayesian decision approach to rainfall thresholds based flood warning, Hydrology and Earth System Sciences, 10, 413-426, 2006.

Mascaro, G., Vivoni, E.R., and Deidda, R., Implications of ensemble quantitative precipitation forecast errors on distributed streamflow forecasting, Journal of Hydrometeorology, 11(1), 69–86, doi:10.1175/2009JHM1144.1, 2010.

Mascaro, G., R. Deidda, and M. Hellies, On the nature of rainfall intermittency as revealed by different metrics and sampling approaches, Hydrology and Earth System Sciences, 17, 355–369, doi:10.5194/hess-17-355-2013, 2013a.

Mascaro, G., M. Piras, R. Deidda, and E.R. Vivoni, Distributed hydrologic modeling of a sparsely monitored basin in Sardinia, Italy, through hydrometeorological downscaling, Hydrology and Earth System Sciences, 17, 4143–4158, 2013b.

Maurer, E.P. and H.G. Hidalgo, Utility of daily vs. monthly large-scale climate data: an intercomparison of two statistical downscaling methods, Hydrology and Earth System Sciences, 12, 551–563, doi: 10.5194/hess-12-551-2008, 2008.

Maurer, E.-P., L.-D. Brekke, T. Pruitt, Contrasting lumped and distributed hydrology models for estimating climate change impacts on California watersheds, Journal of the American Water Resource Association, 46 (5), 1024–1035, 2010.

Mausbach, M.J., and A.R. Dedrick, The length we go: Measuring environmental benefits of conservation practices, Journal of Soil and Water Conservation, 59(5): 96A-103A, 2004.

Maxwell, R.M., F.K. Chow, and S.J. Kollet, The groundwater–land-surface–atmosphere connection: Soil moisture effects on the atmospheric boundary layer in fully-coupled simulations, Advances in Water Resources, 30(12), 2447–2466, doi:10.1016/j.advwatres.2007.05.018, 2007.

Merz, R., J. Parajka, and G. Bloschl, Time stability of catchment model parameters: Implications for climate impact analyses, Water Resources Research, 47, 1–17, 2011.

Meyer, S., M. Blaschek, R. Duttmann, and R. Ludwig, Improved hydrological model parametrization for climate change impact assessment under data scarcity - The potential of field monitoring techniques and geostatistics, Science of The Total Environment, 543, 906-923, 2016.

Milano, M., D. Ruelland, S. Fernandez, A. Dezetter, J. Fabre, E. Servat, J.M. Fritsch, S. Ardoin-Bardin, G. Thivet, Current state of Mediterranean water resources and future trends under climatic and anthropogenic changes, Hydrological Sciences Journal, 58, 498–518, 2013a.

Montaldo, N., J.D. Albertson, and M. Mancini, Vegetation dynamics and soil water balance in a water-limited Mediterranean ecosystem on Sardinia, Italy, Hydrology and Earth System Sciences, 12, 1257–1271, 2008.

Monteith, J.L., Evaporation and environment, Symposia of the Society of Experimental Biology, 19, 205–234, 1965.

Montenegro, S., and R. Ragab, Impact of possible climate and land use changes in the semi-arid regions: a case study from North Eastern Brazil, Journal of Hydrology, 434-435, 55–68, 2012.

Montgomery, D.R., and E. Foufoula-Georgiou, Channel network source representation using digital elevation models, Water Resources Research, 29(12), 3925-3934, 1993.

Moore, I.D., Infiltration equations modified for surface effect, J. Irrig. Drain. Div. Trans. ASAE, 107, 71–86, 1981a.
Moore, I.D., Effect of surface sealing on infiltration, Trans. ASAE, 24, 1546–1553, 1981b.

Morel-Seytoux, H.J., and J. Khanji, Derivation of an equation of infiltration, Water Resources Research, 10, 795–800, 1974.

Muma, M., S.J. Gumiere, A.N. Rousseau, C. Scudeler, C. Paniconi, Implementation of a root water extraction module in CATHY: Comparison of four empirical root-density distribution models. Four Decades of Progress in Monitoring and Modeling of Processes in the Soil-Plant-Atmosphere System: Applications and Challenges, 19-21 juin, Naples, Italy, Procedia Environmental Sciences, 19, 57-66, 2013.

Muma, M., S.J. Gumiere, A.N. Rousseau, Assessment of the impact of subsurface agricultural drainage on soil water storage and flows of a small watershed. Water, 8(8), 326, doi:10.3390/w8080326, 2016.

Murphy J.M., D.H.M. Sexton, D.N. Barnett, G.S. Jones, M.J. Webb, M. Collins et al., Quantification of modeling uncertainties in a large ensemble of climate change simulations. Nature, 430:768–72, 2004.

Najafi, M., H. Moradkhani, and I. Jung, Assessing the uncertainties of hydrologic model selection in climate change impact studies. Hydrol. Process. 25, 2814– 2826, 2011.
Orlandini, S., and R. Rosso, Diffusion wave modeling of distributed catchment
dynamics, Journal of Hydrologic Engineering, 1(3), 103-113, 1996.

Nakićeović, N., J. Alcamo, G. Davis, H.J.M. de Vries, J. Fenhann, S. Gaffin, K. Gregory, A. Grubler, T.Y. Jung, T. Kram, E.L. La Rovere, L. Michaelis, S. Mori, T. Morita, W. Papper, H. Pitcher, L. Price, K. Riahi, A. Roehrl, H-H Rogner, A. Sankovski, M. Schlesinger, P. Shukla, S. Smith, R. Swart, S. van Rooijen, N. Victor, and Z. Dadi, Emissions Scenarios, A Special Report of Working Group III of the Intergovernmental Panel on Climate Change. Cambridge University Press: Cambridge; 559, 2000.

Nash, J.E., and J.V. Sutcliffe, River flow forecasting through conceptual models part I—A discussion of principles, Journal of Hydrology, 10(3), 282–290, 1970.

Neitsch, S.L., J.G. Arnold, J.R. Kiniry, J.R. Williams, and K.W. King,
Soil and water assessment tool theoretical documentation—version 2005
Soil and water research laboratory, agricultural research service, US Department of Agriculture, Temple, 2005.

Neuman, S.P., Wetting front pressure head in the infiltration model of Green and Ampt, Water Resources Research, 12, 564–565, 1976.

Niu, G.-Y., C. Paniconi, P.A. Troch, R.L. Scott, M. Durcik, X. Zeng, T. Huxman, and D. C. Goodrich, An integrated model of catchment-scale ecohydrological processes: 1. Model description and tests over an energy-limited watershed, Ecohydrology, 7, 427–439, 2014.

Noto, L.V., Ivanov, V.Y., Bras, R.L., and Vivoni, E.R., Effects of initialization on response of a fully-distributed hydrologic model, Journal of Hydrology, 352(1-2), 107–125, doi:10.1016/j.jhydrol.2007.12.031, 2008.

O'Callaghan, J.F., and D.M. Mark, The extraction of drainage networks from digital elevation data, Computer Vision Graphics and Image Processing, 28, 323-344, 1984.

Orlandini, S., and G. Moretti, Determination of surface flow paths from gridded elevation data, Water Resources Research, 45, W03417, doi:10.1029/2008WR007099, 2009a.

Orlandini, S., and R. Rosso, Diffusion wave modeling of distributed catchment dynamics, Journal of Hydrologic Engineering, 1(3), 103-113, 1996.

Orlandini, S. and R. Rosso, Parameterization of stream channel geometry in the distributed modeling of catchment dynamics, Water Resources Research, 34(8), 1971- 1985, 1998.

Orlandini, S., G. Moretti, M. Franchini, B. Aldighieri, and B. Testa, Path-based methods for the determination of nondispersive drainage directions in grid-based digital elevation models, Water Resources Research, 39(6), 1144, doi:10.1029/2002WR001639, 2003.

Panday, S., and P.S. Huyakorn, A fully coupled physically-based spatially-distributed model for evaluating surface/subsurface flow, Advances in Water Resources, 27, 361–82, 2004.

Paniconi, C, and M. Putti, A comparison of Picard and Newton iteration in the numerical solution of multidimensional variably saturated flow problems, Water Resources Research, 30(12), 3357-3374, 1994.

Paniconi, C. and E.F. Wood, A detailed model for simulation of catchment scale subsurface hydrologic processes, Water Resources Research, 29(6), 161-178, 1993.

Paniconi, C. and M. Putti, Physically based modeling in catchment hydrology at 50: Survey and outlook, Water Resources Research, 51, 7090–7129, doi:10.1002/ 2015WR017780, 2015.

Parlange, J.-Y., W.L. Hogarth, and M.B. Parlange, Optimal analysis of the effect of a surface crust, Soil Science Society of America Journal, 48, 494–497, 1984b.

Patil, S.D., and M. Stieglitz, Comparing spatial and temporal transferability of hydrological model parameters, Journal of Hydrology, 525, 409-417, 2015.

Penman, H.L., Natural evaporation from open water, bare soil and grass, P. R. Soc. London, Ser-A, 193, 120–145, 1948.

Perra, E., M. Piras, R. Deidda, C. Paniconi, G. Mascaro, and E.R. Vivoni, On the parameter transferability across distributed hydrologic models in a semi-arid Mediterranean catchment, Hydrological Processes (in preparation), 2018.

Perra E., M. Piras, R. Deidda, C. Paniconi, G. Mascaro, E.R. Vivoni, P. Cau, P.A. Marras, R. Ludwig, and S. Meyer, Multimodel assessment of climate change-induced hydrologic impacts for a Mediterranean catchment, Hydrology and Earth System Sciences (submitted), 2018.

Perrin, C., C. Michel, and V. Andreassian, Does a large number of parameters enhance model performance? Comparative assessment of common catchment model structures on 429 catchments, Journal of Hydrology, 242, 275–301, 2001.

Piras, M., Evaluation of climate change impacts on the hydrologic response of a sparsely-monitored basin in Sardinia, Italy, through distributed hydrologic simulations and hydrometeorological downscaling, PhD Thesis, University of Cagliari, Italy, 2014.

Pitman, A., and A. Henderson-Sellers, Recent progress and results from the project for the intercomparison of landsurface parameterization schemes, Journal of Hydrology, 213, 128–135. http://dx.doi.org/10.1016/S0022-1694(98)00206-6, 1998.

Puigdefábregas, J., and T. Mendizabal, Perspectives on desertification: western Mediterranean, Journal of Arid Environments, 39, 209–224, 1998.

Pulina, M. A., L'evapotraspirazione potenziale in Sardegna in funzione dello studio del regime idrico dei suoli, Studi Sassaresi, Annali della Facoltà di Agraria dell'Università di Sassari, 1986.

Rawls, W. J., D.L. Brakensiek, and K.E. Saxton, Estimation of soil properties, T. ASAE, 1316–1328, 1982.

Reed S., V. Koren, M. Smith, Z. Zhang, F. Moreda, D.J. Seo, and DMIP Participants, Overall Distributed Model Intercomparison Project results, Journal of Hydrology, 298(1–4), 60–34, 2004.

Refsgaard, J., and J. Knudsen, Operational validation and intercomparison of different types of hydrological model, Water Resources Research, 32, 2189–2202. http:// dx.doi.org/10.1029/96WR00896, 1996.

Refsgaard, J., J. Vandersluijs, J. Brown, and P. Vanderkeur, A framework for dealing with uncertainty due to model structure error, Advance in Water Resoures, 29, 1586–1597, 2006.

Ren, H., Z. Hou, M. Huang, J. Bao, Y. Sun, T. Tesfa, and L.R. Leung, Classification of hydrological parameter sensitivity and evaluation of parameter transferability across 431 US MOPEX basins, Journal of Hydrology, 536, 92-108, 2016.

Rieger, W., Winter, F., Disse, M., Uncertainties of soil parameterisation in process- based simulation of distributed flood control measures, Advances in Geoscience, 2010.

Rosenberg, N.J., D.L. Epstein, D. Wang, L. Vail, R. Srinivasan, and J.G. Arnold, Possible impacts of global warming on the hydrology of the Ogallala aquifer region, Climate Change 42(4): 677-692, 1999.

Rummukainen, M., State-of-the-art with regional climate models, WIREs Climate Change, 1, 82–96, doi:10.1002/wcc.8, 2010.

Rutter, A. J., K.A. Kershaw, P.C. Robins, and A.J. Morton, A predictive model of rainfall interception in forests: 1. Derivation of the model from observation in a plantation of Corsican pine, Agrilultural and Forest Meteorology, 9, 367–384, 1971.

Safari, A., F. De Smedt, and F. Moreda, WetSpa model application in the Distributed Model Intercomparison Project (DMIP2), Journal of Hydrology, 418–419, 78–89. http://dx.doi.org/10.1016/j.jhydrol.2009.04.001, 2012.

Schulla, J., Hydrologische Modellierung von Flussgebieten zur Abschatzung der Folgen von Klimaanderungen. Zurcher Geographische Schriften, Heft 69, ETH Zurich, pp. 187, 1997.

Schulla, J., K. Zoellmann, and W. Kinzelbach, Sustainable agriculture and water management in semi arid regions, Second Inter-Regional Conference on Environment-Water, September 1–3, Lausanne, 1999.

Schulla, J., Model description WaSiM (Water balance Simulation Model), Hydrology Software Consulting, Regensdorferstrasse, Zurich, 2015.

Schulla, J. and Jasper, K., Model Description WASIM-ETH (Water Balance Simulation Model ETH), ETH-Zurich, Zurich, 2001.

SCS, Estimation of Direct Runoff from Storm Rainfall, National Engineering Handbook, Section 4 – Hydrology, USDA, 10.1–10.24pp.

Scudeler, C., C. Paniconi, D. Pasetto, M. Putti, Examination of the seepage face boundary condition in subsurface and coupled surface/subsurface hydrological models, Water Resources Research, DOI: 10.1002/2016WR019277, 2017.

Seibert, J., Reliability of model predictions outside calibration conditions, Nord. Hydrol., 34, 477–492, 2003.

Seiller G., F. Anctil, and C. Perrin, Multimodel evaluation of twenty lumped hydrological models under contrasted climate conditions, Hydrology and Earth System Sciences, 16, 1171–1189, 2012.

Seoni, A., Modelli di preannuncio delle piene in piccoli bacini ed incertezze legate alla densita' della rete pluviometrica, PhD Thesis, University of Cagliari, Italy, 2015.

Silvestro, F., S. Gabellani, F. Giannoni, A. Parodi, N. Rebora, R. Rudari, and F. Siccardi, A hydrological analysis of the 4 November 2011 event in Genoa, Natural Hazard and Earth System Sciences, 12, 2743–2752, 2012.

Singh, V.P., Kinematic Wave Modeling in Water Resources: Surface Water Hydrology, John Wiley, Hoboken, N.J, 1996.

Smith, R.E., C. Corradini, and F. Melone, Modeling infiltration for multistorm runoff events, Water Resources Research, 29, 133–144, 1993.

Smith, M., K., Georgakakos, and X. Liang, Special issue: the distributed model intercomparison project (DMIP), Journal of Hydrology, 298, 1–3. http://dx.doi.org/10.1016/j. jhydrol.2004.05.001, 2004.

Smith, M., V. Koren, Z. Zhang, Y. Zhang, S. Reed, Z. Cui, F. Moreda, B. Cosgrove, N. Mizukami, E. Anderson, and DMIP 2 Participants, Results of the DMIP2 Oklahoma experiments, Journal of Hydrology, 418–419, 17–48, http://dx.doi.org/10.1016/j. jhydrol.2011.08.056, 2012.

Sousa, P.M., R.M. Trigo, P. Aizpurua, R. Nieto, L. Gimeno, R. Garcia-Herrera, Trends and extremes of drought indices throughout the 20th century in the mediterranean, Natural Hazards and Earth System Sciences, 11 (1), 33–51. http://dx.doi.org/10.5194/nhess-11-33- 2011, 2011.

Stonefelt, M.D., T.A. Fontaine, and R.H. Hotchkiss, Impacts of climate change on water yield in the upper Wind River basin, Journal of the American Water Resource Association, 36(2): 321-336, 2000.

Sulis, M., S.B. Meyerhoff, C. Paniconi, R.M. Maxwell, M. Putti, and S.J. Kollet, A comparison of two physics-based numerical models for simulating surface water–groundwater interactions, Advances in Water Resources, 33, 456-467, 2010.

Sulis, M., C. Paniconi, and M. Camporese, Impact of grid resolution on the integrated and distributed response of a coupled surface–subsurface hydrological model for the des Anglais catchment, Quebec, Hydrological Processes, 25, 1853–1865, 2011.

Sulis, M., C. Paniconi, C. Rivard, R. Harvey, and D. Chaumont, Assessment of climate change impacts at the catchment scale with a detailed hydrological model of surface-subsurface interactions and comparison with a land surface model, Water Resources Research, 47, W01513, doi:10.1029/2010WR009167, 2011.

Sulis, M., Paniconi, C., Marroccu, M., Huard, D., and Chaumont, D.: Hydrologic response to multimodel climate output using a physically based model of groundwater/surface water interactions, Water Resources Research, 48, W12510, doi:10.1029/2012WR012304, 2012.

Tarboton, D.G., A new method for the determination of flow directions and contributing areas in grid digital elevation models, Water Resources Research, 33(2), 309-319, 1997.

Taylor, C., G. Al-Mashidani, and J.M. Davis, A finite element approach to watershed runoff, Journal of Hydrology, 21, 231–46, 1974.

Tebaldi, C., R.L. Smith, D. Nychka, L.O. Mearns, Quantifying uncertainty in projections of regional climate change: a Bayesian approach to the analysis of multimodel ensembles, Journal of Climate 18, 1524–1540, 2005.

Thompson, J.R., A.J. Green, D.G. Kingston, and S.N. Gosling, Assessment of uncertainty in river flow projections for the Mekong River using multiple GCMs and hydrological models, Journal of Hydrology, 486,1-30, 2013.

Thornthwaite, C.W., and J.R. Mather, The water balance, Climatology, 8 (l), Laboratory of Climatology, Centerton, NJ, 1955.

Todini, E. and L. Ciarapica, The TOPKAPI model, Mathematical Models of Large Watershed Hydrology, V.P. Singh et al. (Eds.), Water Resources Publications, 12, Littleton, Colorado, 2001.

Tooth, S., Arid geomorphology: investigating past, present and future changes, Progress in Physical Geography 31, 319–335, 2007.

USDA Soil Conservation Service, National Engineering Handbook, Section 4 Hydrology, Chapters 4-10, 1972.

VanderKwaak, J.E, and K. Loague, Hydrologic-response simulations for the R-5 catchment with a comprehensive physics-based model, Water Resources Research, 37(4), 999–1013, 2001.

van der Linden, P. and J.F.B. Mitchell, ENSEMBLES: Climate change and its impacts: Summary of research and results from the ENSEMBLES project, Met Office Hadley Centre, Exeter, UK, 2009.

Van Genuchten, M.T., and D.R. Nielsen, On describing and predicting the hydraulic properties of unsaturated soils, Annales Geophysicae, 3(5), 615-628, 1985.

Vandervaere, J.-P., M. Vauclin, R. Haverkamp, C. Peugeot, J.-L. Thony, and M. Gilfedder, Prediction of crust-induced surface runoff with disc infiltrometer data, Soil Science, 163, 9–21, 1998.

Vansteenkiste, T., M. Tavakoli, V. Ntegeka, F. De Smedt, O. Batelaan, F. Pereira, P. Willems, Intercomparison of hydrological model structures and calibration approaches in climate scenario impact projections, Journal of Hydrology, 519, 743–755, http://dx.doi.org/10.1016/j.jhydrol.2014.07.062, 2014a.

Vansteenkiste, T., M. Tavakoli, N. Van Steenbergen, F. De Smedt, O. Batelaan, F. Pereira, and P. Willems, Intercomparison of five lumped and distributed models for catchment runoff and extreme flow simulation, Journal of Hydrology, 511, 335– 349. http://dx.doi.org/10.1016/j.jhydrol.2014.01.050, 2014b.

Vaze, J., D.A. Post, F.H.S. Chiew, J.-M. Perraud, N.R. Viney, and J. Teng, Climate non-stationarity – Validity of calibrated rainfall-runoff models for use in climate change studies, Journal of Hydrology, 394, 447–457, 2010.

Velázquez, J.A., J. Schmid, S. Ricard, M.J. Muerth, B. Gauvin St-Denis, M. Minville, D. Chaumont, D. Caya, R. Ludwig, and R. Turcotte, An ensemble approach to assess hydrological

models' contribution to uncertainties in the analysis of climate change impact on water resources, Hydrology and Earth System Sciences, 17, 565-578, 2013.

Vicente-Serrano, S.M., and J.M. Cuadrat-Prats, Trends in drought intensity and variability in the middle Ebro valley (NE of the Iberian peninsula) during the second half of the twentieth century. Theoretical and Applied Climatology, 88 (3–4), 247–258. http://dx.doi.org/10. 1007/s00704-006-0236-6, 2007.

Vischel, T., G. Pegram, S. Sinclair, and M. Parak, Implementation of the TOPKAPI model in South Africa: Initial results from the Liebenbergsvlei catchment, Water SA, 34(3), 331-342, 2008.

Vivoni, E. R., V.Y. Ivanov, R.L. Bras, and D. Entekhabi, Generation of triangulated irregular networks based on hydrological similarity, Journal of Hydrologic Engineering, 9(4), 288–302, doi:10.1061/ASCE1084-0699(2004)9:4(288), 2004.

Vivoni, E.R., V.Y. Ivanov, R.L. Bras, and D. Entekhabi, On the effects of triangulated terrain resolution on distributed hydrologic model response, Hydrological Processes, 19(11), 2101–2122, doi:10.1002/hyp.5671, 2005.

Vivoni, E.R., Entekhabi, D., Bras, R.L., Ivanov, V.Y, Van Horne, M.P, Grassotti, C., and Hoffman, R.N., Extending the predictability of hydrometeorological flood events using radar rainfall nowcasting, Journal of Hydrometeorology, 7(4), 660–677, 2006.

Vivoni, E.R., Rodriguez, J.C., and Watts, C.J., On the spatiotemporal variability of soil moisture and evapotranspiration in a mountainous basin within the North American monsoon region, Water Resources Research, 46, W02509, 1-18, doi:10.1029/2009WR008240, 2010.

Vivoni, E.R., A. Rango, C.A. Anderson, N.A. Pierini, A.P. Schreiner-McGraw, S. Saripalli, and A. S. Laliberte, Ecohydrology with unmanned aerial vehicles. Ecosphere 5(10):130, http://dx.doi.org/10.1890/ES14-00217.1, 2014.

Volk, M., J. Hirschfeld, G. Schmidt, C. Bohn, A. Dehnhardt, S. Liersch, and L. Lymburner, A SDSS-based ecological-economic modeling approach for integrated river basin management on different scale levels: The project FLUMAGIS. Water Resour Manage 21:2049–2061, DOI 10.1007/s11269-007-9158-z, 2007.

Whisler, F.D, A.A. Curtis, A. Niknam, and M.J.M. Römkens, Modeling infiltration as affected by soil crusting, in Proceedings of the Fort Collins Third International Hydrology Symposium, Fort Collins, Colorado, June 1977, pp. 400–413, 1979.

Wigmosta, M.S., L.W. Vail, and D.P. Lettenmier, A distributed hydrology-vegetation model for complex terrain, Water Resources Research, 30,1165-1679, 1994.

Wollmuth, J.C, and J.W. Eheart, Surface water withdrawal allocation and trading systems for traditionally riparian areas, Journal of the American Water Resources Association 36(2): 293–303, 2000.

Wood, A.W., L.R. Leung, V. Sridhar, and D.P. Lettenmaier, Hydrologic implications of dynamical and statistical approaches to downscaling climate model outputs, Climatic Change, 62(1-3), 189–216, 2004.

Xoplaki, E., J.F. González-Rouco, J. Luterbacher, H. Wanner, Mediterranean summer air temperature variability and its connection to the large-scale atmospheric circulation and SSTs. Climate Dynamics, 20 (7), 723–739. http://dx.doi.org/10.1007/s00382- 003-0304-x, 2003.

Xu, C.Y., Operational testing of a water balance model for pre- dicting climate change impacts, Agricultural and Forest Meteorology, 98–99, 295–304, 1999.

Xu, C.Y., and V.P. Singh, Review on regional water resources assessment under stationary and changing climate, Water Resources Management 18 (6), 591– 612, 2004.

Xu, C., E. Widen, and S. Halldin, Modelling hydrological consequences of climate change – Progress and challenges, Advances in Atmospheric Sciences, 22, 789-797, 2005.

Yen, H., A. Sharifi, L. Kalin, G. Mirhosseini, and J.G. Arnold, Assessment of model predictions and parameter transferability by alternative land use data on watershed modeling, Journal of Hydrology, 527, 458-470, 2015.